



# Proceedings of Forum “Math-for-Industry” 2022 -Mathematics of Public Health and Sustainability-

**Chief Editor : Philip Broadbridge**

**Editors: Luke Bennetts, Melanie Roberts and Kenji Kajiwara**

九州大学マス・フォア・インダストリ研究所

# **Proceedings of Forum “Math-for-Industry” 2022 -Mathematics of Public Health and Sustainability-**

■ **Chief Editor:**

Philip Broadbridge

■ **Editor:**

Luke Bennetts, Melanie Roberts and Kenji Kajiwara

## About MI Lecture Note Series

The Math-for-Industry (MI) Lecture Note Series is the successor to the COE Lecture Notes, which were published for the 21st COE Program “Development of Dynamic Mathematics with High Functionality,” sponsored by Japan’s Ministry of Education, Culture, Sports, Science and Technology (MEXT) from 2003 to 2007. The MI Lecture Note Series has published the notes of lectures organized under the following two programs: “Training Program for Ph.D. and New Master’s Degree in Mathematics as Required by Industry,” adopted as a Support Program for Improving Graduate School Education by MEXT from 2007 to 2009; and “Education-and-Research Hub for Mathematics-for-Industry,” adopted as a Global COE Program by MEXT from 2008 to 2012.

In accordance with the establishment of the Institute of Mathematics for Industry (IMI) in April 2011 and the authorization of IMI’s Joint Research Center for Advanced and Fundamental Mathematics-for-Industry as a MEXT Joint Usage / Research Center in April 2013, hereafter the MI Lecture Notes Series will publish lecture notes and proceedings by worldwide researchers of MI to contribute to the development of MI.

October 2022

Kenji Kajiwara

Director, Institute of Mathematics for Industry

## Proceedings of Forum “Math-for-Industry” 2022 -Mathematics of Public Health and Sustainability-

MI Lecture Note Vol.93, Institute of Mathematics for Industry, Kyushu University

ISSN 2188-1200

Date of issue: June 19, 2023

Editors: Philip Broadbridge, Luke Bennetts, Melanie Roberts and Kenji Kajiwara

Publisher:

Institute of Mathematics for Industry, Kyushu University

Graduate School of Mathematics, Kyushu University

Motooka 744, Nishi-ku, Fukuoka, 819-0395, JAPAN

Tel +81-(0)92-802-4402, Fax +81-(0)92-802-4405

URL <https://www.imi.kyushu-u.ac.jp/>

## Prologue

During 21<sup>st</sup>–24<sup>th</sup> November 2022, we were privileged to host the Forum “Math-for-Industry” 2022 (FMfI2022), following a long tradition of successful events around the Asia Pacific region, under the auspices of the Asia Pacific Consortium of Mathematics for Industry (APCMfI). The event was held at the City Campus of La Trobe University, conveniently located in the heart of Melbourne’s business district. More broadly, this event was hosted by Australian members of APCMfI. The organising committee included representatives from Monash University, the University of Adelaide, Griffith University and Kyushu University, as well as several from La Trobe University.

The chosen theme for FMfI2022 was “Mathematics for Public Health and Sustainability”, encompassing two of the most challenging areas that are faced by humanity. Mathematical modelling in these two areas involves some common features. Both deal with complex systems of many variables influenced by human behaviour and environmental influences (earthquakes, volcanism, droughts, floods, storms) that can be predicted only with a high degree of uncertainty. To some extent, these systems can be modelled by deterministic dynamics that inform our basic understanding, but with important unpredictable fluctuations of external forces as well as uncertainty in the values of model parameters. A variety of mathematical tools is needed, including: forward and inverse problems of differential and integral equations; uncertain parameter estimation; stochastic equations; discrete agent simulation; operations research and game theory. To this end, we invited several excellent and influential speakers, all of whom are very busy people that freely committed their time to this worthy cause. Also, there was a variety of interesting and attractive posters that generated much discussion. By tradition, FMfI showcases only invited plenary talks plus posters by students and early-career researchers.

It occurred to the organisers that the modelling of important complex systems requires the use of ‘Statistics and Mathematical Modelling in Combination’ (SMMC). That combination is easier said than done. The majority of mathematical scientists devote most of their time to one or the other end of the statistics—mathematics spectrum. Therefore, we decided to run a workshop SMMC2022 on that combined theme, as technical background. SMMC2022 was held in the week preceding FMfI from 16<sup>th</sup>–18<sup>th</sup> November. This gave us the opportunity to call for contributed talks as well as inviting several plenary speakers who had examples of successful research at the interface of mathematical science disciplines.

Both events received very supportive feedback from participants. Thank you to all those who prepared talks and posters, providing stimulation at a very high standard. Neither event could have run without the generous support of APCMfI, La Trobe University (especially the Australia Branch of IMI-Kyushu-U, La Trobe Asia and the School of Computing, Engineering and Mathematical Sciences), the Institute of Mathematics for Industry Kyushu University (for International Program Grant and sponsorship of student prizes), and the Australian Mathematical Sciences Institute (AMSI) for a workshop grant. We express our gratitude to all benefactors and supporters. We acknowledge the work of the organising committee and program committee that met regularly throughout most of the year, reliably coordinated by the tireless administrative officer Diana Heatherich. Finally, we thank all who attended, either in person or by electronic communications during a difficult pandemic. We had registrants from Australia, New Zealand, Japan, Malaysia, USA, India, and the Netherlands.

Due to many competing demands, we have not insisted on full papers being submitted by speakers. They were given the opportunity to contribute full papers, projected presentation pages, extended abstracts or original abstracts. Documents from both events have been combined here. They have been categorised by broad topic: SARS-Corona virus modelling; other public health issues; environmental models; and combined methods of mathematics/statistics. We hope that there will be something of interest for all readers, that it might spread the word on who is active in these fields, and that it might encourage people to participate in FMfI and other APCMfI and IMI events in future.

Editors Philip Broadbridge, Melanie Roberts, Luke Bennetts, and Kenji Kajiwara,  
March 2023

# Contents

Prologue · · · · ·	i
History of the Forums "Math-for-Industry" · · · · ·	1
Forum and Conference Committees · · · · ·	3
SMMC Conference Schedule · · · · ·	4
FMFI2022 Forum Schedule · · · · ·	6
Abstracts: SARS-Corona epidemics. · · · · ·	9
Abstracts: General Public Health · · · · ·	13
Abstracts: Environmental Modelling · · · · ·	16
Abstracts: Mathematical/Statistical Methods · · · · ·	22
Poster abstracts · · · · ·	30
Papers and Presentations · · · · ·	33
M. Banerjee, Samiran Ghosh, and Vitaly Volpert: Epidemic to immuno-epidemic models of COVID-19 · · · · ·	35
S. Kaji: HOMOLOGICAL FEATURES OF 3D MEDICAL IMAGES · · · · ·	53
A. D. Hartono, Tôn Việt Tạ and Linh Thi Hoai Nguyen: A Geometrical Structure for Predator-Avoidance Fish Schooling · · · · ·	75
M. Roberts: MERGE and the role of gully erosion modelling to protect water quality on the Great Barrier Reef · · · · ·	91
S. Taylor: Mathematical Modelling of nitrogen management on dairy farms · · · · ·	97
L. Bennetts: Modelling flexural strains at the outer margins of Antarctic ice shelves caused by ocean waves · · · · ·	109
W. Schilders: Mathematics: key enabling technology for scientific machine learning · · · · ·	121
POSTER SESSION · · · · ·	159

## History of the Forums "Math-for-Industry"

The first of these forums was initiated by the Institute of Mathematics for Industry (IMI) at Kyushu University in Japan in 2010. As part of its international program, IMI has continued to support participation throughout the Asia-Pacific region in its philosophy of relating high-level mathematics to industry needs. In 2014, this outreach was broadened with the formation of Asia Pacific Consortium of Mathematics for Industry (APCMfi), which is now the host organisation, consisting of members from the entire region, plus some from further afield. Except for one postponement during the height of the novel coronavirus pandemic, forums have been held annually with great success:

2008 Sep 16-17

Tokyo, Japan

Consortium of Math-for-Industry

2009 Nov 9-13

Fukuoka, Japan

Casimir Force, Casimir Operators and the Riemann Hypothesis

-- Mathematics for Innovation in Industry and Science—

2010 Oct 21–23

Fukuoka, Japan

Information Security, Visualization, and Inverse Problems, on the basis of Optimization Techniques

2011 Oct 24–28

Honolulu, USA

TSUNAMI - Mathematical Modelling Using Mathematics for Natural

Disaster: Prediction, Recovery and Provision for the Future

2012 Oct 22–26

Fukuoka, Japan

Information Recovery and Discovery

2013 Nov 4–8

Fukuoka, Japan

The Impact of Applications on Mathematics

2014 Oct 27–31

Fukuoka, Japan

Applications + Practical Conceptualization + Mathematics = Fruitful Innovation

2015 Oct 26–30

Fukuoka, Japan

The Role and Importance of Mathematics in Innovation

2016 Nov 21–23

Brisbane, Australia

## Agriculture as a Metaphor for Creativity in all Human Endeavours

2017 Oct 23–26

Honolulu, USA

Responding to the Challenges of Climate Change: Exploiting, Harnessing  
and Enhancing the Opportunities of Clean Energy

2018 Nov 17-21

Shanghai, PRC

Big Data Analysis, AI, Fintech, Math in Finance and Economics

2019 Nov 18–21

Auckland, NZ

Mathematics for the Primary Industries and the Environment

2021 Dec 13-16

Hanoi, Vietnam

Mathematics for Digital Economy

2022 Nov 21-24

Melbourne, Australia

Mathematics for Public Health and Sustainability

## Forum and Conference Committees

### Organising Committee and Programme Committee

- Professor Marcel Jackson, La Trobe University, Chair, Organising Committee
- Emeritus Professor Philip Broadbridge, La Trobe University, Chair, Programme Committee
- Associate Professor Joel Miller, La Trobe University
- Dr Peter Van Der Kamp, La Trobe University
- Associate Professor Luke Bennetts, University of Adelaide
- Dr Melanie Roberts, Griffith University
- Dr Christopher Lenard, La Trobe University
- Dr Anja Slim, Monash University
- Dr Rebecca Chisholm, La Trobe University
- Associate Professor Winston Sweatman, Massey University, New Zealand
- Professor Luke Prendergast, La Trobe University
- Professor Osamu Saeki, Kyushu University
- Professor Kenji Kajiwara, Kyushu University
- Diana Heatherich, La Trobe University, Secretariat

Advisers: Professors Zainal Bin Abdul Aziz, President APCFMI  
Dr Pierluigi Cesana (Poster Competition Organiser)  
Dr Shizuo Kaji, Treasurer APCMfl.

This combined committee met fortnightly throughout most of 2022.



## SMMC Conference Schedule

### Wednesday 16 Nov

9:35–10:25 Jukka **Corander**

Robust and scalable inference for simulator-based models

10:30–10:45 Morning Tea

10:45–11:35 Shizuo **Kaji**

Modelling preference with hyperplane arrangement

11:40–12:00 Yvonne **Stokes**

Chemical signalling and tissue response: a moving boundary problem in biology

12:00–12:20 Rahil **Valani**

Dynamics of inertial particle focusing in curved ducts

12:20–12:40 Soukaina **Hadiri**

Some results on the mixed bifractional Brownian motion

12:40–2:00 Lunch

2:00–2:50 David **Price**

Supporting government response to COVID-19 through model-based situational assessment

2:55–3:10 Afternoon Tea

3:10–4:00 Melanie **Roberts**

MERGE and the role of gully erosion modelling to protect water quality on the Great Barrier Reef

### Thursday 17 November

10:45 – 11:35 Oliver **Maclaren**

Data, Models and Uncertainty: Perspectives and Tools

11:40 – 12:00 Sarah **Vollert**

A sequential method for efficiently parameterising ensemble ecosystem models

12:00 – 12:20 Jordan **Pitt**

Model predictions of wave overwash extent into the marginal ice zone

12:20 – 12:40 Adeshina **Adekunle**

A new mathematical modelling framework for capturing and forecasting Australia COVID-19 waves: transitioning from Delta wave into Omicron wave

12:40 – 2:00 Lunch

2:00 – 2:50 Natalie **Thamwattana**

Interaction between nanostructures: relation between their atomic distributions and modelling approaches

2:55 – 3:10 Afternoon Tea

3:10 – 4:00 Kei Hirose

Penalized likelihood approach in multivariate regression with missing values and its application to materials properties prediction

**Friday, 18 Nov**

10:10–10:30 Chris **Drovandi**

Likelihood-Free Methods and Model Misspecification

10:30–10:45 Morning Tea

10:45–11:35 iadine **Chad`es**

Developing AI Decision Tools for Conservation

11:40–12:00 **Ton** Viet Ta

Fish Schooling

12:00–12:20 Matthew **Adams**

Analysis of model sloppiness: what can it do, and what's next?

12:20–12:40 Saddam **Abbasi**

Identifying state of the process using ML algorithms

12:40–2:00 Lunch

2:00–2:50 Emma **McBryde**

The application of mathematics to pandemics: some examples of modelling used during COVID-19

2:55–3:10 Afternoon Tea

3:10–3:30 Komal **Singla**

Symmetry Analysis and Exact solutions of fractional order (2+1)-dimensional Burgers system

3:30–3:50 Manoj **Kumar**

Analysis of Diffusive Size-Structured Population Model and Optimal Birth Control

## FMFI2022 Forum Schedule

Monday, 21 November

9:15–10:00

Opening & Acknowledgement of Country

Professor Marcel Jackson

Mr Adam Cuneen, Victoria's Commissioner to North Asia

Deputy Consul General Mr Shunsuke Saito, Consulate General of Japan

Professor Chris Pakes, Pro Vice Chancellor (Graduate & Global Research)

Professor Zainal Aziz, President of APCMfi

10:00–10:50 Wil **Schilders**

Mathematics: key enabling technology for scientific machine learning

10:50–11:20 Morning Tea

11:20–12:10 Bhavna **Antony**

Artificial Intelligence Approaches for Diagnosis and Management of Glaucoma

12:00–2:00 Lunch

2:00–2:50 Emma **McBryde**

The application of mathematics to pandemics: some examples of modelling used during COVID-19

2:50–3:10 Afternoon Tea

3:10–4:00 Oliver **Maclaren**

Identifiability analysis and predictive uncertainty for complex mathematical and simulation models

4:00–6:00 Free

6:00–7:00 Malay **Banerjee**

Christie Eliezer Memorial Lecture

Epidemic to immuno-epidemic models of COVID-19

## Tuesday, 22 November

9:15-10:05 Jukka **Corander**

Advances in likelihood-free inference with applications to evolutionary epidemiology

10:15–10:30 Morning Tea

10:30–11:20

Natalie **Thamwattana**

Modelling clogging in granular assembly when treating acidic groundwater

11:20–12:10 Luke **Bennetts**

Modelling flexural strains at the outer margins of Antarctic ice shelves caused by ocean waves

12:10–2:00 Lunch

2:00–2:50 Masayo **Hirose**

An Assessment of Prediction Error under Area Level Model with Arc-Sin Transformation

2:50–3:10 Afternoon Tea

3:10–4:00

Luke **Prendergast**

Some considerations for measuring and interpreting heterogeneity in meta-analysis

## Wednesday, 23 November

9:15-10:05 Andrea **Bertozzi**

Energy minimizing surfaces for nanovial technology

10:15–10:30 Morning Tea

10:30–11:20 David **Price**

Evaluation of a pharmacokinetic-pharmacodynamic model for predicting parasitological outcomes in Phase 2 studies of new antimalarial drugs

11:20 – 12:10 Stephen **Taylor**

Mathematical Modelling of nitrogen management on dairy farms

12:10 - 2:00 Lunch

2:00 – 2:50 Shizuo **Kaji**

Homological features of 3D medical images

3:10 – 5:00 Poster Session (Hybrid)

5:00 – 6:00 Free

6:00 Forum Dinner

## Thursday, 24 November

9:15-10:05 Hugh **Possingham**

Decision science thinking applied to nature conservation

10:15–10:30 Morning Tea

10:30–11:20 iadine **Chad`es**

Challenges of developing decision tools to guide conservation decisions

11:20–12:10 Melanie **Roberts**

The effect of sediment heterogeneity on sediment yield during gully erosion

12:10–2:00 Lunch

2:00–2:50 Freya **Shearer** and Gerard **Ryan**

Modelling through the crisis: developing methods to support decision-making in the COVID-19 pandemic

3:00–3:10 Zainal Aziz and Pierluigi Cesana

Poster prize awards

3:10-3:20 Kenji Kajiwara

Invitation to FMfl2023 Fukuoka

3:20-3:30 Phil Broadbridge

Summing up and Closing.

## **Abstracts: SARS-Corona epidemics.**

### *Epidemic to immuno-epidemic models of COVID-19*

(See also a full report in this volume)

**Malay Banerjee**, IIT Kanpur, India.

Abstract: A wide range of multi-compartment models is available to study the epidemic progression of SARS-CoV-2. Variation in the period of infectivity, the time required for recovery, and days spent at the hospital during the disease severity vary significantly from one individual to another. These phenomena are the factors behind considering multiple compartments to study the epidemic progression due to COVID-19. The main objective of this talk is to discuss a new modeling approach for the COVID-19 epidemic, which involves distributed recovery and death rates and the variable infectivity based upon the immunity level of the individuals. The infection transmissibility rate depends upon the immune response's strength and antibody level due to vaccination and acquired immunity. The proposed model helps to evaluate the COVID-19 epidemic situation in some countries.

### *The application of mathematics to pandemics: some examples of modelling used during COVID-19*

**Emma McBryde**, James Cook University, Australia.

Abstract: Mathematical models have been applied to explain infectious diseases outbreaks for over a century, but have never been taken so seriously as during the recent COVID-19 pandemic, during which they were used to synthesize evidence and inform public health action. This talk will discuss some of the models used at state level, national level and globally. It will discuss limitations and future directions for modelling.

When Australia closed its borders it did so on advice based on layered transmission and mobility models. This work suggested that by February 2020, several countries had already had cases of SARS CoV-2, without knowing it. Flight mobility suggested where the likely epidemic would spread and correctly identified changes in epicentre to Europe and later South America. I will discuss some of the modelling results that suggested this, and the importance of the early international travel restrictions. One of the first pieces of available evidence about COVID-19 was its very specifically age-based effects, with children both less likely to acquire COVID and less likely to spread it. We used this information — along with age-specific contact matrices — to assess the potential risks and benefits of school closure. We also used age-based matrices to investigate optimal vaccine distribution at a time when vaccines were scarce. Results show that prioritising the most vulnerable (older age) was almost always a better strategy than prioritising the highest transmitters (20–30 year olds). I will finish by discussing model refinements that are being made currently and a vision for open-science in the modelling emerging infectious diseases space.

### Modeling the Covid-19 Pandemic

**Andrea Bertozzi**, University of California Los Angeles, USA.

Abstract: The COVID-19 pandemic placed epidemic modeling at the forefront of worldwide public policy making. Modeling and forecasting COVID-19 has been challenge. In my talk, I will describe several regional-scale models for forecasting and assessing the course of the pandemic. We used parsimonious models for early-time data, and developed an accessible framework for generating policy-relevant insights into the disease. We also look at the role of network structure and on the dynamics of opinion spread and optimal policies under real-world conditions.

### Modelling through the crisis: developing methods to support decision-making in the COVID-19 pandemic

**Freya Shearer** and **Gerard Ryan**, University of Melbourne, Australia.

Abstract: Here we will talk about a range of modelling and data-analytics work conducted on a regular and ad hoc basis since 2020 to provide government health decision-makers with information to manage the COVID-19 pandemic. We will first discuss the novel metric of “Transmission Potential” (TP), which is the average potential for transmission in the community. TP can be combined with case data in a semi-mechanistic framework to calculate a continuous risk metric. In times of ongoing transmission, this metric is equivalent to the effective reproduction number of a virus, while in times of low or no transmission, the metric reverts to TP — providing decision-makers with a tool that is applicable at all stages of outbreak and suppression.

We describe the incorporation of changes to adapt the framework to novel variants and the rollout of the vaccination programme, and the downstream uses of this work in case and clinical forecasting, and contributions to the “National Plan to Reopening”. We will discuss both the technical developments and policy implications of the work.

## *Data, Models and Uncertainty: Perspectives and Tools*

**Oliver Maclaren**, University of Auckland, New Zealand.

Abstract: Complex mathematical and simulation models are central to science, engineering, and policymaking. However, model sophistication frequently outpaces available data while interpretational issues can make drawing causal conclusions difficult. This talk will cover my research interests in methods for bridging the gap between data and complex mathematical models representing scientific and engineering understanding. I will illustrate with examples such as my work on COVID-19 modelling for policymakers, parameterisation of cell, tissue, and population dynamics models in biology, and large-scale uncertainty quantification for geothermal reservoir simulation models. I will discuss the challenges of model development, model interpretation, parameter identifiability, prediction vs. parameter estimation and mechanistic understanding, and how new and old statistical uncertainty quantification methods can help us use complex mechanistic models more effectively. I will highlight high-level conceptual issues and promising, practical, computationally efficient methods. A key theme throughout will be the interplay between traditional applied mathematical modelling, statistics, and newer areas such as causal inference.

A key element of epidemic decision-making is situational awareness — that is, knowing the current and potential future status of the epidemic. Outputs from mathematical and statistical models have provided enhanced situational awareness to governments throughout the course of the COVID-19 pandemic. Key analyses include estimation of the effective reproduction number ( $R_{\text{eff}}$ ), forecasting of epidemic activity, and forecasts of ward- and ICU-bed demand. Accurate and timely estimation of  $R_{\text{eff}}$  enables the tracking and planning of progress towards the control of outbreaks. Short-term forecasts of daily case incidence and hospital bed occupancy provide information on future health system requirements, which supports both clinical and public health planning.

In this talk, I will describe Australia’s situational awareness modelling program for COVID-19 through 2020–21. I will provide an overview of the modelling outputs reported to key government decision-making committees on (at least) a weekly basis since April 2020, and highlight some challenges with providing near-real-time analytic support.



*A new mathematical modelling framework for capturing and forecasting Australia COVID-19 waves: transitioning from Delta wave into Omicron wave.*

**Adeshina I. Adekunle**<sup>1\*</sup>, Mingmei Teo<sup>1</sup>, August Hao<sup>2</sup>, Gerard Ryan<sup>2</sup>, Nick Golding<sup>2</sup>, Rob Moss<sup>2</sup> and Peter Dawson<sup>1+</sup>

\* speaker

+ corresponding author

<sup>1</sup> Dept. of Defence, Australia

<sup>2</sup> University of Melbourne, Australia.

Abstract: Covid-19 pandemic may be subsiding, but the damage caused by the SARS-CoV2 virus will take long time to amend. Many governments adopted series of public health control measures to reduce the burden of this disease during different SARS-CoV2 strain specific waves. These measures include lockdown, isolations, quarantine, and facemask wearing. To proffer these measures in Australia, the Australian Government relied on forecasting outputs from the National Situational Assessment Team. In the work, we provide particle filter forecasts for the Delta and Omicron strain waves in Australia using an auto stochastic compartmental model. The reliability of the forecasting approach is demonstrated.

## Abstracts: General Public Health

### *Homological features of 3D medical images* (see also, the projected presentation, in this volume)

**Shizuo Kaji**, Institute of Mathematics for Industry, Kyushu University, Japan.

Abstract: Modern medical imaging techniques have enabled access to the interior of the human body in the form of not only 2D images but also 3D volumes. It is, however, not easy to utilise the 3D information and analysis is often limited to a slice-by-slice investigation. We need a set of features for volumetric data to take full advantage of the 3D measurements. On the one hand, radiomic features have been proposed to capture the textural characteristics of a volume. They are computed from small patches of a volume and encode only local properties. On the other hand, persistent homology (PH) provides computational machinery to extract the global structure of a volume. In this talk, we present our software, Cubical Ripser [1], for efficient computation of persistent homology of volumetric data. Then, we define a few types of invariants of a volumetric image based on PH and demonstrate their clinical relevance to abnormality quantification and detection in lung CT [2].

#### References

- [1] S. Kaji, T. Sudo, and K. Ahara, Cubical Ripser: Software for computing persistent homology of image and volume data, arXiv:2005.12692
- [2] N. Tanabe, S. Kaji, et al., A homological approach to a mathematical definition of pulmonary fibrosis and emphysema on computed tomography, J Appl Physiol, vol 131-2, 2021

### *Energy minimizing surfaces for nanovial technology*

**Andrea Bertozzi**, University of California Los Angeles, USA.

Abstract: For nearly 40 years, drugmakers have used genetically engineered cells as tiny drug factories. Such cells can be programmed to secrete compounds that yield drugs used to treat cancer and autoimmune conditions such as arthritis. I will talk about recent work from UCLA to design tiny containers that can be used to sort and to select cells based on what type they are, and which compounds — and how much of those compounds — they secrete. The methodology involves templating droplets using amphiphilic microparticles. These particles are observed to hold nearly equal volumes of aqueous liquid when dispersed in an oil-water mixture. I will discuss mathematical theory to rigorously prove that through random interactions, a system of such particles achieves this state. I will also discuss efficient numerical methods for computing low energy states for various microparticle shapes and show some examples of how these particles can be used to study single cell secretion.

*Evaluation of a pharmacokinetic-pharmacodynamic model for predicting parasitological outcomes in Phase 2 studies of new antimalarial drugs*

**David Price**, Doherty Institute for Infection and Immunity, University of Melbourne and Royal Melbourne Hospital, and Centre for Epidemiology and Biostatistics, Melbourne School of Population and Global Health, University of Melbourne, Australia.

**Abstract:** The unrelenting rise of multidrug resistant malaria demands the continuous development of novel antimalarial compounds from preclinical studies in human volunteers to Phase 3 clinical trials in patients. Mechanistic pharmacokinetic-pharmacodynamic (PK-PD) models, fit in a Bayesian hierarchical framework, are routinely used to predict parasite-time profiles in the presence of a drug to evaluate the potential of these new treatments and explore optimal dosing regimens. But, how well do these models estimate the biological characteristics of the drug and parasites?

In the context of a Phase 2 study of a new antimalarial drug, cipargamin, we performed a simulation-estimation study to evaluate the performance of this modelling and estimation framework to recover the characteristics of the treatment and parasite dynamics. We simulated cipargamin concentration and parasitaemia profiles that reproduce the observed profiles for 8 volunteers enrolled in a Phase 2 study. Cipargamin was administered on day 7 following inoculation of malaria parasites. The pre- and post-treatment parasitaemia profiles were simulated using our biologically informed PD model, which captures the life cycle of the parasite in the red blood cell. Estimation of the PK-PD parameters was performed using a Bayesian hierarchical model with STAN.

The population PK model parameters describing the absorption, distribution, and clearance of cipargamin were estimated with minimal bias and the posterior predictive checks captured the simulated PK profiles. The PD model was fitted to the parasitaemia profiles of each simulated dataset using the estimated PK parameters. The posterior predictive checks demonstrate that our PK-PD model successfully captures the central trend and variability of both the pre- and post-treatment simulated parasitaemia profiles.

*Advances in likelihood-free inference with applications to evolutionary epidemiology*

**Jukka Corander**, University of Oslo, Norway and University of Helsinki, Finland.

Abstract: Likelihood-free inference has evolved from a seminal idea to a powerful tool for advanced statistical and mathematical modeling in roughly 20 years. Currently both computational statistics and machine learning communities are actively contributing to development of new methods for calibrating simulator-based models in the light of data or other constraints. We discuss some of the recent advances in such inference methods and illustrate them with models for epidemics and pathogen population evolution.

*Interaction between nanostructures: relation between their atomic distributions and modelling approaches*

**Natalie Thamwattana**, University of Newcastle, Australia.

Abstract: Applications of nanomaterials are found in many areas, including renewable energy, electronics, textiles, food technology, environment, health care and medicine. Understanding mechanics of these materials is important as it can help to optimise their performances. In this talk, we consider structures of nanomaterials, the role that molecular structures play in determining an approach for modelling intermolecular interactions and their applications.

## **Abstracts: Environmental Modelling**

### *A Geometrical Structure for Predator-Avoidance Fish Schooling*

(See also a full report in this volume)

Aditya Dewanto Hartono, **Ton Viet Ta**<sup>\*1</sup> and Linh Thi Hoai Nguyen<sup>2</sup>

<sup>1</sup> Mathematical Modeling Laboratory, Department of Agro-environmental Sciences, Kyushu University, Japan

\* Corresponding author

<sup>2</sup> Institute of Mathematics for Industry, Kyushu University, Japan.

Abstract: In this talk, we introduce our mathematical models of stochastic differential equations for fish schooling. Structural stability of models against noise is then studied numerically. Patterns obtained from the models which are consistent with real observations are presented.

### *Mathematical modelling of nitrogen management on dairy farms*

(See also the projected presentation, in this volume)

**Stephen Taylor**, Graeme Wake and Tony Pleasants

University of Auckland, New Zealand.

Abstract: New Zealand's climate allows for full year outdoor grazing of dairy cows and a very efficient dairy industry. One downside is the nitrogen-containing chemicals that get deposited on fields through fertilising or cows' urine, because these chemicals end up in fresh water streams. In order to understand how to mitigate this, we model this nitrogen deposition and its dynamics on a dairy farm.

*MERGE and the role of gully erosion modelling to protect water quality on the Great Barrier Reef*

(See also the full report, in this volume)

**Melanie Roberts**, Griffith University, Australia.

Abstract: Gully erosion is the majority source of fine sediment that reaches the Great Barrier Reef (GBR), degrading water quality and contributing to poor outcomes including coral death. Consequently, gully remediation is a significant focus of activities to improve GBR water quality. The MERGE gully erosion model was developed in partnership with Queensland Government and the Queensland Water Modelling Network to provide a process-based model to inform gully rehabilitation actions at specific sites. In this talk, I introduce the MERGE model and share the outcomes of a pilot study to explore the on-ground application of the model.

**Melanie Roberts**, Griffith University, Australia.

Abstract: Gully erosion is the majority source of fine sediment that ultimately reaches the Great Barrier Reef (GBR), while also contributing to the pool of bioavailable nutrients in the lagoon. Particulate nitrogen is transported with sediment to the GBR, degrading water quality and contributing to poor outcomes including algal blooms, and potentially crown-of-thorns starfish outbreaks. Quantifying the surface area of eroded sediment is important to estimate the particulate nitrogen load, and thereby prioritise interventions. The MERGE gully erosion model was developed in partnership with Queensland Government and the Queensland Water Modelling Network to provide a process-based model to inform gully rehabilitation actions at specific sites. In this talk I introduce MERGE-D, which extends MERGE to account for heterogeneities in sediment properties, providing an improved estimate of sediment surface area, and hence particulate nitrogen loads.

*Modelling clogging in granular assembly when treating acidic groundwater*

**Natalie Thamwattana**, University of Newcastle, Australia.

Abstract: Acid sulphate soils (ASS) are naturally occurring sediments occupying over 200,000 km<sup>2</sup> of land in Australia. Acidic groundwater resulting from the oxidation of pyrite (FeS<sub>2</sub>) in ASS is a major environmental concern particularly in the coastal regions. When exposed to air during flood mitigation drainage or upon excavation (e.g. coal mining), FeS<sub>2</sub> can rapidly oxidise to form sulphuric acid, leading to contamination of the groundwater and causing acid drainage in underground coal mines. To treat acidic groundwater, permeable reactive barriers (PRBs) are introduced to neutralize acidity induced by pyrite oxidation in ASS terrain. PRBs (alkaline materials, e.g. crushed recycled concrete, ash, blast-furnace slag and calcitic limestone CaCO<sub>3</sub>) are used as an underground filter to eradicate the contaminants through chemical and/or biological processes. However, this clogging can reduce the porosity of PRBs which in turn reduces their longevity and functionality. In this talk, we discuss modelling clogging in PRBs which is due to the accumulation of bacteria and reactive aggregates becoming coated with chemical precipitates, and the effect of the clogging on the porosity of PRBs over time.

*Modelling flexural strains at the outer margins of Antarctic ice shelves caused by ocean waves*

**Luke Bennetts**, University of Adelaide, Australia.

Abstract: The extent of Antarctic sea ice is hitting record lows in response to climate change. This is exposing the Antarctic coastline to the most energetic waves on the planet that exist in the Southern Ocean. In particular, ocean waves are increasingly able to reach ice shelves that fringe about half the Antarctic coastline, which has implications for future global sea level rise. Energetic waves bend and flex the outer margins of the ice shelves, and the flexural strains imposed can propagate fractures, cause icequakes, initiate iceberg calving, and even trigger disintegration events, particularly when the ice shelf is already weakened by warming temperatures. I will present a mathematical model of ocean wave transfer to ice shelf flexure, and a series of approximations that generate predictions over a spectrum of wave frequencies and for realistic ice shelf and seabed geometries. I will discuss results for Antarctica's largest ice shelf, the Ross Ice Shelf.

*Model predictions of wave overwash extent into the marginal ice zone*

**Jordan Pitt\*** and Luke Bennetts, University of Adelaide, Australia.

\* speaker

Abstract: Overwash is an important aspect of the dynamics in the marginal ice zone where sea ice and ocean waves interact. Overwash dissipates wave energy, and the presence of water on top of sea ice can drive growth or melting, depending on the local thermodynamic conditions. The presence of water on floes is also important for biologic and chemical processes. While overwash has been observed and investigated under experimental conditions, it has not yet been studied in the marginal ice zone. One reason for this lack of in-situ measurements and observations is due to the marginal ice zone being highly dynamic, and the onset of overwash only occurring under specific and sensitive conditions. To facilitate future observations we have produced a stochastic model of the extent of overwash into fields of sea ice by combining a new model of the onset of overwash and a standard transmission model. This combined transmission and overwash model is validated against experimental observations and is used to provide the extent of overwash for various realistic ice field and wave field conditions.

## Decision science thinking applied to nature conservation

**Hugh Possingham**, University of Queensland, Australia.

Abstract: Ecology has always had a lot of mathematical theory, which blossomed in the 1960s–1980s. One of the applied branches of ecology is nature conservation (the others are pest management and harvesting). Mathematical theory for nature conservation in the late part of the last century was naïve – ignoring important issues such as finances, efficiency and risk. Over the past 30 years our group has created a range of approaches for making conservation decisions using applied mathematics and economics – such as where to place protected areas, which threatened species to invest in, how much to spend on monitoring and whether to restore or protect habitat. I will discuss the basic maths that underpins these approaches.

## Challenges of developing decision tools to guide conservation decisions

**Madeline Chadwick**, CSIRO, Australia.

Abstract: Over the last 10 years, we have developed decision tools to help make informed decisions to help protect biodiversity in the face of limited resources. Developing decision tools for the conservation of biodiversity poses unique challenges to researchers, e.g. poor data context, urgent decision-making and human operated systems to cite a few. I will summarise these challenges and lessons learned from our experience developing the Integrated Spatial Prioritisation (ISP) tool and testing Artificial Intelligence decision tools in the context of adaptively managing species and their associated threats for the Saving our Species Program (NSW). While the ISP is used to guide current investment as a conservation planning tool, more needs to be done to make AI decision tools relevant to managers in areas such as interpretability and trust.



## Effect of slow-fast time scale on spatio-temporal pattern formation

**Malay Banerjee**, IIT Kanpur, India.

Abstract: Spatiotemporal pattern formation in interacting population models is an interesting field of study as it can capture the stationary as well as dynamic patchy distribution of population within their habitat. Introduction of nonlocal interaction in the spatiotemporal model can produce stationary pattern by a spatiotemporal model with Rosenzweig-MacArthur reaction kinetics [MBVV]. On the other hand, it is evident that growth of various prey and their predators take place at different rates when measured with respect to a fixed time scale. This fact is incorporated into the mathematical model by introducing different time-scales into the growth equations. The resulting models (with temporal reaction kinetics only), in general, exhibit two different types of oscillatory behavior, namely, canard oscillation and relaxation oscillation [PRCSPMB]. The main objective of this talk is to describe a spatiotemporal model for interacting population with nonlocal interaction term and slow-fast time scale, and discuss various scenarios of stationary and non-stationary pattern formation.

### References

[MBVV] Banerjee, M., Volpert, V. (2017). Spatio-temporal pattern formation in Rosenzweig-MacArthur model: Effect of nonlocal interactions. *Ecological Complexity* 30: 2–10.  
[PRCSPMB] Ray Chowdhury, P., Petrovskii, S., Banerjee, M. (2021). Oscillations and pattern formation in a slow-fast prey-predator system. *Bulletin of Mathematical Biology* 83: 110.

## Analysis of Diffusive Size-Structured Population Model and Optimal Birth Control

**Manoj Kumar**, IIT Mandi, India.

Abstract: This work addresses the optimal birth control problem for invasive species in a spatial environment. We apply the method of semigroups to qualitatively analyze a size-structured population model in which individuals occupy a position in a spatial environment. With insect population in mind, we study the optimal control problem which takes fertility rate as a control variable. With the help of adjoint system, we derive optimality conditions. We obtain the optimality conditions by fixing the birth rate on three different sets. Using Ekeland's variational principle, the existence, and uniqueness of optimal birth controller to the given population model which minimizes a given cost functional is shown. A concrete example is also given to see the behaviour of population density.

*A sequential method for efficiently parameterising ensemble ecosystem models*

**Sarah Vollert\***, Chris Drovandi, and Matthew Adams, Queensland University of Technology, Australia.

\* speaker

Abstract: Ensemble ecosystem models are valuable decision-making tools for understanding the effects of conservation actions and human impacts on threatened species. Models parameterised with dynamic systems constraints help us understand ecosystems with limited data availability. However existing methods are computationally inefficient, preventing larger networks from being studied. Using Bayesian approaches, we build on current methods to overcome this technical obstacle. Compared with the existing method, we find that using a sequential Monte Carlo approach yields similar parameter inferences and model predictions while being significantly faster. Consequently, we can study larger and more realistic networks, improving ecosystem modelling capabilities.

## **Abstracts: Mathematical/Statistical Methods**

### *Mathematics: key enabling technology for scientific machine learning*

(See also the projected presentation, in this volume)

**Wil Schilders**, Eindhoven University of Technology & TU Munich Institute of Advanced Studies, The Netherlands.

Abstract: Artificial Intelligence (AI) will strongly determine our future prosperity and well-being, also in the area of public health and sustainability. Due to its generic nature, AI will have an impact on all sciences and business sectors, our private lives and society as a whole. AI is pre-eminently a multidisciplinary technology that connects scientists from a wide variety of research areas, from behavioural science and ethics to mathematics and computer science. Without downplaying the importance of that variety, it is apparent that mathematics can and should play an active role. All the more so as, alongside the successes of AI, also critical voices are increasingly heard. As Robbert Dijkgraaf (former director of the Princeton IAS, now our minister of science and education) observed in May 2019: “Artificial intelligence is in its adolescent phase, characterised by trial and error, self-aggrandisement, credulity and lack of systematic understanding.” Mathematics can contribute to the much-needed systematic understanding of AI, for example, greatly improving reliability and robustness of AI algorithms, understanding the operation and sensitivity of networks, reducing the need for abundant data sets, or incorporating physical properties into neural networks needed for superfast and accurate simulations in the context of digital twinning. Mathematicians absolutely recognise the potential of artificial intelligence, machine learning and (deep) neural networks for future developments in science, technology and industry. At the same time, a sound mathematical treatment is essential for all aspects of artificial intelligence, including imaging, speech recognition, analysis of texts or autonomous driving, implying it is essential to involve mathematicians in all these areas. In this talk, we highlight the role of mathematics as a key enabling technology within the emerging field of scientific machine learning. And we will end with the important adage: “Real intelligence is needed to make artificial intelligence work.”

## *Some considerations for measuring and interpreting heterogeneity in meta-analysis* (extended abstract)

**Luke A. Prendergast**, Department of Mathematical and Physical Sciences La Trobe University, Australia.

Abstract: Used to combine summary statistics from several studies, the huge increase in available data over the last few decades has seen a rapid increase in the usage of meta-analytic methods. Meta-analysis can guide researchers in determining new hypotheses to test, alert policy and other decision makers of previously undetected associations between important variables and interventions, and provide at least a starting point for evidence-based debate.

Heterogeneity in meta-analysis refers to the variation in study characteristics (e.g., differences in cohorts, intervention strategies etc.) that leads to variation in outcomes across studies. While many perceive heterogeneity to be a nuisance since it increases estimator variance, the presence of heterogeneity can itself be very insightful. In this talk we will discuss heterogeneity, consider a variety of heterogeneity measures (including some that should be used more often) and highlight why the most common heterogeneity measure,  $I^2$  is often misinterpreted [1]. We also provide some examples of how heterogeneity can offer valuable insight and along the way see the consequences of not appropriately acknowledging the presence of heterogeneity. Differences in cohort and subpopulation demographics, variations of treatment regimes, etc. means that heterogeneity in the effect of interest almost always needs to be assumed present. For example, it may be reasonable to assume that age and gender are associated with severity and treatment of COVID-19 and in the context of meta-analysis this means assuming that effects vary depending on such characteristics. With this in mind, prediction intervals (e.g., [3]), underused in the context of meta-analysis, can be used as an estimate of a range in which most (e.g., 95%) effects fall, including those for missing studies and future studies.

Another measure that can be useful is the coefficient of variation (CV, [5]) which measures the heterogeneity standard deviation relative the magnitude of the effect. This can be useful since variation among large effects may not be clinically meaningful, whereas variation between small effects can indicate differences in effects that can have very different implications depending on cohort demographics, treatment conditions, etc. Given that very large values of the CV can result due to small effects, we provide transformations of the CV on the scale [0, 1] that may be preferable for interpretation and which also have reliable confidence intervals [2].

An analysis of heterogeneity may also be useful in addition to reporting findings regarding the effect of interest. For example, the standardised mean difference (SMD), assumes that within each study, the population variances in each of two treatment arms are equal. Whether this assumption seems reasonable overall can be tested using a meta-analysis of ratio of variances [4]. Here, while a meta-analysis may indicate that, on average, the assumption may approximately hold (e.g., a mean ratio of variances close to one), heterogeneity can reveal that there can be violations to this assumption for at least some studies. Finally, we

briefly look at how a meta-regression analysis (see [6]) can be useful to both explore potential sources of heterogeneity and to better understand the consequences of heterogeneity for the research question at hand. Throughout we consider several data examples and use visualisations to highlight why it is important to appropriately acknowledge the presence of heterogeneity.

## References

1. M. Borenstein, J. P. T. Higgins, L. V. Hedges, and H. R. Rothstein. Basics of meta-analysis: I<sup>2</sup> is not an absolute measure of heterogeneity. *Research Synthesis Methods*, 8(1):5–18, 2017.
2. M. Cairns and L. A. Prendergast. On ratio measures of heterogeneity for meta-analyses. *Research Synthesis Methods*, 13(1):28–47, 2022.
3. J. Int'Hout, J. P. A. Ioannidis, M. M. Rovers, and J. J. Goeman. Plea for routinely presenting prediction intervals in meta-analysis. *BMJ Open*, 6(7):e010247, 2016.
4. L. A. Prendergast and R. G. Staudte. Meta-analysis of ratios of sample variances. *Statistics in Medicine*, 35(11):1780–1799, 2016.
5. B. Takkouche, C. Cadarso-Suarez, and D. Spiegelman. Evaluation of old and new tests of heterogeneity in epidemiologic meta-analysis. *American Journal of Epidemiology*, 150(2):206–215, 1999.
6. S. G. Thompson and J. P. T. Higgins. How should meta-regression analyses be undertaken and interpreted? *Statistics in Medicine*, 21(11):1559–1573, 2002.

## Likelihood-Free Methods and Model Misspecification

**Chris Drovandi**, Queensland University of Technology, Australia.

**Abstract:** Statistical approaches for likelihood-free inference such as approximate Bayesian computation (ABC) and Bayesian synthetic likelihood (BSL) are now widely adopted in many scientific disciplines for calibrating complex statistical models with intractable likelihood functions. In this talk, I will discuss the behaviour of ABC and BSL under the commonly encountered problem of model misspecification. ABC has some inherent robustness while BSL can exhibit some strange behaviour under misspecification. However, I show how BSL can be extended to make it robust to misspecification, and to identify which features of the data it cannot match.

## An Assessment of Prediction Error under Area Level Model with Arc-Sin Transformation

**Masayo Y. Hirose**\*<sup>1</sup>, Malay Ghosh<sup>2</sup> and Tamal Ghosh<sup>2</sup>

<sup>1</sup>Institute of Mathematics for Industry, Kyushu University, Japan,

<sup>2</sup>University of Florida, USA.

\* speaker

**Abstract:** An empirical best linear unbiased predictor can contribute to more efficiency, especially when the sample size within each area is not large enough to make reliable direct estimates. However, the natural back transformation could produce a bias with the arc-sin transformed data, especially when the sample size within an area is not large enough. In this study, we find explicit empirical Bayes estimators that correct biases asymptotically. Moreover, assessing its mean squared prediction error is also essential. We, therefore, explicitly obtain the second-order unbiased estimators of these mean squared prediction errors, maintaining strict positivity. The data analysis result will be shown in conclusion to apply the proposed method to the positive rate in PCR testing for COVID-19.

*Penalized likelihood approach in multivariate regression with missing values and its application to materials properties prediction*

**Kei Hirose**, Institute of Mathematics for Industry, Kyushu University, Japan.

Abstract: In the field of materials science and engineering, statistical analysis has recently been used to predict multiple material properties from an experimental design. These material properties correspond to response variables in the multivariate regression model. We conduct a penalised maximum likelihood procedure to estimate model parameters. In some cases, there may be a relatively large number of missing values in the response variables, owing to the difficulty of collecting data on material properties. We, therefore, propose a method based on the expectation-maximisation (EM) algorithm to incorporate a correlation structure among the response variables into a statistical model.

*Identifiability analysis and predictive uncertainty for complex mathematical and simulation models*

**Oliver Maclaren**, University of Auckland, New Zealand.

Abstract: Complex mathematical and simulation models are increasingly central in science, engineering, industry, and policy-making. COVID-19 modelling is a notable example: the New Zealand government heavily used modelling to inform its policy and received praise for an effective, science-informed approach to managing the pandemic. In addition, numerous less visible but still impactful examples of modelling work play a significant role in modern society and industry. These examples range from managing natural resources like geothermal reservoirs using numerical simulation models to elaborate theoretical mathematical models designed to understand wound healing and tumorigenesis in epithelia. However, constructing a complex simulation model is only the first step in realising its potential value: we next need to reliably connect it to empirical data to ensure its relevance to the real world. A key barrier to connecting models and data is the lack of identifiability of complex models and parameters. Identifiability refers to the ability to uniquely determine model parameters from ideal data, while practical identifiability refers to reliably estimating parameters from imperfect data. While identifiability is closely related to mechanistic understanding and is the traditional goal of scientific studies, in some applications, we may care more about model predictions than identifiability. However, the relationship between identifiability analysis and the construction of reliable predictive uncertainty bands needs more study for complex mechanistic models. In this talk, I will discuss likelihood-based frequentist tools for diagnosing parameter identifiability and constructing model predictions and the trade-offs and relationships between the two goals.

### *Robust and scalable inference for simulator-based models*

**Jukka Corander**, University of Oslo, Norway and University of Helsinki, Finland.

Abstract: Simulator-based models are becoming increasingly popular in many research domains across academia and industry. Calibration of such models in the light of data and quantification of uncertainty about model parameters are key challenges for practical applications and the topic has received accelerating attention during the past decade. We will discuss various inference techniques for simulator-based models that improve computational feasibility by adopting techniques from machine learning to build surrogate models for the approximate likelihood or posterior. Several of these approaches are available in the open-source software platform Engine for Likelihood-Free Inference (ELFI): [elfi.ai](http://elfi.ai).

### *Modelling preference with hyperplane arrangement*

**Shizuo Kaji**, Institute of Mathematics for Industry, Kyushu University, Japan.

Abstract: A person's preference on a set of options, such as political parties and film genres, can be modelled by a (partial) order on the set. Modelling preference data collected from many individuals with various tastes is a subject of preference learning. There are two major approaches to modelling preference data; based on the distance on orders and based on a utility function defined over the set of options. These approaches lack flexibility (or are biased) since too much structure is forced on the preference data to be modelled by the mathematical structure that the models utilise. Instead, we rely on a geometric entity, hyperplane arrangement, to model preference data. The geometric and combinatorial structure of hyperplane arrangement provides a good balance of flexibility and regularisation.



### Identifying state of the process using ML algorithms

Saddam Akber Abbasi<sup>1\*</sup>, Mohammed Ahmed<sup>1</sup>, and Adegoke Nurudeen<sup>2</sup>

<sup>1</sup> Qatar University, Qatar.

\* Speaker

<sup>2</sup> The University of Sydney, Australia.

Abstract: A process working under the random cause of variation is considered in-control whereas if special cause variations are in effect, the process is considered to be out-of-control. To identify the state of the process, control charts are widely used as a tool of the Statistical Process Control tool-kit. Control chart functionality mostly depends on a set of assumptions that may not be valid for many real-life processes. In this study, we will be applying a set of ML algorithms to identify the state of the process. The process begins by providing a number of examples (in-control and out-of-control) for training the ML models. Once the models are trained, their performance will be assessed and compared using the probability of correct detection. This study will provide an alternative to the control charts for efficient and robust process monitoring.

### Analysis of model sloppiness: what can it do, and what's next?

Matthew Adams\*, Gloria Monsalvo-Bravo, Sarah Vollert, Imke Botha, and Christopher Drovandi, Queensland University of Technology, Australia.

\* speaker

Abstract: When performing statistical fitting of deterministic models to data, using either frequentist or Bayesian approaches, uncertainty in model parameters is often estimated. However, this uncertainty can have a complex, non-linear structure which has implications for how best to interpret and/or improve the model. This talk discusses “analysis of model sloppiness”, a tool for unveiling this parameter uncertainty structure. Applications of this analysis include: (1) uncovering controlling mechanisms underlying the system being modelled, (2) informing which parameter measurements need to be prioritised in future experiments, (3) guiding strategic model reduction, and (4) diagnostically comparing the accuracy of different model-data fitting algorithms.

### *Some results on the mixed bifractional Brownian motion*

**Soukaina Hadiri**, University IBN Zohr, Morocco.

Abstract: In this work, firstly, we introduce a new Gaussian process as an extension of the well-known bifractional Brownian motion as a linear combination of a finite number of independent bifractional Brownian motions. We have chosen to call this process the mixed bifractional Brownian motion. Secondly, we study some stochastic properties and characteristics of this process: The Holder continuity, the self-similarity, the quadratic variation, the Markov property and the differentiability of the trajectories, the long-range dependence, the stationarity of the increments and the behavior of the noise generated by the increments of this process. We believe that our process can be a possible candidate for models which involve self-similarity, long range dependence and non-stationarity of increments.

### *Dynamics of inertial particle focusing in curved ducts*

**Rahil Valani**, University of Adelaide, Australia.

Abstract: Particles suspended in fluid flow through a curved duct can focus to stable equilibrium positions in the duct cross-section due to the balance of two dominant forces — inertial lift force and secondary drag force. Such particle focusing is exploited in various medical and industrial technologies aimed at separating particles by size. In this talk, I will present results of our numerical investigation of the dynamics of neutrally buoyant particles in fluid flow through curved ducts with rectangular cross-sections. I will show that rich bifurcations take place in the particle equilibria as a function of the duct bend radius. I will also offer insights on how these bifurcations in combination with particle dynamics can be exploited to separate particles of different sizes in circular and spiral ducts.

## Poster abstracts

Since its inception, FMfl has conducted an exhibition of posters displaying the research of current and recent students. There are sessions when exhibitors can casually discuss their work with forum registrants. A special session is allocated in the main presentation room where each poster exhibitor can project and discuss their poster for 5 minutes.

Non-student registrants are given a voting slip to choose their top three posters in order. This helps to inform a poster committee consisting of the organisers and the APCMfl executive. One first prize and a small number of excellent posters are chosen. The values of prizes are limited by donations but we have had generous support from IMI-Kyushu University.

### \*\*Quantitative Stochastic Homogenization of Parabolic Equations with Lower Order Terms

Man **YANG**, Kyushu University

Abstract: I am a doctoral student at Kyushu University. I received my master's degree in mathematics from Kyushu University in 2022 and my bachelor's degree in Mathematics from Shanghai University in 2019. My research area is probability theory and more precisely, I study the stochastic homogenization theory currently. I am also interested in the relationship between stochastic differential equations and homogenization theory.

### \*\*The critical points of the elastic energy among curves pinned at endpoints

Kensuke **YOSHIZAWA**, Kyushu University

Abstract: I am a postdoctoral researcher at Institute of Mathematics for Industry in Kyushu University. I got my Ph.D. at Tohoku University in 2022 under the supervision of Prof. Shinya Okabe. My poster is devoted to the presentation of optimal shapes of ideal elastic rods whose endpoints are fixed (up to zeroth order), thorough the mathematical analysis of the corresponding variational problem.

### Expected number of zeros of Gaussian analytic function with finitely dependent Gaussian coefficients

Kohei **NODA**, Kyushu University

Abstract: I'm a doctoral student in Graduate School of Mathematics for Innovation, Kyushu University. My research area is probability theory and complex analysis related to statistical mechanics of Coulomb systems. In particular, I'm studying zeros process of Gaussian analytic function and random matrix theory under supervisor Professor Tomoyuki Shirai in my doctoral course. Also, I'm supported by WISE program (MEXT) at Kyushu University. This is joint work with Tomoyuki SHIRAI, Kyushu University

*Study on recurrences of random walks on growing  $k$ -ary trees*

Shuma **Kumamoto**

Abstract: Shuma Kumamoto received his B.S. degree in physics and M.S. degree in informatics from Kyushu University in 2020 and 2022, respectively. He is currently a Ph.D. student in mathematics at Kyushu University. His research interest includes random walk. This is joint work with Shuji Kijima, Shiga University and Tomoyuki Shirai, Kyushu University.

*Embedding spherical quandles in pin groups*

Kentaro **YONEMURA**, Kyushu University

Abstract: I am a student in Japan and am interested in knot theory and the quandle, an algebraic system related to knot theory. These days, the quandle class with a manifold structure, called smooth quandle, is my hot topic. I am looking forward to talking with you and discussing the future of mathematics.

*Lyapunov Regularity for Planar Piecewise Expanding Maps*

Kodai **YAMAMOTO**, Kyushu University

Abstract: I am a master course student at Joint Graduate School of Mathematics for Innovation, Kyushu University. My supervisor is Prof. Masato Tsujii at Kyushu University. I mainly study dynamical systems, especially structural stability and hyperbolicity. Recently, I am interested in Lyapunov regularity and have been researching this since I was an undergraduate student.

This is joint work with Yushi NAKANO, Tokai University and Teruhiko SOMA, Tokyo Metropolitan University.

Model Selection in Statistical Learning Theory

Naoki **NAKAMURA**, Kyushu University

Abstract: According to Occam's Razor, we should not assume too much when explaining things. In the context of Statistical learning theory, this means that we should adopt the simplest model. In general, the optimization problem for finding sparse simpler accurate model is NP-hard. Thus, practitioners don't try searching for simpler models. Currently, this problem is abandoned in machine learning. So, it is important that we answer the following practical questions: Can we show that an accurate and simpler model exists?

Multiple Zeta Values and Euler's reflection formula for the Gamma function

Karin **Ikeda**, Kyushu University

Abstract: I am Karin Ikeda, a first year master course student at Kyushu University. My supervisor is Professor Masanobu Kaneko. I am currently studying "multiple zeta values". In particular, I have been able to give a purely algebraic proof of an identity which is closely related to Euler's reflection formula for the gamma function. For more details, please see my slides of the talk. Thank you!

This is joint work with Mika Sakata, Osaka University of Health and Sport Sciences.

\*\*\*Parameterising movement parameters in an onchocerciasis transmission model with a population genetic data

Himal **SHRESTHA**, La Trobe University

Abstract: Himal Shrestha is a PhD student at Nematode and Vector Genomics lab at La Trobe University, Australia. He uses genetic, environmental and epidemiological data to model transmission of a neglected tropical disease called river blindness. Himal is interested in spatial modelling and landscape genetics.

This is joint work with Shannon M. Hedtke, La Trobe University, Karen McCulloch, La Trobe University, Warwick N. Grant, La Trobe University and Rebecca Chisholm, La Trobe University.

\*\*\*Best Poster Award.

\*\*Excellent Poster Award.

## **Papers and Presentations**

Speakers were given the option of publishing abstracts, extended abstracts, projected presentations, or written research papers.

Appended from hereon, are the released presentations and research papers. These have been reviewed under the direction of the editors. We are particularly grateful to the authors.

# Epidemic to immuno-epidemic models of COVID-19

Malay Banerjee<sup>a,1</sup>, Samiran Ghosh<sup>a</sup>, Vitaly Volpert<sup>b,c</sup>

<sup>a</sup> Department of Mathematics & Statistics, IIT Kanpur, Kanpur - 208016, India

<sup>b</sup> Peoples Friendship University of Russia (RUDN University)

6 Miklukho-Maklaya St, 117198 Moscow, Russia

<sup>c</sup> Institut Camille Jordan, UMR 5208 CNRS, University Lyon 1

69622 Villeurbanne, France

## 1 Motivation and developments of mathematical modelling in epidemiology

Mathematical models in epidemiology have played a crucial role in understanding and predicting the spread of various infectious diseases. The models have evolved over time and have become more complex to capture the various factors that influence the spread of diseases. During the COVID-19 pandemic, mathematical models have played a crucial role in understanding the progression of the disease, predicting the impact of interventions, and informing policy decisions.

One of the earliest models was developed by Daniel Bernoulli in the XVIII century. In the early 20th century, Kermack and McKendrick developed a set of differential equations that described the spread of infectious diseases in a closed population [1, 2, 3]. More recent developments in mathematical epidemiology include multi-compartmental models [4, 5], which divide the population into different groups based on their disease status, such as susceptible, infected, and recovered etc. These models can also include factors such as age, gender, and geographic location. Nonlinear transmission rate models account for the fact that the rate of transmission of a disease may change as the number of infected individuals increases [6]. Multi-patch models take into account the fact that infectious diseases can spread across different geographic regions, each with their own population and transmission dynamics [7, 8]. Agent-based models simulate the behavior of individual agents, such as people, and how they interact with each other and their environment [9]. Network models describe the spread of diseases on networks, such as social networks or transportation networks [10, 11]. Overall, mathematical models in epidemiology have provided valuable insights into the spread of infectious diseases and have helped inform public health policies and interventions.

## 2 Multi-compartmental epidemic model

Compartmental epidemic models are the most commonly used mathematical models to describe the spread of an epidemic disease. The use of a compartmental model can help in understanding the

---

<sup>1</sup>Corresponding author.

complex dynamics of the epidemic, as well as the effectiveness of different intervention strategies in controlling the spread of the disease. It can also be used to predict the future trajectory of the epidemic and inform policy decisions on the optimal interventions to use. The very basic nature of an epidemic can be captured by the well known classical SIR-type models, which is mainly based upon three compartments, susceptible ( $S$ ), infected ( $I$ ) and removed ( $R$ ). But, to understand the epidemic progression in more details, more compartments need to be incorporated in the modelling. There are many developments towards the multi compartmental epidemic models [4, 5]. In the context of the COVID-19, the progression of epidemic was not easy to track, and it was necessary to consider all possible compartments that take into account all the complexities of the infection including all stages of the infection, as well as the complexities in the social restrictions (e.g., quarantine, lock downs etc.). In [12], we considered multiple compartments based on the different stages of the disease and the different interventions used to control the spread of the virus. Specifically, we used the following compartments: susceptible ( $S(t)$ ), exposed population who are at the beginning of the incubation period and cannot spread the disease ( $E_1(t)$ ), exposed population who are at the end of the incubation period and can spread the disease ( $E_2(t)$ ), symptomatic ( $I_s(t)$ ), asymptomatic ( $I_a(t)$ ), quarantined ( $Q(t)$ ), hospitalized ( $J(t)$ ), recovered ( $R(t)$ ). Each compartment is connected to others through a set of ordinary differential equations that describe the flow of individuals between the compartments. The model is depicted in the flow chart Fig. 1 and is given in the system (2.1).

$$\frac{dS}{dt} = -\frac{\beta S}{N}(I_s + p_1 I_a + p_2 E_2 + p_3 Q + p_4 J), \quad (2.1a)$$

$$\frac{dE_1}{dt} = \frac{\beta S}{N}(I_s + p_1 I_a + p_2 E_2 + p_3 Q + p_4 J) - \mu E_1, \quad (2.1b)$$

$$\frac{dE_2}{dt} = \mu E_1 - \delta E_2, \quad (2.1c)$$

$$\frac{dI_a}{dt} = (1 - \sigma)\delta E_2 - \eta I_a, \quad (2.1d)$$

$$\frac{dI_s}{dt} = \sigma\delta E_2 - (\rho_1 + \zeta_1 + \zeta_2 + \zeta_3)I_s, \quad (2.1e)$$

$$\frac{dQ}{dt} = \zeta_1 I_s - (\xi_1 + \xi_2)Q, \quad (2.1f)$$

$$\frac{dJ}{dt} = \zeta_3 I_s + \xi_1 Q - (\rho_2 + \nu)J \quad (2.1g)$$

$$\frac{dR}{dt} = \eta I_a + \zeta_2 I_s + \xi_2 Q + \nu J, \quad (2.1h)$$

subjected to non-negative initial conditions  $S(0), E_1(0), E_2(0), I_a(0), I_s(0), Q(0), J(0), R(0) \geq 0$ , and the interpretation of the are given in the paper [12]. The basic reproduction number and controlled reproduction number for the model (2.1), are respectively given by (details are in [12]):

$$\mathcal{R}_0 = \beta \left[ \frac{p_2}{\delta} + \frac{(1 - \sigma)p_1}{\eta} + \frac{\sigma}{\rho_1 + \zeta_2} \right], \quad (2.2)$$

and



$$\mathcal{R}_c = \beta \left[ \frac{p_2}{\delta} + \frac{p_1(1-\sigma)}{\eta} + \frac{\sigma}{\rho_1 + \zeta_1 + \zeta_2 + \zeta_3} + \frac{p_3\zeta_1\sigma}{(\rho_1 + \zeta_1 + \zeta_2 + \zeta_3)(\xi_1 + \xi_2)} \right. \\ \left. + \frac{p_4\sigma\zeta_3}{(\rho_1 + \zeta_1 + \zeta_2 + \zeta_3)(\rho_2 + \nu)} + \frac{p_4\sigma\xi_1\zeta_1}{(\rho_1 + \zeta_1 + \zeta_2 + \zeta_3)(\xi_1 + \xi_2)(\rho_2 + \nu)} \right]. \quad (2.3)$$

During this work, social restriction was the only control measure for COVID-19 worldwide, and the social interactions were completely monitored by the government time to time. For that reason we considered the transmission rate as time dependent and we considered two different choice of transmission rate as shown in Fig. 2 and the corresponding model fitting with the data of Germany is shown in Fig. 3. The fitted parameter values are available in the paper [12]. Interestingly, in Fig. 3 the data are fitted well in the case of continuous  $\beta(t)$  as compared to the discontinuous choice of  $\beta(t)$ . The same model is fitted with data from other countries [12].

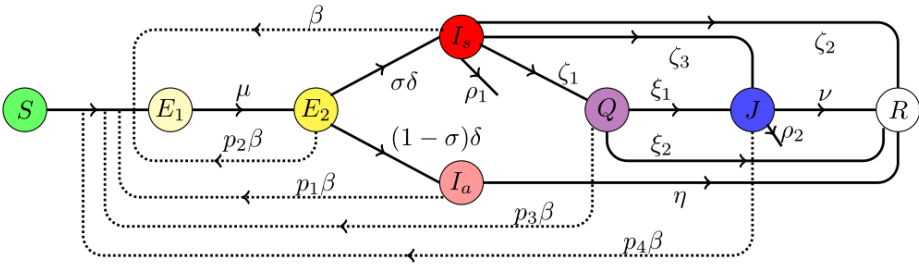


Figure 1: Schematic diagram for the progression of disease described by the model (2.1). Solid arrows represent the transfer from one compartment to another while the dotted line with arrow denote the compartments responsible for disease transmission. Associated rates are mentioned accordingly.

Then we extend our proposed model to a two-group model. We divide the whole population into two groups and this may be a group following the protocols and the other group not following the protocols; or, the grouping can be made by the age of individuals, etc. The extended two group model is given by (details of the variables and parameters are given in [12]):

$$\frac{dS_1}{dt} = -\frac{S_1}{N} [\beta_{11}(I_{s_1} + p_{11}I_{a_1} + p_{12}E_{12}) + \beta_{12}(I_{s_2} + p_{21}I_{a_2} + p_{22}E_{22}) + \beta_Q Q + \beta_J J], \quad (2.4a)$$

$$\frac{dS_2}{dt} = -\frac{S_2}{N} [\beta_{21}(I_{s_1} + p_{31}I_{a_1} + p_{32}E_{12}) + \beta_{22}(I_{s_2} + p_{41}I_{a_2} + p_{42}E_{22}) + \beta_Q Q + \beta_J J], \quad (2.4b)$$

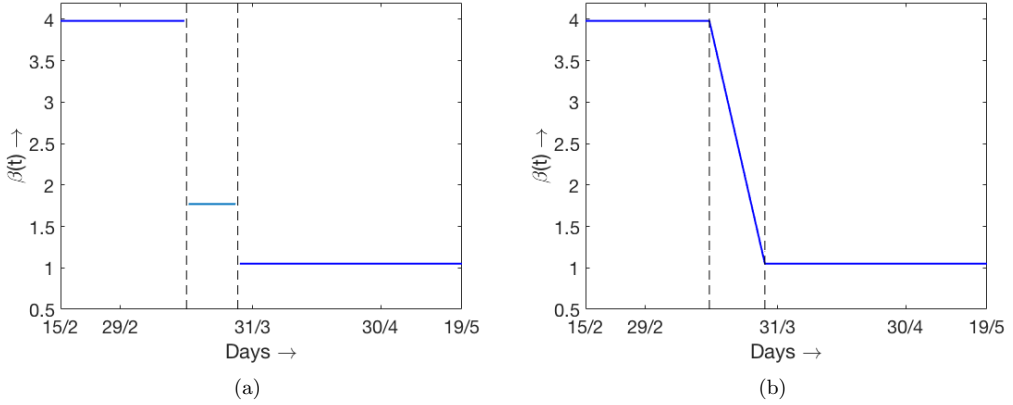


Figure 2: The values of  $\beta$  changing with time  $t$  and used in (a) blue curve in Fig. 3 and (b) magenta curve in Fig. 3 respectively.

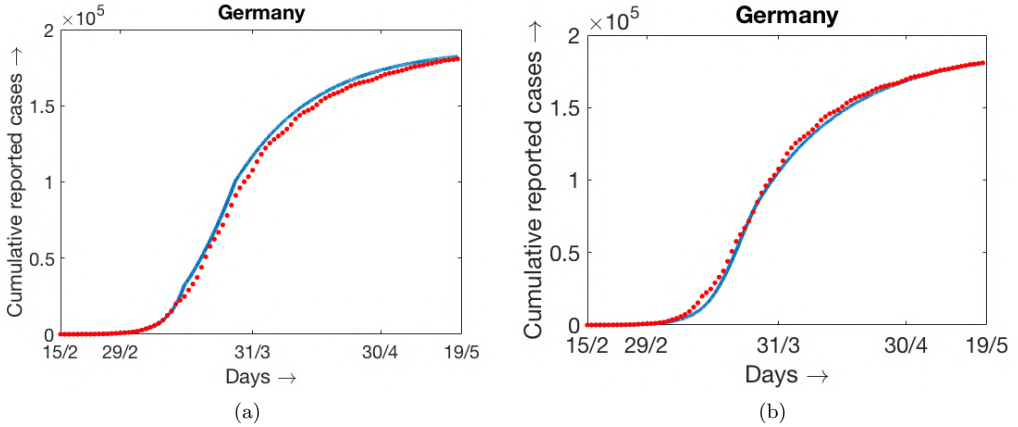


Figure 3: Blue curves indicate the model simulation and the red dotted curves indicate the reported data for cumulative infected population. Simulation results are obtained for two different forms of  $\beta(t)$ , (a) with  $\beta(t)$  as shown in Fig. 2a; (b) with  $\beta(t)$  as shown in Fig. 2b.

$$\frac{dE_{11}}{dt} = \frac{S_1}{N} [\beta_{11}(I_{s_1} + p_{11}I_{a_1} + p_{12}E_{12}) + \beta_{12}(I_{s_2} + p_{21}I_{a_2} + p_{22}E_{22}) + \beta_Q Q + \beta_J J] - \mu_1 E_{11}, \quad (2.4c)$$

$$\frac{dE_{21}}{dt} = \frac{S_2}{N} [\beta_{21}(I_{s_1} + p_{31}I_{a_1} + p_{32}E_{12}) + \beta_{22}(I_{s_2} + p_{41}I_{a_2} + p_{42}E_{22}) + \beta_Q Q + \beta_J J] - \mu_2 E_{21}, \quad (2.4d)$$

$$\frac{dE_{12}}{dt} = \mu_1 E_{11} - \delta_1 E_{12}, \quad (2.4e)$$

$$\frac{dE_{22}}{dt} = \mu_2 E_{21} - \delta_2 E_{22}, \quad (2.4f)$$

$$\frac{dI_{a_1}}{dt} = (1 - \sigma_1)\delta_1 E_{12} - \eta_1 I_{a_1}, \quad (2.4g)$$

$$\frac{dI_{a_2}}{dt} = (1 - \sigma_2)\delta_2 E_{22} - \eta_2 I_{a_2}, \quad (2.4h)$$

$$\frac{dI_{s_1}}{dt} = \sigma_1 \delta_1 E_{12} - (\rho_{11} + \zeta_{11} + \zeta_{12} + \zeta_{13}) I_{s_1}, \quad (2.4i)$$

$$\frac{dI_{s_2}}{dt} = \sigma_2 \delta_2 E_{22} - (\rho_{21} + \zeta_{21} + \zeta_{22} + \zeta_{23}) I_{s_2}, \quad (2.4j)$$

$$\frac{dQ}{dt} = \zeta_{11} I_{s_1} + \zeta_{21} I_{s_2} - (\xi_1 + \xi_2) Q, \quad (2.4k)$$

$$\frac{dJ}{dt} = \zeta_{12} I_{s_1} + \zeta_{22} I_{s_2} + \xi_1 Q - (\rho_2 + \nu) J, \quad (2.4l)$$

$$\frac{dR}{dt} = \eta_1 I_{a_1} + \eta_2 I_{a_2} + \zeta_{13} I_{s_1} + \zeta_{23} I_{s_2} + \xi_2 Q + \nu J. \quad (2.4m)$$

Now considering one group for the people who follow protocols and the other group for people who do not follow protocols, we define the quantity  $K$  (coefficient of social interaction) by  $K = S_1/N$ , where,  $N$  is the total population and  $S_1$  is the total population in the first group. Numerically we observed that  $K$  is very sensitive and a very small increment in  $K$  can lead to a larger epidemic outbreak (see Fig. 4). Using the model (2.4), we fit the trend of larger second wave in Spain in Fig. 5 (the estimated parameter values are given in the paper [13]).

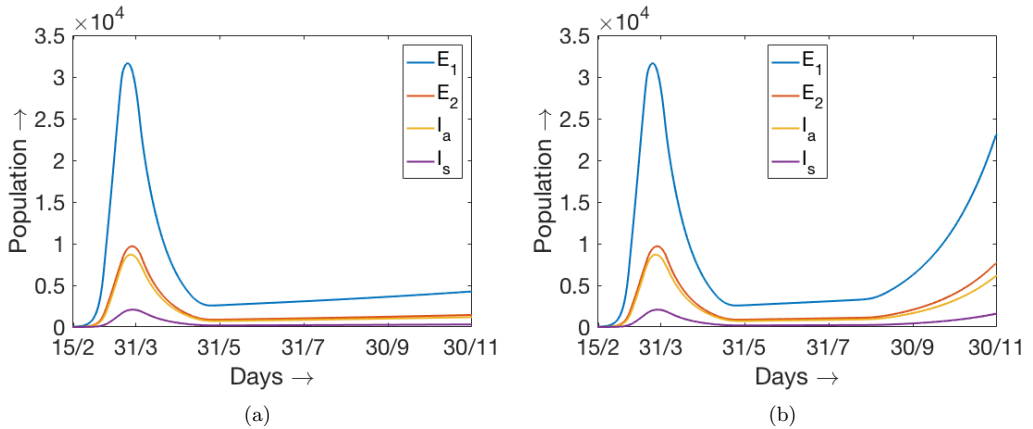


Figure 4: Time evolution of  $E_1$ ,  $E_2$ ,  $I_a$  and  $I_s$  obtained from the numerical simulation of the two models (2.1) and (2.4) from 15th February to 30th November 2020 as described in the text. Two different values of  $K$  are used for the duration 1st September to 30th November, (a)  $K = 0.1$  and (b)  $K = 0.15$ .

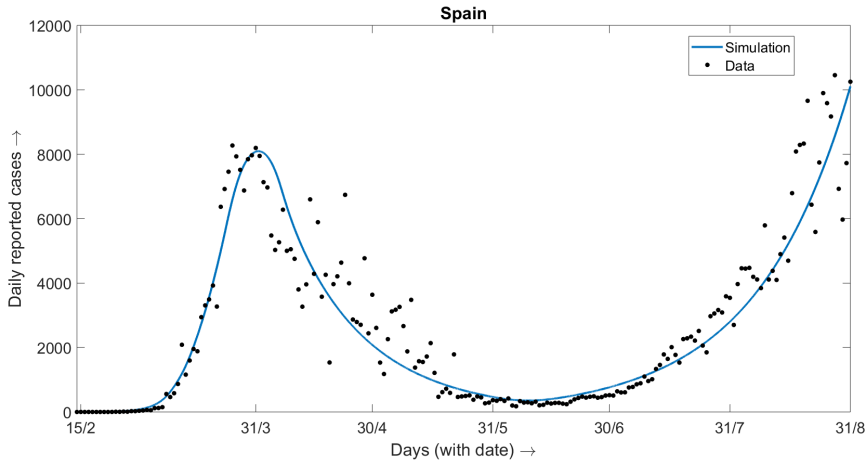


Figure 5: Fitting of the model (2.4) with the data for Spain. The fitted parameter values are available in the paper [13].

### 3 Model with distributed recovery and death rates

While multi-compartmental classical epidemiological models have been successful in predicting and controlling the spread of infectious diseases, there are still limitations and assumptions that need to be taken into account. More advanced models that incorporate more complex and realistic assumptions about the transmission dynamics of diseases can provide more accurate predictions and help in designing effective control strategies. Classical epidemiological models, such as SIR, are systems of ordinary differential equations for the number of susceptible people (S), infected (I) and recovered (R). These models are based on two main assumptions: the first assumption is that the number of new infections is proportional to the number of susceptible and the number of infected (i.e., their product). This assumption, although empirical, can be justified under certain circumstances. The second assumption of the classical epidemiological models, which states that the number of recoveries and deaths are proportional to the total number of infections at a given time, is based on the idea that the duration of infectiousness is fixed and independent of the number of infected individuals. However, this assumption may not hold true in all cases.

Suppose, for definiteness, that the disease lasts, on average, two weeks and the probability of recovery is 95%. Then at time  $t$ ,  $0.95J(t - t_0)$  will recover and  $0.05J(t - t_0)$  will die, where  $t_0 = 14$  days,  $J(t - t_0)$  is the number of people who fell ill two weeks ago. Thus, the number of recovered people at time  $t$  is determined by the number of cases at time  $t - t_0$ , and not by the total number of infected people at time  $t$ . These two values can be very different, especially during periods of exponential growth or decline in the epidemic. Therefore, instead of the usual SIR model, we get a model with a delay, and the magnitude of the delay is determined by the duration of the disease [14]. In [14], we developed the delay model (which is entirely determined by the daily number of new cases  $J(t)$ ), given by:

$$\frac{dS(t)}{dt} = -J(t), \quad (3.5a)$$

$$\frac{dI(t)}{dt} = J(t) - J(t - \tau), \quad (3.5b)$$

$$\frac{dR(t)}{dt} = r_0 J(t - \tau), \quad (3.5c)$$

$$\frac{dD(t)}{dt} = d_0 J(t - \tau). \quad (3.5d)$$

Here  $J(t) = \beta \frac{S(t)}{N} I(t)$  and  $J(t) = 0$  for all  $t < 0$ .

**Determination of disease duration from data:** Using the model (3.5), we can determine the disease duration  $\tau$  from the the epidemiological data for daily number of infected  $J(t)$  and the number of infected individuals  $I(t)$ , using the equation

$$\frac{dI(t)}{dt} = J(t) - J(t - \tau).$$

Let  $I(t)$  have maximum at  $t = t_m$ . Set  $I(t_m) = I_m$ . Then  $J(t_m) = J(t_m - \tau)$ , i.e., the daily number of infected is same at two different time points  $t = t_m$  and  $t = t_m - \tau$ . From the real data of the active infected individuals  $I(t)$ , we can find the day on which the daily number of active cases is maximal and it determines  $t_m$ . From the data of daily reported cases  $J(t)$ , we can observe that  $J(t)$  crosses its maximum at some time before  $t_m$ . Now we have to find the value of  $J(t)$  such that  $J(t_m)$  will be equal to  $J(t_m - \tau)$ , which in turn determines the disease duration  $\tau$ . Hence considering the delay model, using the real data of daily new cases  $J(t)$  and active cases  $I(t)$  around a peak, we can find the disease duration  $\tau$ .

We illustrate this method using the data of  $J(t)$  and  $I(t)$ , taken from *Worldometer* for COVID-19 in Italy. We have collected the daily new reported data  $J(t)$  and active case data  $I(t)$  for Italy from February 21, 2020 to May 31, 2021 (which captures the first three peaks in Italy). To have smoother data, we use 7-days' moving average, the data on  $j$ -th day replaced by the average data from  $(j - 3)$ th day to  $(j + 3)$ th day. As the concerned method is focused on the peaks, the error at the beginning and end of the time interval is immaterial. In Italy, during the first peak (in April 2020), the peak of  $I(t)$  is attained at  $t_m = 51$  (Fig. 6(a)) and the peak of  $J(t)$  is attained before on  $t = 32$  which is less than  $t_m$  (Fig. 6(b)). First we find that  $J(t_m = 51) = 4.17 \times 10^3$  and then find  $J(32) = 4.15 \times 10^3 \approx J(t_m = 51)$ . This implies  $J(t_m - \tau) = J(32)$  and consequently, we can calculate  $\tau = 19$  as the disease duration during the first peak. Similarly, during the second peak (in November 2020) and third peak (in March 2021), we have estimated the disease duration as  $\tau = 20$  days and  $\tau = 14$  days, respectively. Similarly, the value of  $\tau$  is estimated for some other countries which are available in the paper [14].

**Distributed recovery and death rates:** For instance, if the disease has different levels of severity or if there are differences in treatment availability, the duration of the disease may vary among infected individuals. In such cases, the assumption of a fixed duration of the disease may not be appropriate, and more complex models may be required to account for these factors. It is necessary to take into account not only the average duration of the disease, but also the probability

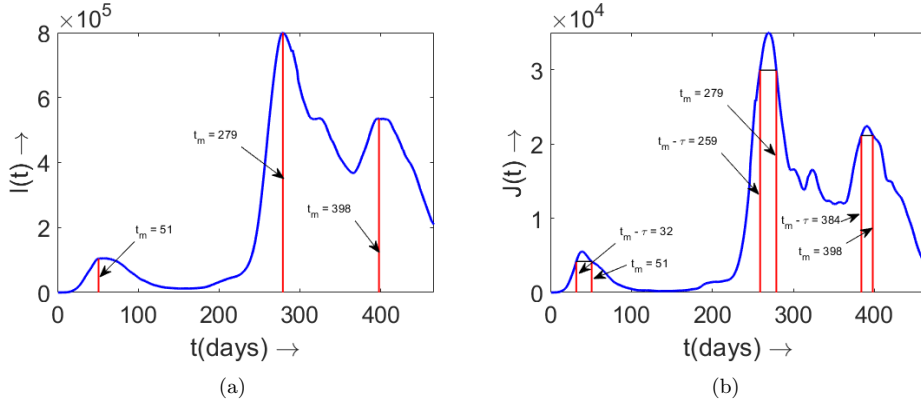


Figure 6: Estimation of the disease duration  $\tau$  using the data around different peaks of COVID-19 in Italy. Time  $t = 0$  corresponds to February 21, 2020. The obtained value of  $\tau$  is 19 days for the first peak, 20 days for the second peak and 14 days for the last peak.

of recovery (or death) depending on the time elapsed after infection. Such data are available in the literature and they allow us to formulate and study a model with distributed parameters [13]. Let  $r(t - \eta)$  and  $d(t - \eta)$  be the recovery and death rates depending on the time-since-infection  $t - \eta$ . Then the number of new recovery and death at time  $t$  are respectively given by:

$$\int_0^t r(t - \eta)J(\eta)d\eta, \quad \int_0^t d(t - \eta)J(\eta)d\eta.$$

Then the model looks like:

$$\frac{dS}{dt} = -J(t), \quad (3.6a)$$

$$\frac{dI}{dt} = J(t) - \int_0^t r(t - \eta)J(\eta)d\eta - \int_0^t d(t - \eta)J(\eta)d\eta, \quad (3.6b)$$

$$\frac{dR}{dt} = \int_0^t r(t - \eta)J(\eta)d\eta, \quad (3.6c)$$

$$\frac{dD}{dt} = \int_0^t d(t - \eta)J(\eta)d\eta, \quad (3.6d)$$

where,  $J(\eta) = \beta S(t)I(t)/N$ , with the initial condition  $S(0) = N$ ,  $I(0) = I_0 > 0$ ,  $R(0) = 0$ ,  $D(0) = 0$  and  $J(t) = 0$  for  $t \leq 0$ .

**Reduction to classical SIR model and delay model:** Our proposed model (3.6a)-(3.6d) can be reduced to some simpler models for some particular and simpler choices of the recovery and death distributions. If we choose:

$$r(t - \eta) = \begin{cases} r_0 & , \quad t - \tau < \eta \leq t \\ 0 & , \quad \eta < t - \tau \end{cases}, \quad d(t - \eta) = \begin{cases} d_0 & , \quad t - \tau < \eta \leq t \\ 0 & , \quad \eta < t - \tau \end{cases}, \quad (3.7)$$

where  $\tau > 0$  is disease duration,  $r_0$  and  $d_0$  are some constants, then the model (3.6a)-(3.6d) reduces to the following classical SIR model

$$\frac{dS}{dt} = -\beta \frac{S}{N} I, \quad (3.8a)$$

$$\frac{dI}{dt} = \beta \frac{S}{N} I - (r_0 + d_0)I, \quad (3.8b)$$

$$\frac{dR}{dt} = r_0 I, \quad \frac{dD}{dt} = d_0 I. \quad (3.8c)$$

On the other hand, if we choose  $r(t-\eta) = r_0\delta(t-\eta-\tau)$ ,  $d(t-\eta) = d_0\delta(t-\eta-\tau)$ , where  $r_0$ ,  $d_0$  are constants,  $r_0 + d_0 = 1$ , and  $\delta$  is the Dirac delta-function, then the model (3.6a)-(3.6d) reduces to the delay model (3.5) discussed earlier.

**Estimation of recovery and death distributions:** It is common to use gamma distribution to model the time it takes for an individual to recover or die from an infectious disease. To estimate the recovery rate function  $r(t)$  and death rate function  $d(t)$  for the COVID-19 epidemic, we fit a gamma distribution to the data for 120 recovered patients and 31 dead individuals in China (see [13] for details).

The gamma distributions fitted to the recovery and death data are respectively given by (see Fig. 7a, Fig. 7b respectively):

$$f_1(t) = \frac{1}{b_1^{a_1}\Gamma(a_1)} t^{a_1-1} e^{-\frac{t}{b_1}}, \quad f_2(t) = \frac{1}{b_2^{a_2}\Gamma(a_2)} t^{a_2-1} e^{-\frac{t}{b_2}},$$

with  $a_1 = 8.06275$ ,  $b_1 = 2.21407$ ,  $a_2 = 6.00014$  and  $b_2 = 2.19887$ .

Let  $p_0$  represents the survival probability, which is estimated to be 0.97 for COVID-19. Then the distributed rate functions  $r(t)$  and  $d(t)$  are given by:

$$r(t) = p_0 f_1(t), \quad d(t) = (1 - p_0) f_2(t).$$

**Model validation:** To validate our model with distributed recovery and death rates, we compare the output (i.e., the sum of daily recoveries and deaths) of the model with the actual data on infected individuals, recoveries, and deaths. Using the estimated functions for  $r(t-\eta)$ ,  $d(t-\eta)$ , and taking the number  $J(t)$  of real data on daily infection, we find the sum of daily recoveries and deaths by the expression (as per the model (3.6a)-(3.6d)):

$$\Sigma(t) = \int_0^t r(t-\eta)J(\eta)d\eta + \int_0^t d(t-\eta)J(\eta)d\eta. \quad (3.9)$$

This  $\Sigma(t)$  is compared with the real data of sum of recoveries and deaths. Fig. 8 shows the result of such comparison for China from 23rd January, 2020 to 15th April, 2020 with the data from *Worldometer* (7-day moving average). Recoveries and deaths can also be determined as a proportion of active cases (as per the SIR model)

$$\sigma(t) = (r_0 + d_0)I(t).$$

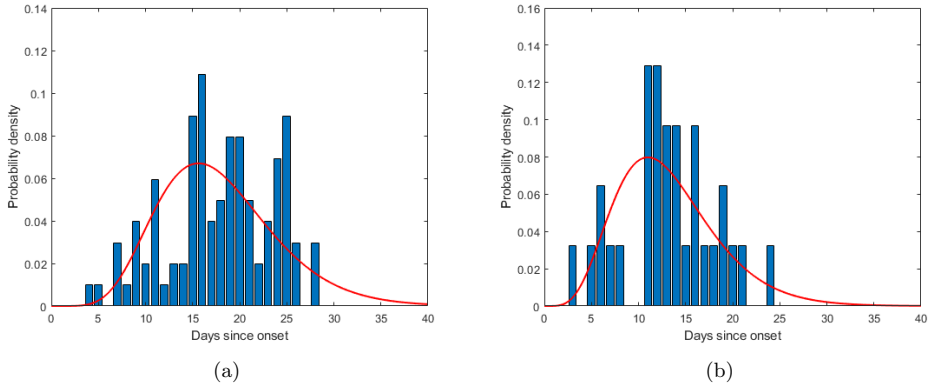


Figure 7: Probability distribution for recovery (a) and death (b) as a function of days-post-infection.

Here  $I(t)$  is taken from the data and  $r_0 + d_0 = 1/16$ . It can be observed from Fig. 8 that the SIR model overestimates the sum of recovered and dead, whereas the model with distributed recovery and death rates fits the real data much better. Validation for other countries are also performed and are given in the paper [13], and in all the cases it is observed that the classical SIR model overestimates the total recovery and death, whereas, our proposed model with distributed recovery and death rates can fit the total recovery and death quite well.

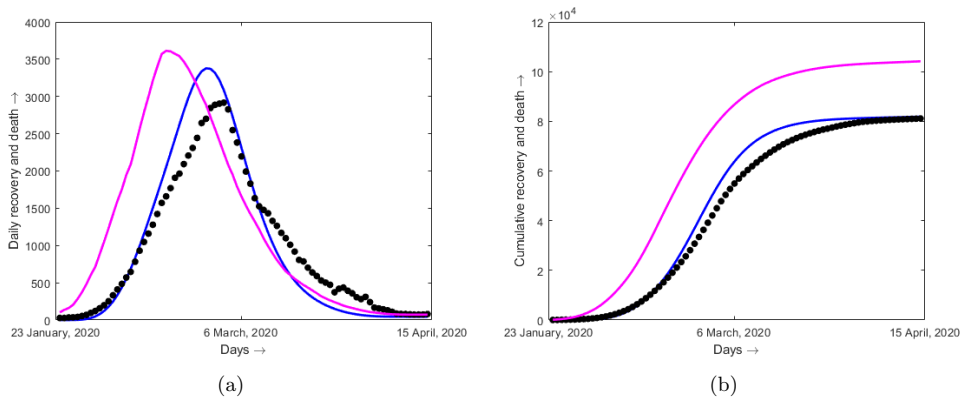


Figure 8: In the left panel, the blue curve shows the number  $\Sigma(t)$  of recovered and dead in the distributed model, the magenta curve corresponds to  $\sigma(t)$  in the SIR model, and the black dots correspond to the 7-day moving average of daily recoveries and death in China. The right panel shows the corresponding cumulative recovery and death.



## 4 Immuno-epidemic model

The dynamics of within-host interactions between the pathogen and the host immune system play a crucial role in the spread of infectious diseases in populations. Understanding the complex interactions between pathogens and the immune system is essential for predicting the course of an outbreak, developing effective treatments and vaccines, and designing public health strategies to control the spread of the disease. The contagiousness of an infection depends on the time after infection and can be assessed through the viral load within the body of an infected individual. Thus, an immune-epidemiological model is obtained, which is a system of integrodifferential equations and most efficiently and adequately describes the interaction of the development of the disease at the individual and population levels. The model proposed in [15] looks like:

$$\frac{dS}{dt} = -\frac{S}{N} \int_0^t \beta(t-\eta)J(\eta)d\eta, \quad (4.10)$$

$$\frac{dI}{dt} = \frac{S}{N} \int_0^t \beta(t-\eta)J(\eta)d\eta - \int_0^t r(t-\eta)J(\eta)d\eta - \int_0^t d(t-\eta)J(\eta)d\eta, \quad (4.11)$$

where  $\beta(t-\eta)$  is the disease transmission rate depending on the time since infection  $t-\eta$ . Here we assume that  $\beta(t-\eta)$  is proportional to the total viral load  $P(t-\eta)$  inside the body at the time since infection  $t-\eta$ .

In addition, taking into account vaccination, as well as the gradual decrease in immunity over time, we obtain more detailed model given by:

$$S(t) = N - (I(t) + D(t) + m(t)N). \quad (4.12)$$

$$\frac{dI}{dt} = \frac{S}{N} \int_0^t \beta(t-\eta)J(\eta)d\eta - \int_0^t r(t-\eta)J(\eta)d\eta - \int_0^t d(t-\eta)J(\eta)d\eta, \quad (4.13)$$

$$\frac{dR}{dt} = \int_0^t r(t-\eta)J(\eta)d\eta, \quad \frac{dD}{dt} = \int_0^t d(t-\eta)J(\eta)d\eta, \quad (4.14)$$

where  $m(t)$  is the level of immunity in the system at time  $t$  that takes into account the immunity waning. The relation of the immunity level  $m(t)$  with the immunity due to vaccination and the acquired immunity can be defined by:

$$m(t) = \frac{1}{N} \left( \int_0^t \phi(t-\eta)V'(\eta)d\eta + \int_0^t \psi(t-\eta)R'(\eta)d\eta \right), \quad (4.15)$$

where  $V(t)$  is the number of vaccinated individuals at time  $t$ , and  $V'(t)$  is the rate of vaccination,  $R'(t)$  is the rate of recovery,  $\phi(t)$  describes how immunity changes with time, and  $\psi(t)$  describes how acquired immunity changes in time. More detailed explanations of the variable  $m(t)$  that captures the effect of multiple vaccine doses and the effectiveness against new emerging strains, are given in the paper [15].

The model (4.12)-(4.14) allows an accurate prediction of the further development of the epidemic (see Fig. 9).

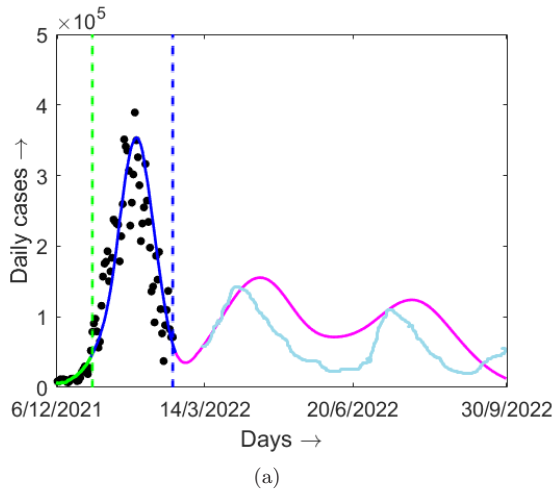


Figure 9: Prediction of daily cases in France. The cyan curve is the real data and magenta curve is the model prediction.

## 5 Age-dependent immuno-epidemic model

The immunological condition of an individual can play a significant role in the progression of a disease. The immune system varies from person to person, and various factors such as age, genetics, underlying health conditions, and lifestyle choices can influence the immune response to an infection. As a result, the susceptibility to a particular disease and its severity can vary significantly among individuals and populations. For example, in case of malaria, although anyone can get infected with malaria, young children are particularly vulnerable due to their underdeveloped immune systems. Similarly, HIV attacks the immune system, and the risk of infection is highest in individuals between the ages of 20 – 45 years who are sexually active and may engage in high-risk behaviors. The recent coronavirus disease (COVID-19) is also an example of how the age group can affect the severity of a disease. According to studies, older adults and individuals with underlying health conditions such as diabetes, hypertension, and cardiovascular disease are more likely to develop severe illness and have a higher mortality rate than younger, healthier individuals. Overall, understanding the immunological condition of individuals and populations is crucial for developing effective prevention and treatment strategies for various infectious diseases.

To take into account these aspects, as a possible extension of the previous models, we consider the age-dependent infectivity, recovery and chance of death due to severe infection. Individual's immune strength plays a crucial role behind the replication of virus particles within the body, development of symptom and also responsible for the time required for recovery. This immunological factors also vary with the age group and as a result the rate of infectivity and the time of recovery varies from one age group to another. In the paper [16], we proposed and analyzed an age-dependent immuno-epidemic model with time dependent recovery and death rates.

Let  $J(x, t)$  denote the number of newly infected individuals of age  $x$  at time  $t$ , while  $S(x, t)$ ,

$I(x, t)$ ,  $R(x, t)$ , and  $D(x, t)$  represent the numbers of susceptible, infected, recovered and dead individuals. Suppose,  $W(x)$  is the total viral load inside an infected individual of age  $x$ . Then we obtain the following age-dependent model:

$$\frac{\partial S(x, t)}{\partial t} = -\alpha(x)S(x, t) \int_0^\infty W(y)I(y, t)dy \quad (\equiv -J(x, t)), \quad (5.16a)$$

$$\begin{aligned} \frac{\partial I(x, t)}{\partial t} &= \alpha(x)S(x, t) \int_0^\infty W(y)I(y, t)dy - \int_0^t r(x, t - \eta)J(x, \eta)d\eta \\ &\quad - \int_0^t d(x, t - \eta)J(x, \eta)d\eta, \end{aligned} \quad (5.16b)$$

$$\frac{\partial R(x, t)}{\partial t} = \int_0^t r(x, t - \eta)J(x, \eta)d\eta, \quad (5.16c)$$

$$\frac{\partial D(x, t)}{\partial t} = \int_0^t d(x, t - \eta)J(x, \eta)d\eta, \quad (5.16d)$$

where  $\alpha(x)$  is the susceptibility function,  $r(x, t - \eta)$  and  $d(x, t - \eta)$  are the recovery and death rates for individuals of age  $x$ , depending on the time-since-infection  $t - \eta$ . The initial conditions are:

$$S(x, 0) = S_0(x) > 0, \quad I(x, 0) = I_0(x) > 0, \quad R(x, 0) = 0 \quad \text{and} \quad D(x, 0) = 0. \quad (5.17)$$

In the context of COVID-19 in New Zealand, we estimated all the age-dependent parameters involved in the model (5.16). The details of the estimated parameters are available in the paper [16]. Using these estimated parameters, the model fitting with the data of Omicron in New Zealand is shown in Fig. 10. Black dots in Fig. 10 represent the real data on daily new cases of Omicron in New Zealand, and the blue curve is the simulation result of the model (5.16). We can observe

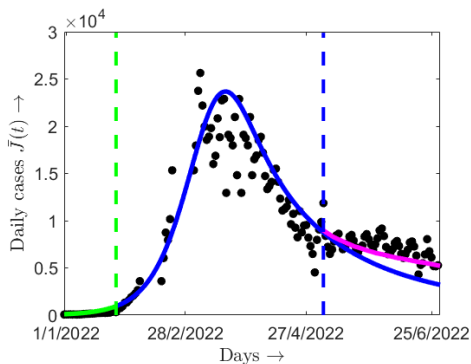


Figure 10: Comparison of new daily cases in modelling and data: model fitting (green), model validation (blue). The black dots are the real data for Omicron in New Zealand. The magenta curve corresponds to modelling with the increased disease transmission rate due to the emergence of new strain in April, 2022.

that modelling results fit quite well the real data up to the end of April, 2022. From the end of

April 2022, new daily cases have some increase instead of further decreasing predicted by the model (Fig. 10). A possible explanation of this discrepancy is related to the emergence of new strain BA.2 (instead of the previous BA.1) for which vaccination can be less efficient due to immune escape or which can have a slightly larger transmission rate. In order to describe this effect, we slightly change the susceptibility function  $\alpha(x)$ , in the beginning of May, 2022. The corresponding result is shown by the magenta curve in Fig. 10, which shows a larger number of daily cases. More details about the fitting are given in [16].

Also, the age-dependent model (5.16) is able to capture the influence the effect of initial age distribution of the susceptible population  $S_0(x)$ , on the epidemic progression. We consider three hypothetical functions representing the age-dependent initial susceptible population distribution  $S_0(x)$ , as shown in Fig. 11(a) by different colors. These cases differ by the proportion of younger age groups with the same total population (integral). Then we perform the numerical simulation of system (5.16a)-(5.16d) and characterize infection progression by the total number of newly infected individuals for all age groups:

$$\bar{J}(t) = \int_0^{100} J(x, t) dx$$

(Fig. 11(b)). We observe that the maximum number of infected and the time to maximum can change significantly depending on the initial age-dependent distribution of the susceptible population. If proportion of the young age groups increases (green curves), then the maximal number of newly infected individuals also increases while the time to maximum decreases. This is related to higher infection transmission by younger population (see Fig. 1 (b) in [16]). In the case of a smaller proportion of these age groups (red curves), the maximal number of new infections decreases and the time to maximum increases. Though it can be difficult to justify this conclusion with the data from different countries because of the influence of numerous other factors (climate, economy, social restrictions) and different methods of data collection, if we restrict this comparison to some neighboring European countries, for which these differences can be less essential, then some tendency can be observed (Fig. 12).

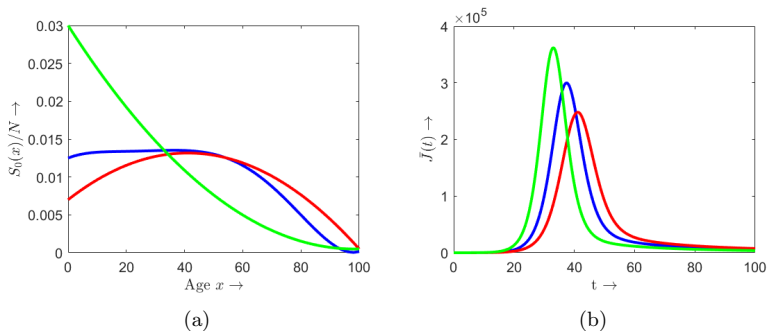


Figure 11: (a) Different age structures  $S_0(x)/N$  of the initial susceptible population with the same total population. (b) Epidemic progression for the three cases in the left panel is shown with the same color.

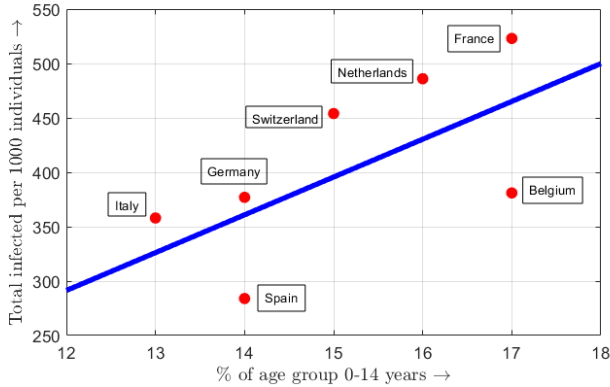


Figure 12: Percentage of the age group 0-14 years (<https://donnees.banquemondiale.org/indicator/SP.POP.0014.T0.ZS>) versus the total number of infection cases from the beginning of epidemic till August 21, 2022 with respect to 1000 people (<https://www.worldometers.info/coronavirus/#countries>).

## 6 Conclusions

Mathematical modelling has played a crucial role in predicting and controlling epidemics, and compartmental models are one of the most commonly used models for this purpose. These models divide the population into different compartments based on their disease status, such as susceptible, infected, and recovered. The models assume that the rate functions, such as the transmission and recovery rates, are constant over time.

However, our observation is that a compartmental model developed entirely in terms of daily new cases, with distributed rate functions depending upon the time since infection, can describe the epidemic progression more effectively, which is an exciting finding. This type of model considers the heterogeneity of immune response in the population and the initial demographic structure of a population, which can significantly influence the epidemic progression. One challenge in developing these models with distributed rate functions is that they require detailed immunological data for a particular infection, which may need to be more readily available. However, as we mentioned, this type of data is available for some countries, which can make it possible to develop more detailed and accurate models.

Our study highlights the importance of considering the heterogeneity of immune response and demographic factors when developing mathematical models to predict and control epidemics. These findings can help public health officials make more informed decisions and take appropriate actions to mitigate the spread of infectious diseases.

## References

- [1] William Ogilvy Kermack and Anderson G McKendrick. A contribution to the mathematical theory of epidemics. *Proc Math Phys Eng Sci*, 115(772):700–721, 1927.
- [2] William Ogilvy Kermack and Anderson G McKendrick. Contributions to the mathematical theory of epidemics. ii.—the problem of endemicity. *Proc Math Phys Eng Sci*, 138(834):55–83, 1932.
- [3] William Ogilvy Kermack and Anderson G McKendrick. Contributions to the mathematical theory of epidemics. iii.—further studies of the problem of endemicity. *Proc. Math. Phys. Eng. Sci.*, 141(843):94–122, 1933.
- [4] Maia Martcheva. *An introduction to mathematical epidemiology*, volume 61. Springer, 2015.
- [5] Fred Brauer, Carlos Castillo-Chavez, and Zhilan Feng. *Mathematical models in epidemiology*, volume 32. Springer, 2019.
- [6] Herbert W Hethcote and P Van den Driessche. Some epidemiological models with nonlinear incidence. *J Math Biol*, 29(3):271–287, 1991.
- [7] Derdei Bichara and Abderrahman Iggidr. Multi-patch and multi-group epidemic models: a new framework. *J Math Biol*, 77(1):107–134, 2018.
- [8] Daozhou Gao and Shigui Ruan. A multipatch malaria model with logistic growth populations. *SIAM J Appl Math*, 72(3):819–841, 2012.
- [9] Rebecca J Rockett, Alicia Arnott, Connie Lam, Rosemarie Sadsad, Verlaine Timms, Karen-Ann Gray, John-Sebastian Eden, Sheryl Chang, Mailie Gall, Jenny Draper, et al. Revealing covid-19 transmission in australia by sars-cov-2 genome sequencing and agent-based modeling. *Nat Med*, 26(9):1398–1404, 2020.
- [10] Shweta Bansal, Bryan T Grenfell, and Lauren Ancel Meyers. When individual behaviour matters: homogeneous and network models in epidemiology. *J R Soc Interface*, 4(16):879–891, 2007.
- [11] Jennifer Lindquist, Junling Ma, P Van den Driessche, and Frederick H Willeboordse. Effective degree network disease models. *J Math Biol*, 62(2):143–164, 2011.
- [12] Swarnali Sharma, Vitaly Volpert, and Malay Banerjee. Extended seiqr type model for covid-19 epidemic and data analysis. *Mathematical Biosciences and Engineering*, 17(6):7562–7604, 2020.
- [13] Samiran Ghosh, Vitaly Volpert, and Malay Banerjee. An epidemic model with time-distributed recovery and death rates. *Bulletin of Mathematical Biology*, 84(8):78, 2022.
- [14] Samiran Ghosh, Vitaly Volpert, and Malay Banerjee. An epidemic model with time delay determined by the disease duration. *Mathematics*, 10(15):2561, 2022.

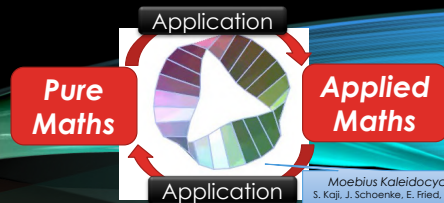
- [15] Samiran Ghosh, Malay Banerjee, and Vitaly Volpert. Immuno-epidemiological model-based prediction of further covid-19 epidemic outbreaks due to immunity waning. *Mathematical Modelling of Natural Phenomena*, 17:9, 2022.
- [16] Samiran Ghosh, Vitaly Volpert, and Malay Banerjee. An age-dependent immuno-epidemiological model with distributed recovery and death rates. *Journal of Mathematical Biology*, 86(2):21, 2023.

# HOMOLOGICAL FEATURES OF 3D MEDICAL IMAGES

Forum "Math-for-Industry" 2022  
 -Mathematics of Public Health and Sustainability-  
 16 November 2022, La Trobe University  
 Shizuo KAJI (IMI, Kyushu U.)

*Physics*  
*Maths Integrates*  
*Medicine*

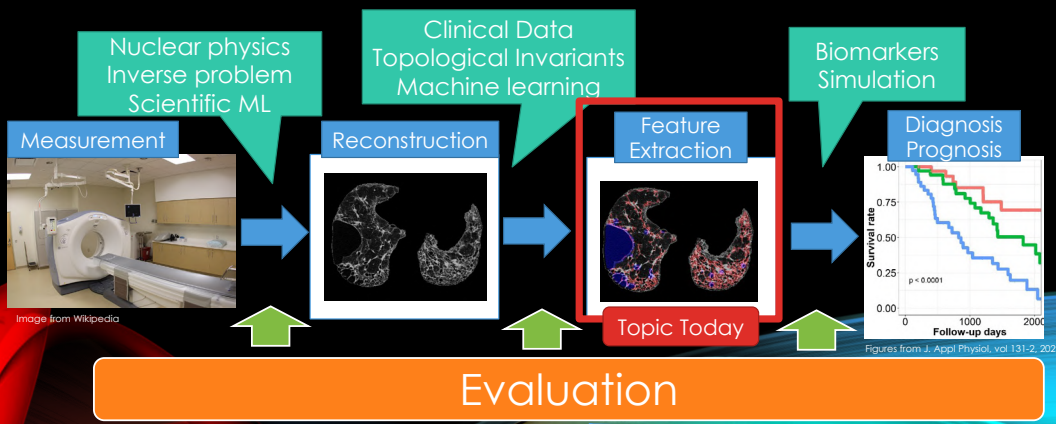
**Applied-Applied  
 Mathematics**



Maebius Kaleidocycle, 2018  
 S. Kaji, J. Schoenke, E. Friedl, M. Grunwald

## Kyoto U. hospital & Tokyo U. hospital & Kyushu U. IMI

A collaborative project on various aspects of medical imaging



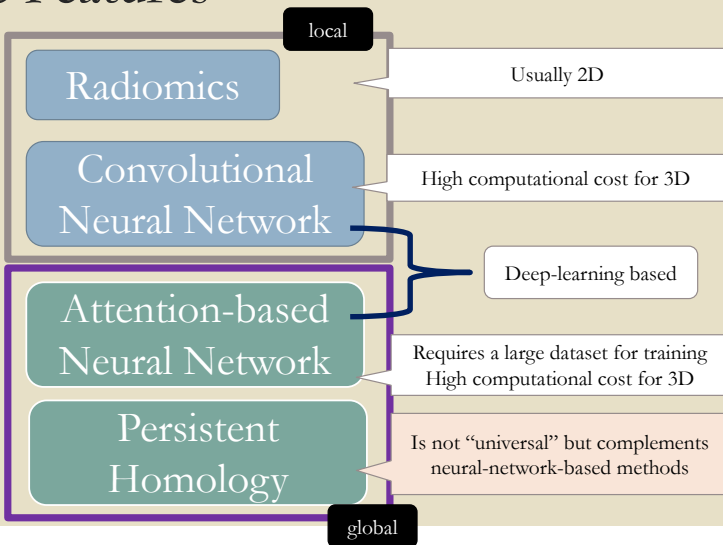
Developing clinically useful methods often leads to theoretically interesting questions



# Deep Learning vs Topology

(Image are taken from Wikipedia unless otherwise stated)

## Medical Image Features



## Deep Neural Nets are shortsighted



(a) Texture image  
 81.4% **Indian elephant**  
 10.3% indri  
 8.2% black swan



(b) Content image  
 71.1% **tabby cat**  
 17.3% grey fox  
 3.3% Siamese cat



(c) Texture-shape cue conflict  
 63.9% **Indian elephant**  
 26.4% indri  
 9.6% black swan

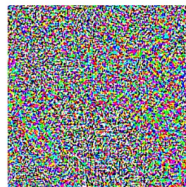
*ImageNet-trained CNNs are biased towards texture; increasing shape bias improves accuracy and robustness*  
 Geirhos et al. 2019

## Deep Neural Nets are shortsighted



$x$   
 "panda"  
 57.7% confidence

+ .007 ×



$\text{sign}(\nabla_x J(\theta, x, y))$   
 "nematode"  
 8.2% confidence

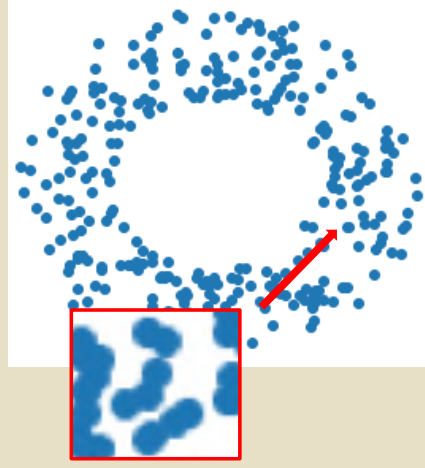
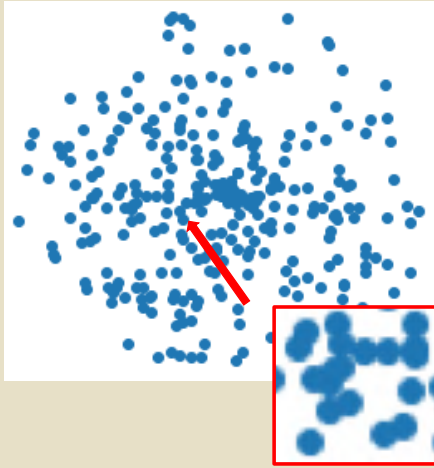
=



$x + \epsilon \text{sign}(\nabla_x J(\theta, x, y))$   
 "gibbon"  
 99.3% confidence

*Explaining and Harnessing Adversarial Examples, Goodfellow et al. 2014*

Deep Nets are too sensitive to local information.  
 Why? Because convolution is a local operation.  
 => Use Topology to capture global characteristic



They look similar locally,  
 but we see a clear difference if we zoom out  
 c.f. Manifolds are locally all Euclidean and homology distinguishes the global topology of them.

Human is good at

- Rough estimation
- Panoramic view
- Discovering rules/**invariance** from a small number of examples
- **Explaining** the reason

DL is good at

- Precise observation
- Memorising/imitating examples
- Processing huge data
- Accurate operation

Topological Data Analysis (TDA)

Deep Learning (DL)

Data-driven local

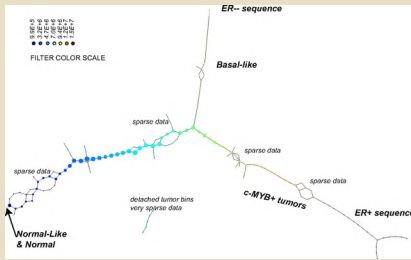
Maths-based global

complementary

Background

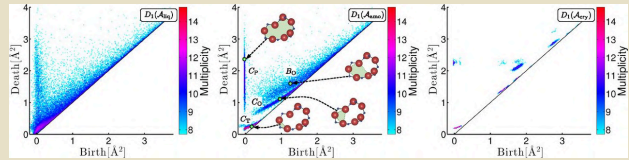
- DL achieves high performance but has some weakness
- TDA has been proven effective in capturing data features that conventional techniques have missed

# Notable applications of TDA (outside image analysis)



Gene expression data of cells

M. Nicholau et al. PNAS 2011  
Topology based data analysis identifies a subgroup of breast cancers with a unique mutational profile and excellent survival.

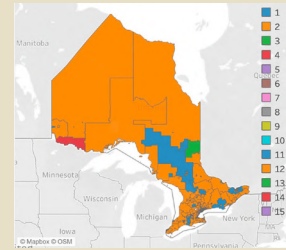


Liquid-Amorphous-Crystalline states of silica

Y. Hiraoka et al. PNAS 2016  
Hierarchical structures of amorphous solids are characterised by persistent homology.

Topological clustering of multilayer networks

M. Yuvaraj et al. PNAS 2021  
Home insurance patterns are detected.



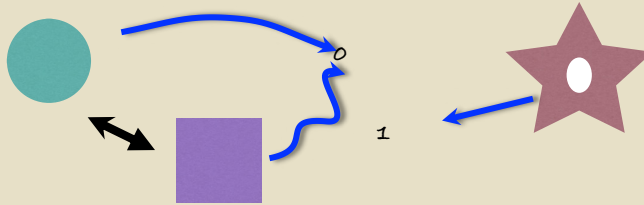
## Tools from Topology

### Homology

## Topological Invariants: Space $\rightarrow$ “Number”

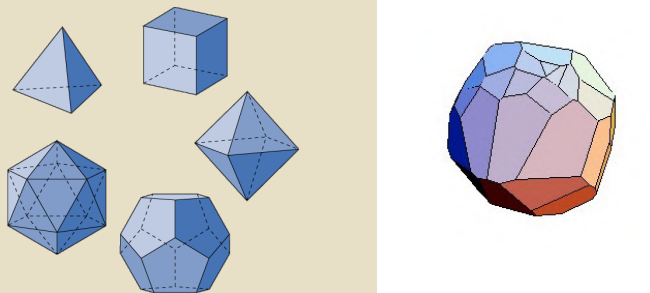
- encode features into “numbers”
- stay unchanged under continuous perturbation
- are computable

It can mean some algebraic structure  
such as group and vector space



## Topological Invariants of a space Ex. Euler's polyhedral theorem

$$\text{Number of F:faces} - \text{E:edges} + \text{V:vertices} = 2$$

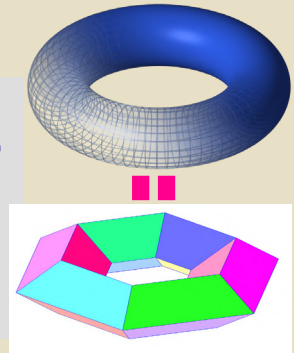
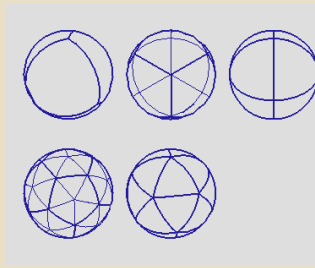


All are topologically a sphere





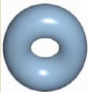

# Topological Invariants of a space

## Sphere vs Doughnuts

- $F-E+V$  is a topological invariant called the **Euler characteristic**
- Sphere **2**
- Sphere with a hole **1**
- Doughnuts **0**



# Homology is a generalisation of Euler characteristic

						
$b_0$ connected component	1	1	1	1	1	1
$b_1$ hole	0	0	1	2	2	0
$b_2$ cavity	0	0	0	1	1	1
Euler characteristic $b_0 - b_1 + b_2$	1	1	0	0	0	2

Example: is the bunny watertight?

**X:** bunny

**b<sub>i</sub>:** i-th betti number

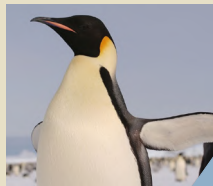
- **b<sub>0</sub>(X)=1**  
(connected)
- **b<sub>1</sub>(X)=7**  
(there are 8 loops)
- **b<sub>2</sub>(X)=0**  
no cavity (not watertight)



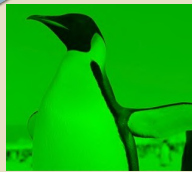
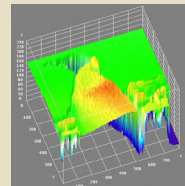
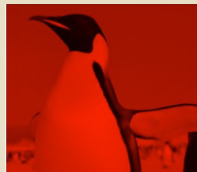
(Stanford bunny)

## Topological Features of Image

# Image = Function on a square or a cube



wikipedia



A colour image is represented by a triple of real-valued functions (R,G,B)

We focus on a monochrome image  
 $f: X \rightarrow R \quad (X \subset R^n, n = 2,3)$

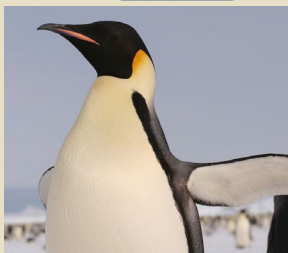
An image processing/analysis method is an operation on the space of functions

# Image processing = Operation on functions

image

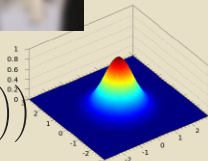


image



Example:  
Convolution

Example of a kernel:  
 $h(x, y) = c \exp\left(-\left(\frac{x^2}{2\sigma_x^2} + \frac{y^2}{2\sigma_y^2}\right)\right)$



$$h * f(x, y) = \int \int h(x - s, y - t) f(s, t) ds dt$$



# Topological Image Analysis

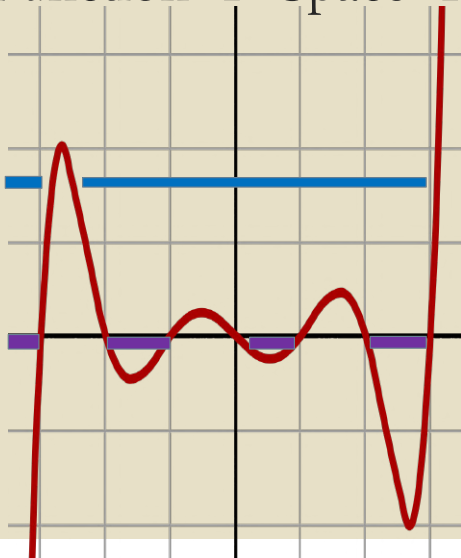
Function  $\rightarrow$  Space  $\rightarrow$  “Numbers”



topological space  $X$   
function  $f: X \rightarrow \mathbb{R}$

Each threshold value  
gives rise to  
the **sub-level set**  
 $\{x \mid f(x) < a\}$

Function  $\rightarrow$  Space  $\rightarrow$  “Numbers”



For each threshold  $a$ , we have a space  
 $X(f,a) := \{x \mid f(x) < a\}$

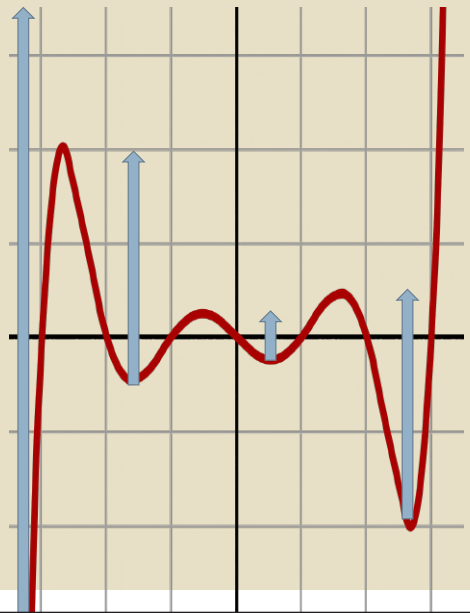
We can compute topological invariants  
of  $X(f,a)$  to obtain image features

Q: How to choose a threshold?

A: We do not choose. Use them all!

## Persistent homology (PH)

- Extension of homology defined for functions over topological spaces
- For each topological feature(cycle), the threshold values with which it was born and destroyed are recorded



Remark:

We can also view PH as a “**continuous relaxation**” of homology.  
Homology is a discrete quantity that is sometimes problematic.  
(e.g, homology can change abruptly with small variation in the input)

## Persistent homology (formal definition)

Increasing sequence of spaces  $\emptyset \subset X_{t_1} \subset X_{t_2} \subset \dots \subset X_{t_m} = X$

Apply the homology functor  
(with coefficients in  $\mathbb{F}_2$ )

PH is by definition the sequence of  $\mathbb{F}_2$ -vector spaces (for each dimension  $d$ )

$$H_d(\emptyset) \rightarrow \dots \rightarrow H_d(X_{t_{i-1}}) \rightarrow H_d(X_{t_i}) \rightarrow \dots \rightarrow H_d(X_{t_{j-1}}) \rightarrow H_d(X_{t_j}) \rightarrow \dots \rightarrow H_d(X)$$

The sequence decomposes into the direct sum of “intervals” having the form

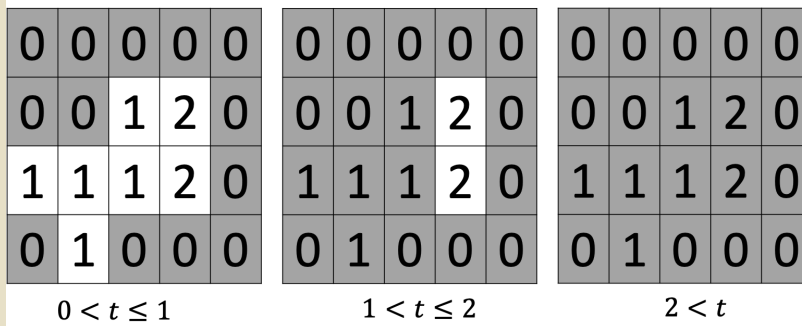
$$0 \longrightarrow \dots \longrightarrow 0 \longrightarrow \mathbb{F}_2 \xrightarrow{\text{Id}} \dots \xrightarrow{\text{Id}} \mathbb{F}_2 \longrightarrow 0 \longrightarrow \dots \longrightarrow 0$$

which correspond to cycles

(= generators = topological features)

represented by  $(t_i, t_j) \in \mathbb{R}^2$

## 2D Example



$\text{PH}_0 = \{(0,1], (0,\infty)\}$  (islands)

$\text{PH}_1 = \{(1,2]\}$  (holes)

A cycle of the form  $(a,b]$  is represented by a point  $(a, b) \in \mathbb{R}^2$

## Software for Persistent Homology computation for image and volumetric data

- **Cubical Ripser** (K-Sudo-Ahara, 2021)
  - Open-source (MIT license), Available at my github repository [https://github.com/shizuo-kaji/CubicalRipser\\_3dim/](https://github.com/shizuo-kaji/CubicalRipser_3dim/)
  - Capable of computing persistent homology of time-series, image, volumetric data
  - One of the fastest program for computing persistent homology of cubical complexes
  - The only program which can handle two major constructions of cubical complexes
  - Python binding that works nicely with Numpy (including DICOM converters)

2D or 3D image

Sublevel sets by sweeping thresholds



Persistent homology

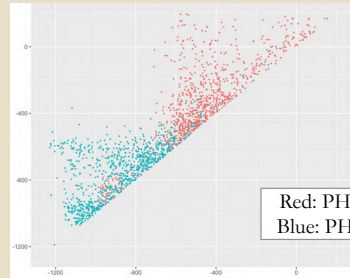
# PH as a feature

Input: Function (over a topological space)



2D, 3D

Output : Persistence Diagram (finite points in  $\mathbb{R}^2$ )



Red:  $PH_0$  cycles  
Blue:  $PH_1$  cycles

Hard to deal with by ML techniques  
=> Convert PH into an additional channel to the original image

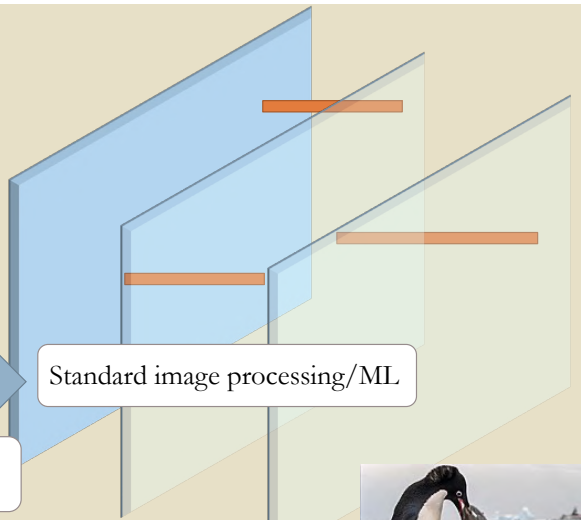
# PH annotated image

For each pixel, assign a histogram of birth and lifetime of cycles which are born at the pixel.  
We obtain an image with additional channels which carries PH information



global information is encoded as the "colour" of pixels

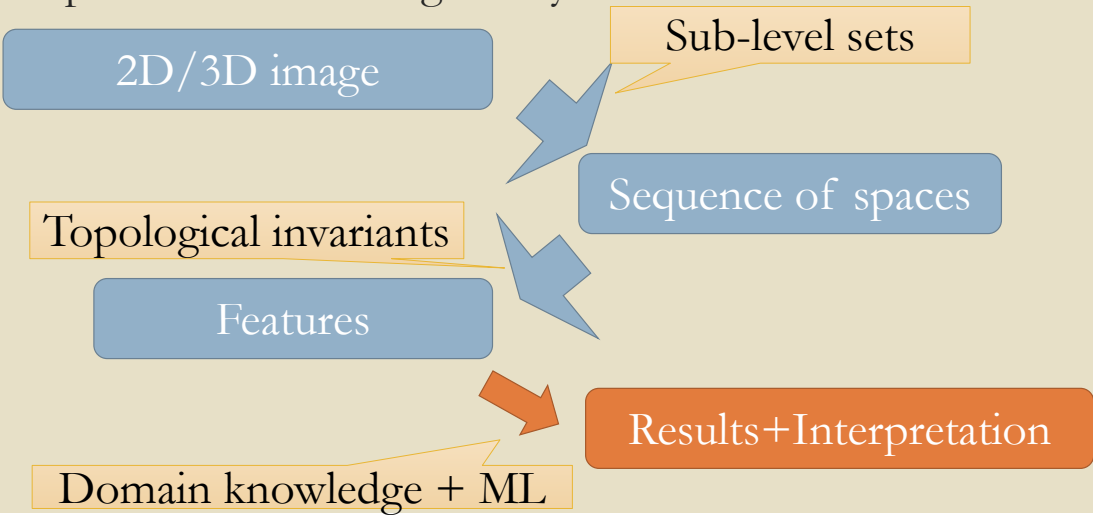
Standard image processing/ML



PH processes the original image so that local and global topological features are encoded as pixel values.  
PH annotated images can be fed to/digested by conventional ML techniques!



## Pipeline of TDA image analysis



## How to cook PH features?

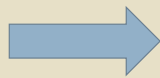
If your priority is in

Performance



Data-driven  
(use DL)

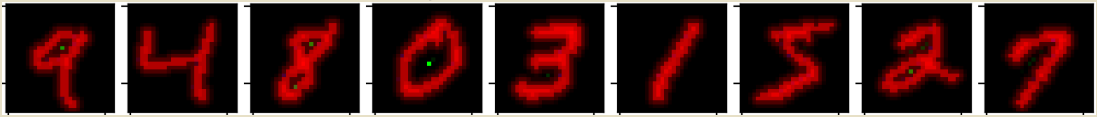
Interpretability



Feature engineering  
using domain knowledge

# Example I : MNIST Digit classification

Green dots are 1-cycles of PH annotation



The MNIST Dataset  
 60k(train)+10k(test) images  
 10 classes (0,1,...,9)  
 28x28 black-and-white images  
 Accuracy of SoTA is over 99.8%

Too easy as a benchmark

We use “Reduced MNIST”

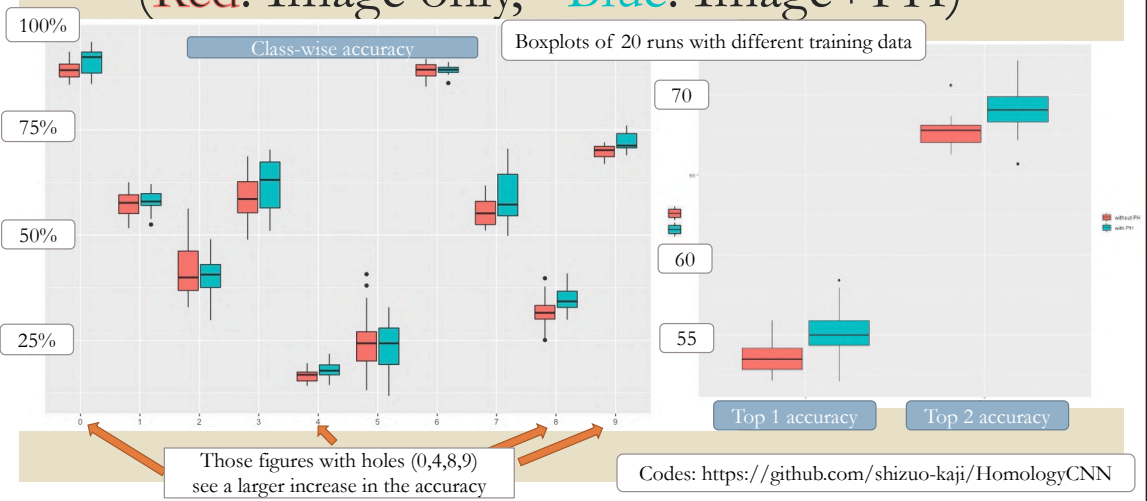
Only 10 training images  
 (one image per class,  
 “small data!”)



Technical remark:

We apply the distance transform before computing PH so that cycles in the image need not be perfectly closed. Also, in this way the size of the loop is encoded as the lifetime. We can do various pre-processing to the original image before taking the sub-level sets.

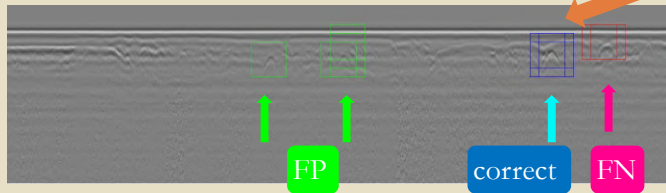
## Reduced MNIST classification results (Red: Image only, Blue: Image+PH)



## Example II: Sinkhole detection in ground penetrating radar image (with S. Choi, T. Kim)

### Difficulty

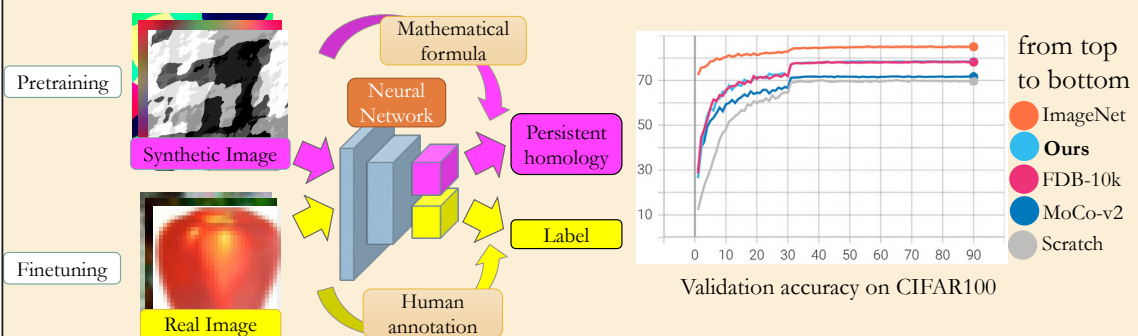
1. No big data (data acquisition is costly)
2. False Negative (overlook) is critical



Collapse in Hakata  
(Nov. 2016 Asahi digital)

We achieved a comparable performance with human experts with only **40 labelled volumes**

## Example III: Training DL models without real data (with Y. Watanabe)



Neural Networks can learn to see from **totally synthetic data by solving a maths problem!**

codes: <https://github.com/shizuo-kaji/PretrainCNNwithNoData>

# Application

## CT analysis of lung disease

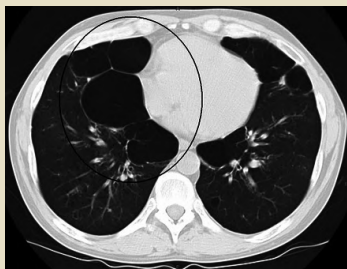
joint with N. Tanabe (Kyoto University Hospital) et al.  
(all figures are from J. Appl Physiol, vol 131-2, 2021 (CC-BY 4.0) unless indicated otherwise)

Goal: diagnose COPD and IPF from CT  
and identify their lesion

(images from Wikipedia)



Healthy



COPD



IPF

COPD: Chronic obstructive pulmonary disease is the third leading cause of death (WHO 2019)

IPF: Idiopathic pulmonary fibrosis is a progressive and irreversible disease

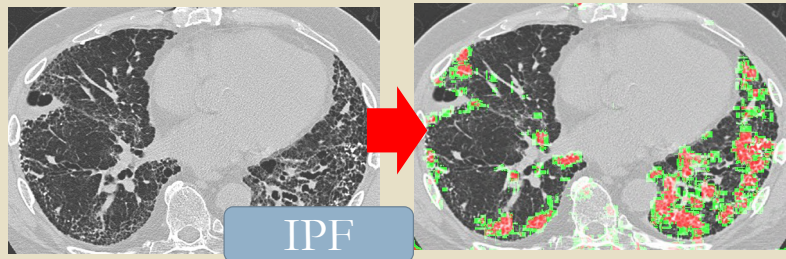
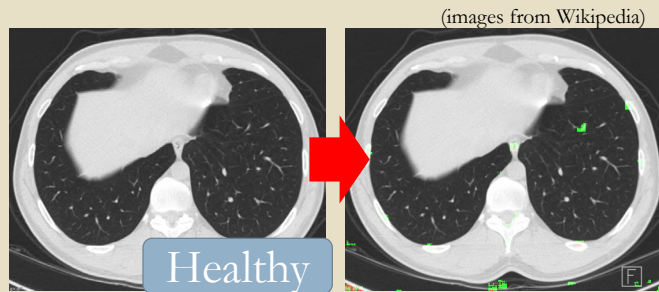


## More concretely

Given a CT volume, **classify** the subject into Healthy, IPF, COPD. Moreover, explain the decision by **localising** lesions that are responsible for the condition.

Available data for each subject

- CT volume
- Label by a medical doctor  
n=45 (training) + 90 (validation)

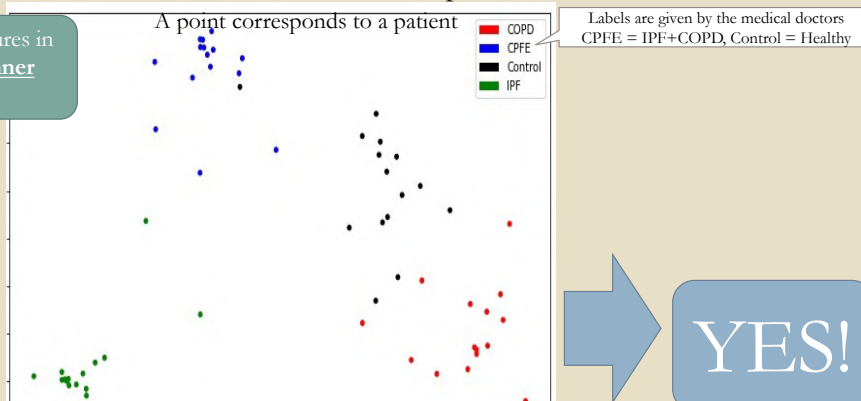


## Preliminary test : Is PH a suitable choice?

We have defined an image feature based on PH.

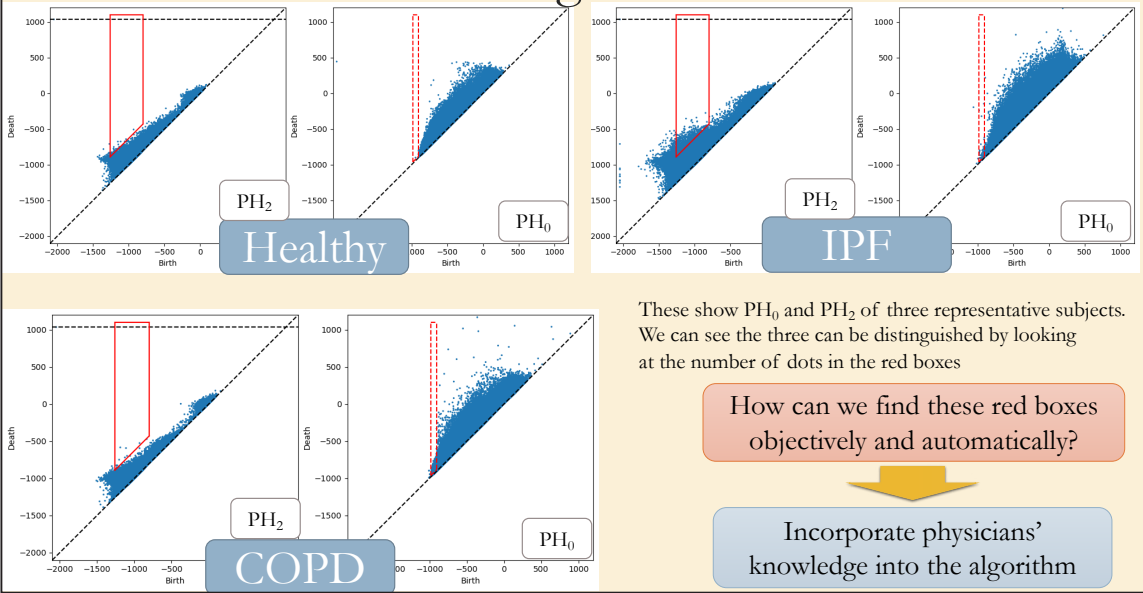
But is it relevant to our current problem?

Let's visualise PH features in an **unsupervised manner** just using CT volumes.



Clear separation of colours even without using the labels

# Difference in PH among conditions

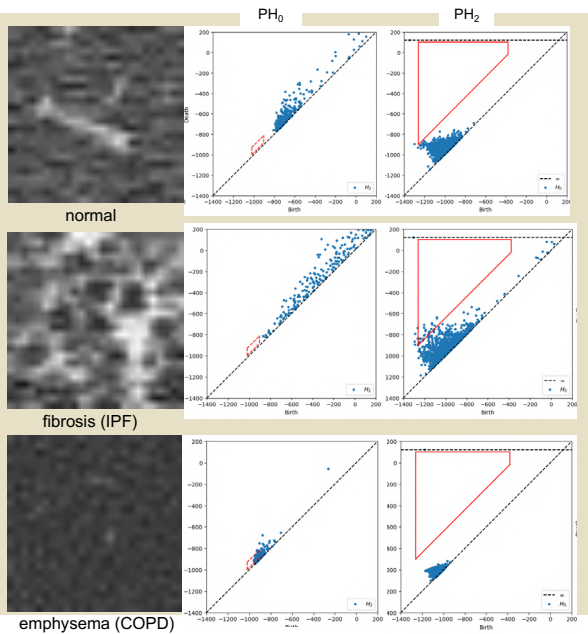


How can we incorporate the experts' knowledge?

Extract doctors' knowledge in terms of ROI selection (ROI = Region of Interest)

Medical doctors select patches typical to the disease and we use them as "training data"

ROIs provide more fine-grained and localised information than the label by telling "what to look at"



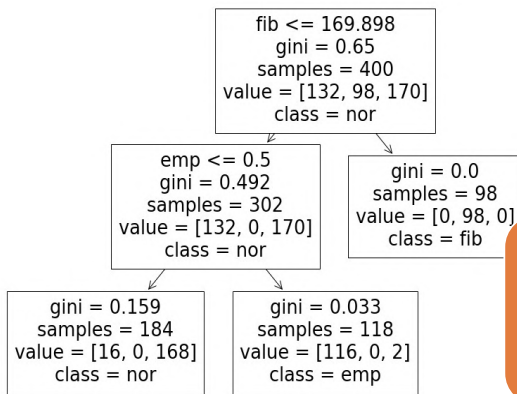
## Learning shallow decision trees from selected ROIs

ML algorithm



Domain knowledge

Note: we need only four parameters to define a box!



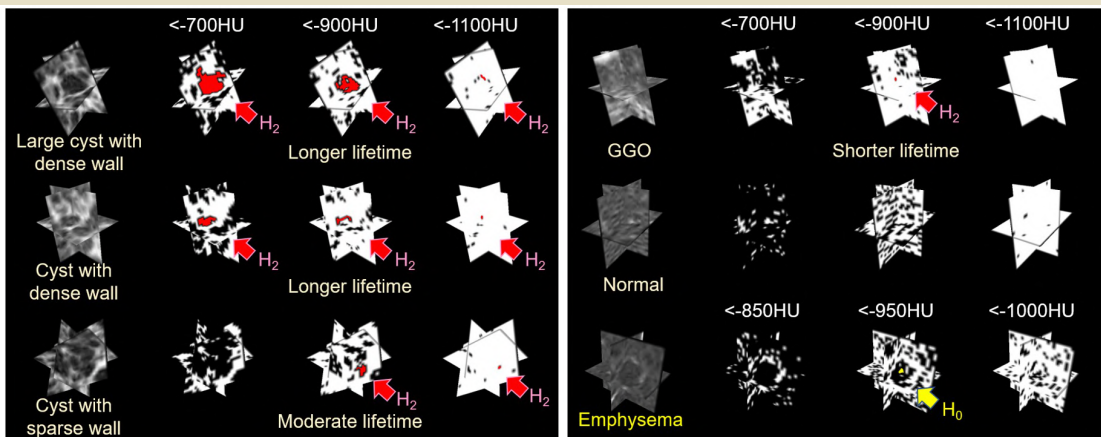
The characteristic cycles (red boxes) in the previous slide are determined by the classification accuracy of the ROIs.

Visual cue  
(physician friendly)



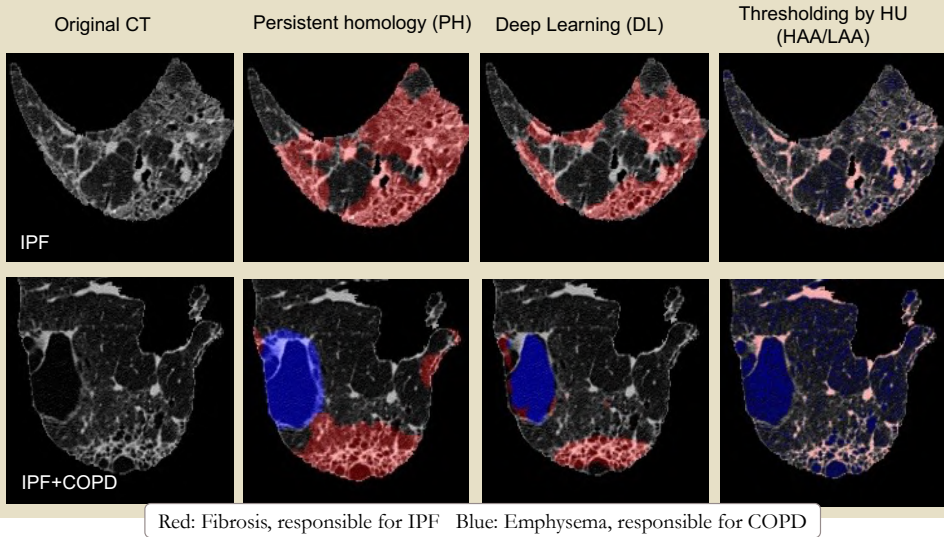
Numerical  
features in terms  
of PH  
(computer friendly)

## The characteristic cycles are interpretable

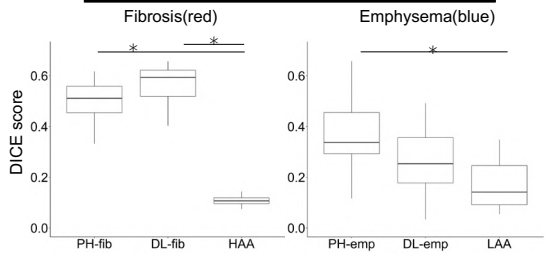


Physicians work in the image domain. Mathematicians work in the PH domain.  
Physicians have strong sense with visuals while mathematicians are more comfortable with “numbers”.  
So it is a good idea to go back and forth frequently between these two domains.

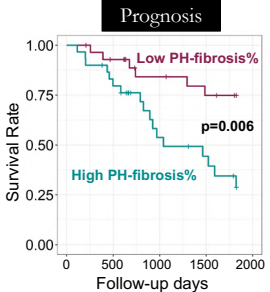
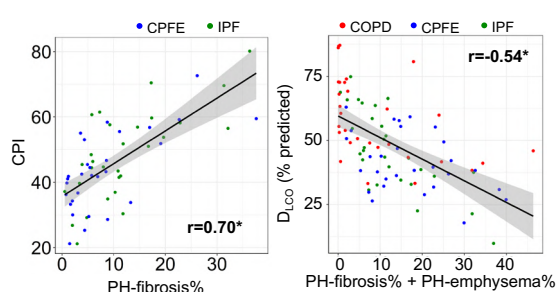
# Comparison of different segmentation methods



## Segmentation agreement with medical doctors



## Clinical merit

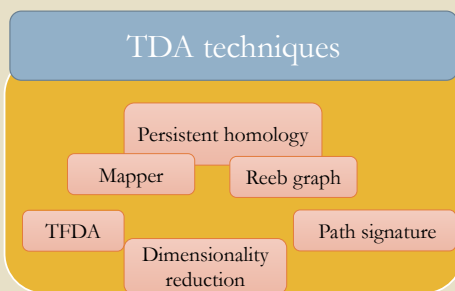


## Correlation with lung function

## Summary

- Topology (persistent homology) provides a way to extract image/volume features that are not easy to obtain by conventional method
- Global and invariant features encoded by persistent homology (PH) complement those (mainly local) features obtained by deep learning (DL) and can be used in conjunction to boost performance
- PH-based image analysis has some advantages:
  - robust and easily **transferable** ( $\Leftrightarrow$  DL needs re-training)
  - **interpretable** ( $\Leftrightarrow$  DL is often a blackbox)
  - 3D ( $\Leftrightarrow$  many conventional analyses are 2D slice-based)

## FAQ on Topological Data Analysis (TDA)



- Performance?
  - It depends on the problems as with other tools.
- Computational cost?
  - Computing PH of a 512x512x512 volume takes 5-10 mins.
- Amount of data necessary?
  - Usually much smaller than DL
- Easy to use?
  - There are many 'meta hyper-parameters' to choose. Also, input and outputs are not vectors.
- Explainability?
  - If you can interpret homology in the target domain

To sum up: TDA is in many ways different from conventional techniques. It is a good idea to keep it in your toolbox.

TDA Tutorial with Google Colab:

<https://github.com/shizuo-kaji/TutorialTopologicalDataAnalysis>

Interactive demo on various techniques of Topological Data Analysis (TDA) including persistent homology

# A Geometrical Structure for Predator-Avoidance Fish Schooling

Aditya Dewanto Hartono<sup>1</sup>, Tôn Việt Tạ<sup>1,\*</sup>, and Linh Thi Hoai Nguyen<sup>2</sup>

<sup>1</sup>Mathematical Modeling Laboratory, Department of Agro-environmental Sciences, Kyushu University, Japan

<sup>2</sup>Institute of Mathematics for Industry, Kyushu University, Japan

\*Corresponding author: email [tavietton@agr.kyushu-u.ac.jp](mailto:tavietton@agr.kyushu-u.ac.jp)

## Abstract

This paper conducts a numerical study of a geometrical structure called  $\epsilon$ -school for predator-avoidance fish schools, based on our previous mathematical model. Our results show that during a predator attack, the number of  $\epsilon$ -school increases from one to a certain value. After the attack, the number of  $\epsilon$ -school decreases in the first two predator-avoidance patterns, but continues to increase in the third pattern. A constant value for the number of  $\epsilon$ -school is observed in the last pattern. These findings suggest that when the predator is approaching, each individual in the school focuses more on avoiding the predator, rather than on interacting with its schoolmates. Such a trait is in agreement with real-life behavior in the natural ecosystem.

*Keywords:*  $\epsilon$ -school, Stochastic Differential Equations, Predator-Prey System, Fish Schooling, Predator-Avoidance Patterns

## 1 Introduction

Fish schooling is a remarkable phenomenon in the aquatic world that has captivated many researchers. The synchronized movement of hundreds or even thousands of fish in a school is a complex and highly organized trait. Such unique swarm behavior has

been the subject of numerous studies in various disciplines, including biology, physics, and mathematics.<sup>1-6</sup>

Studying fish schooling from a mathematical point of view is important. We can gain insights into the rules governing the behavior of individuals and have a deeper understanding of the underlying patterns and dynamics of collective behavior in animal groups. Mathematical models can make predictions and analyze the effects of various factors on the behavior of a school of fish, such as the interaction between individual fish, environmental conditions, and external stimuli. This information can have important implications for fields such as fisheries management, wildlife conservation, and aquatic ecology. It can also have practical applications, such as in the design of swarm robotics to accomplish tasks that would be difficult or impossible for a single robot to accomplish on its own, and the design of software for autonomous vehicles (e.g. self-driving cars) that use collision-avoidance rule of fish.

We have studied fish schooling from the mathematical point of view for more than a decade. In Ref. 7, we constructed a stochastic differential equation (SDE) model for fish schooling, which is based on the biological interaction rules outlined by Camazine *et al.*<sup>2</sup> A geometrical analysis of such a model is then presented in Ref. 8. In Ref. 9, we investigated the obstacle-avoiding patterns of fish schools by incorporating an obstacle-avoidance rule into our original model of Ref. 7. Therein, for the first time, we were able to quantify the cohesiveness of fish schools.

In Ref. 10, we developed a mathematical model for the foraging behavior of fish schools. Our results revealed that when fish form a unitary formation in terms of school, they are able to locate the food more effectively: such a trait is one of the benefits of constituting a school that is consistent with real-life situation in the natural ecosystem.<sup>11-14</sup>

In Ref. 15, we proposed a model of SDEs to describe predator-avoidance behavior of a prey fish school. Therein, two different hunting tactics of the predator were integrated into the general SDE model. On the basis of the model, we discovered four anti-predation maneuvers of the prey fish school (hereinafter, we also label them as the predator-avoiding patterns) which are consistent with the behavior in the real aquatic ecosystem. Moreover, we also successfully demonstrated the benefit of constituting a large school of prey fish in better escaping the predator's attack.

Our previous work<sup>15</sup> was mainly focused on demonstrating the capability of the proposed SDE model in recovering simulated predator-avoidance patterns of the schooling prey fish that fit the real patterns. As a consequence, there remains another crucial issue of the anti-predation behavior of the prey fish school that is still not addressed in our earlier study, namely to what extent does the schooling prey fish alter the structural integrity of its school formation as a response to avoid the predator's attack. This study, therefore, aims to investigate the transformation of the structural formation of the schooling prey fish during a predator's attack. To do so, we introduce the so-called  $\epsilon$ -school as a mathematical representation of the geometrical structure of the schooling prey's formation. Here, the notion of  $\epsilon$ -school is integrated in our SDE model of Ref. 15. Based on this framework, we undertake numerical simulations to elucidate the transformation of  $\epsilon$ -school in all the observed four predator-avoidance patterns.

Our SDE model is as follows:<sup>15</sup>

$$\left\{ \begin{array}{l} dx_i(t) = v_i dt + \sigma_i dw_i(t), \quad (i = 1, 2, \dots, N), \\ dv_i(t) = \left[ -\alpha \sum_{j=1, j \neq i}^N \left( \frac{r^p}{\|x_i - x_j\|^p} - \frac{r^q}{\|x_i - x_j\|^q} \right) \right. \\ \quad \times (x_i - x_j) \\ \quad -\beta \sum_{j=1, j \neq i}^N \left( \frac{r^p}{\|x_i - x_j\|^p} + \frac{r^q}{\|x_i - x_j\|^q} \right) \\ \quad \times (v_i - v_j) + H(x_i, y) \left. \right] dt, \\ \quad (i = 1, 2, \dots, N), \\ dy(t) = v dt + \sigma dw_t, \\ dv(t) = F(x_i, v_i, y, v) dt, \end{array} \right. \quad (1)$$

In (1),  $N$  is the size of (prey) fish school;  $x_i(t)$  and  $v_i(t)$  ( $i = 1, 2, \dots, N$ ) respectively denote the position and velocity in  $\mathbb{R}^d$  ( $d = 2, 3$ ) of the  $i$ -th prey fish at time  $t$ ;  $y(t)$  and  $v(t)$  correspondingly represent the position and velocity of the predator at time  $t$ ; and  $\|\cdot\|$  designates the Euclidean norm of a vector.

The first term in Eq. (1) is an SDE for the unknown  $x_i(t)$ , where  $\sigma_i dw_i$  ( $i = 1, 2, \dots, N$ ) denotes a stochastic differentiation of  $d$ -dimensional independent Brownian motion defined in a filtered probability space.<sup>7</sup> The second expression is a deterministic equation for the unknown  $v_i(t)$ . Parameters  $1 < p < q < \infty$  are fixed exponents;  $\alpha$  and  $\beta$  designate positive coefficients of attraction and velocity matching among the individual prey, respectively; and  $r > 0$  depicts the critical distance between two individuals in the school.

The third expression of Eq. (1) is again a stochastic equation for the unknown  $y(t)$  in which  $w(t)$  is a  $d$ -dimensional Brownian motion in the same filtered probability space which is independent of  $w_i(t)$ ,  $i = 1, 2, \dots, N$ . The last term of Eq. (1) is deterministic.

In this study, we include a condition of “being eaten” into the proposed model (1). Such a condition manifests a situation where a particular prey fish is captured by the predator during its attack. Here, the “being eaten” condition applies when the  $i$ -th prey fish is within a distance  $r$  from the approaching predator such that  $\|y - x_i\| < r$ . Consequently, when a prey fish satisfies the “being eaten” condition, the system described by the model changes from  $N : 1$  ( $N$  prey, 1 predator) to  $(N - 1) : 1$ .

The function  $H(x_i, y)$  represents the mechanism adopted by an individual prey fish to avoid the predator. It takes the following remark:

$$H(x_i, y) = \delta \frac{R_1^{\theta_1}}{\|x_i - y\|^{\theta_1}} (x_i - y), \quad (2)$$

where  $R_1 > r$ ,  $\delta$ , and  $\theta_1$  are positive constants.

On the other hand, the function  $F(x_i, v_i, y, v)$  manifests the hunting strategy of the predator. Here, we devised two hunting tactics of the predator, namely (i) the predator attacks the center of the schooling prey (hunting tactic I), and (ii) the predator focuses its attack on the nearest prey (hunting tactic II). The mathematical expressions for each of the prescribed predator’s hunting strategies are respectively defined as follows:

$$F(x_i, v_i, y, v) = - \frac{R_2^{\theta_2}}{\|y - x_c\|^{\theta_2}} \times \left[ \gamma_1 (y - x_c) + \gamma_1 \gamma_2 (v - v_c) \right], \quad (3)$$



$$F(x_i, v_i, y, v) = -\frac{1}{N} \sum_{j=1}^N \frac{R_2^{\theta_2}}{\|y - x_j\|^{\theta_2}} \times \left[ \gamma_1 (y - x_j) + \gamma_1 \gamma_2 (v - v_j) \right]. \quad (4)$$

In Eq. (3),  $x_c$  and  $v_c$  respectively denote the center position and velocity of the schooling prey; we defined them as the average value of the positions and velocities of all the individual prey constituting the school:

$$x_c = \frac{1}{N} \sum_{i=1}^N x_i, \quad v_c = \frac{1}{N} \sum_{i=1}^N v_i. \quad (5)$$

Parameters  $R_2 > r$ ,  $\theta_2$ ,  $\gamma_1$ , and  $\gamma_2$  are positive constants. Meanwhile, in Eq. (4),  $x_j$  designates the position of each individual prey fish.

The organization of this paper is as follows. In the following section, we provide detailed explanation regarding the notion of  $\epsilon$ -school and outline the initial conditions for our simulation based on the model (1). In Section 3, we present the results of the numerical simulations. Lastly, in Section 4, we pose some concluding remarks of the current study.

## 2 Preliminary

In this section, we introduce the concept of  $\epsilon$ -school and establish initial conditions for our simulations based on the model (1). The notion of  $\epsilon$ -school is akin to that of a connected component in an  $\epsilon$ -graph, as seen in graph theory.<sup>16</sup>

At each time step  $t$ , we define an  $\epsilon$ -graph  $G(V(t), E(t))$  where the set of vertices

$$V(t) = \{x_1(t), x_2(t), \dots, x_N(t)\}$$

represents the positions of individuals, and the set of edges

$$E(t) = \{(x_i(t), x_j(t)) \text{ if } \|x_i(t) - x_j(t)\| \leq \epsilon, \\ i, j = 1, 2, \dots, N\}$$

connects any two individuals whose distance does not exceed  $\epsilon$ .

We refer to each connected component of  $G(V(t), E(t))$  as an  $\epsilon$ -school. Furthermore, we denote by  $N_\epsilon(t)$  the number of  $\epsilon$ -schools in the graph  $G(V(t), E(t))$ .

**Remark 1.** *In Ref. 8, we introduced a new definition of  $\epsilon, \theta$ -schooling. The definition states that once the  $\epsilon, \theta$ -schooling structure has been formed, it will be maintained indefinitely, as long as there are no external factors, such as a predator, that disrupt it. However, in the current paper, the structure changes over time as a result of predator attacks. Therefore, the definition of  $\epsilon, \theta$ -schooling is not applicable here.*

In this study, we investigate the transformation of the number of  $\epsilon$ -school structure of the schooling prey fish due to the predator's attack in both two- and three-dimensional spaces ( $d = 2, 3$ ) for the observed four predator-avoidance patterns in our earlier work.<sup>15</sup> In all of the simulations, we employ the model (1) with the hunting tactic chosen among Eq. (3) and Eq. (4), correspondingly. In all of the cases, the number of prey fish is fixed at  $N = 40$ , and the intensity of noise  $\sigma_i = \sigma = 0.01$  ( $i = 1, 2, \dots, N$ ), while other parameters may vary and are specified as necessary. Here, we specifically

choose a moderate value of  $N = 40$  so as to include a reasonable number of individuals in the schooling prey fish to properly illustrate the transformation of the geometrical structure of such a school formation due to a predator's attack. Meanwhile, the values of the magnitude of the white noise for the schooling prey fish and the predator are determined as  $0.001 \leq \sigma_i \leq 0.01$  and  $0.001 \leq \sigma \leq 0.01$ , respectively, thereby allowing a sufficient magnitude of the white noise to invoke stochasticity in our system; a large value of  $\sigma$  should be avoided to prevent a system with an excessively strong stochasticity.<sup>7,8</sup>

The maximum simulation time is prescribed at  $t_{\max} = 3,500$ , during which the solitary predator attacks the schooling prey only once. At the beginning of the simulation ( $t = 0$ ), all prey fish are in an  $\epsilon$ -school formation, while the predator fish is positioned relatively far from the school.

In the following section, we present the results of the numerical simulations for all the observed four predator-avoidance patterns.

### 3 Results

As outlined in the Introduction, our aim in the present study is to elucidate the transformation of the structural formation of the schooling prey fish during the predator's attack. To do so, we integrate the concept of  $\epsilon$ -school described in the Preliminary section into the general model (1).

From our previous work,<sup>15</sup> we obtained four predator-avoidance patterns. We label them as: (i) Pattern I: Split and Reunion, (ii) Pattern II: Split and Separate into Two Groups, (iii) Pattern III: Scattered, and (iv) Pattern IV: Maintain Formation and Distance. In this section, we present the simulation results of each of the observed patterns for two- and three-dimensional simulations, respectively. Let us begin by discussing the simulation results of the two-dimensional cases.

#### 3.1 Two-dimensional space

For the two-dimensional case, the simulations are carried out with a fixed value of  $\epsilon = 0.7$ . The values of other parameters of the model to obtain each of the predator-avoiding patterns are outlined in Table 1, correspondingly. Therein, the associated hunting tactic of the predator for each of the four predator-avoidance patterns is listed in the second column of the table.

Table 1. Parameter settings for two-dimensional simulations of predator-avoidance fish schooling.

Pattern	Hunting Tactic	$\alpha$	$\beta$	$\delta$	$p$	$\theta_1$	$\theta_2$	$\gamma_1$	$\gamma_2$
I	II	15	0.5	1	4	1	0.5	0.08	0.1
II	I	1	0.5	1	4	5	1	0.1	0.1
III	II	1	0.5	5	2	1	2	1	0.1
IV	I	2	0.5	0.1	2	1	1	5	10

Fig. 1 illustrates the results of the simulation for Pattern I (Split and Reunion), displaying the condition of  $\epsilon$ -school as simulation time progresses from the early stage

### 1 - Split and Reunion 2D.jpg

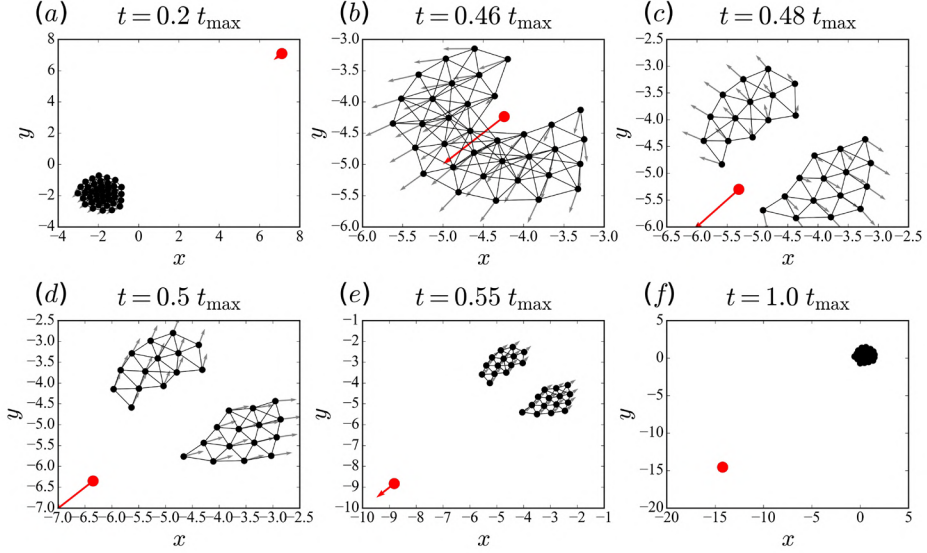


Figure 1. The results of 2D simulation for Pattern I: Split and Reunion. The images demonstrate the behavior of the schooling prey and the predator, as well as the associated condition of  $\epsilon$ -school at: (a)  $t = 0.2t_{\max}$ , (b)  $t = 0.46t_{\max}$ , (c)  $t = 0.48t_{\max}$ , (d)  $t = 0.5t_{\max}$ , (e)  $t = 0.55t_{\max}$ , and (f)  $t = t_{\max}$ , respectively.

until the end of the simulation ( $t_{\max}$ ). Therein, the small black dots manifest the schooling prey, while the large red dot designates the predator. The arrow linked to each of the units denotes the direction of movement of that particular unit at the corresponding time. The individuals constituting an  $\epsilon$ -school (at the corresponding time) are connected to each other through a solid line. Similar configurations apply to the simulation results of other patterns.

As can be seen in Fig 1, as the predator arrives in the vicinity of the prey, the schooling prey reacts accordingly to avoid the predator. Such a maneuver generates a vacuole-form of the schooling prey where each of the individuals tries to get away from the predator (see Fig. 1(b)). At this stage, the associated prey still maintains the unitary school formation, as is depicted by the solid lines connecting each of the individuals.

As the predator progresses along its path, a total number of 11 prey fish is eaten by it. At this stage, all the other “survived” prey responses accordingly by decomposing the unitary formation of the school and temporarily constitutes two smaller groups; each of the groups expands at the right angles away from the direction of the predator’s attack. Evidence for this can be seen in Fig. 1(c), where two number of  $\epsilon$ -schools prevail. As the predator moves away from the “survived” prey, the latter entities recombined to form a unitary school formation behind the predator (Fig. 1(f)), resulting in the recuperation of the number of  $\epsilon$ -school into one.

Now, let us turn our attention to the next Pattern. Fig. 2 displays the corresponding simulation results for Pattern II (Split and Separate into Two Groups). As can be seen in the figure, the behavior of the schooling prey in Pattern II exhibits similar characteristics with Pattern I during the progression periods of the predator’s attack

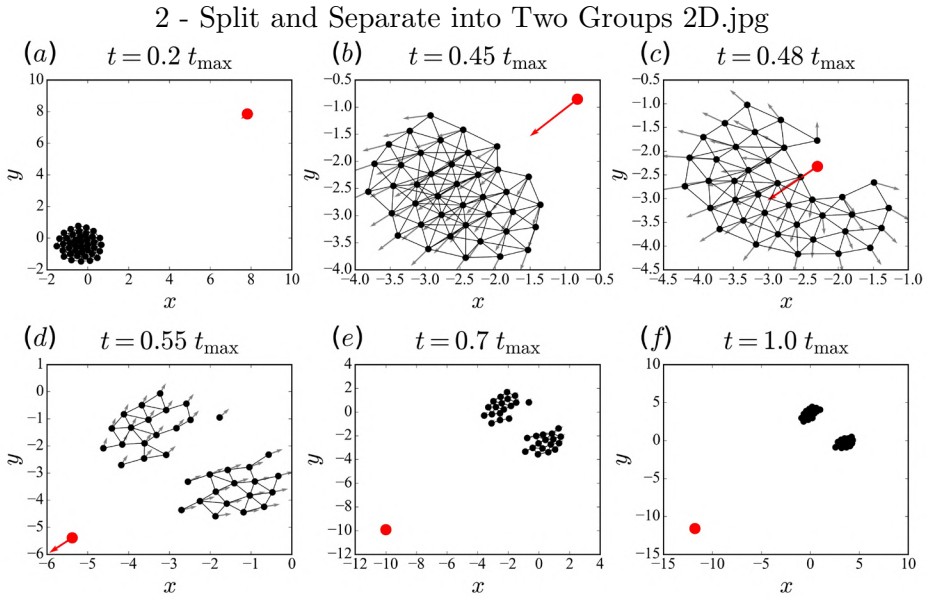


Figure 2. The results of 2D simulation for Pattern II: Split and Separate into Two Groups. The images demonstrate the behavior of the schooling prey and the predator, as well as the associated condition of  $\epsilon$ -school at: (a)  $t = 0.2t_{\max}$ , (b)  $t = 0.45t_{\max}$ , (c)  $t = 0.48t_{\max}$ , (d)  $t = 0.55t_{\max}$ , (e)  $t = 0.7t_{\max}$ , and (f)  $t = t_{\max}$ , respectively.

(see Figs. 2(a) - (d)). In this case, however, a total number of 5 prey fish is eaten by the predator. Another conspicuous difference lies in the periods after the attack. Therein, the two smaller schools of the “survived” prey do not rejoin into a unitary school formation. Evidence for this is in Figs. 2(e) - (f). In accordance with this, the number of  $\epsilon$ -school decreases to two and remains at that level until the end of the allotted simulation time.

Next, we move on to Pattern III (Scattered). Here, another distinctive characteristic of the schooling prey appears: the schooling prey seems to display a panic condition and permanently break the unitary school formation as the simulation proceeds. Because the prey breaks the unitary formation, the predator is in favorable situation to hunt more (available) prey. As a result, the remaining “survived” prey is actively being hunted by the predator, resulting in a continuing panic condition of the individual prey. At the end of the allotted simulation time, a total number of 13 prey fish is eaten by the predator.

As can be seen in Figs. 3(b) - (e), as the predator approaches, the number of  $\epsilon$ -school increases from one into numerous  $\epsilon$ -schools based on the number of “survived” prey at the particular time. Many of these structures consist of only one individual prey fish. Such a condition can be identified in Fig. 3(f), where numerous structures of  $\epsilon$ -school prevail as the simulation arrives at  $t_{\max}$ .

For the last anti-predation maneuver (namely Pattern IV: Maintain Formation and Distance), the schooling prey exhibits vigilant behavior to the nearby predator: it maintains a (relatively) safe distance from the predator during the simulation. Consequently, no prey fish is being eaten by the predator. As shown in Fig. 4, the school

### 3 - Scattered 2D.jpg

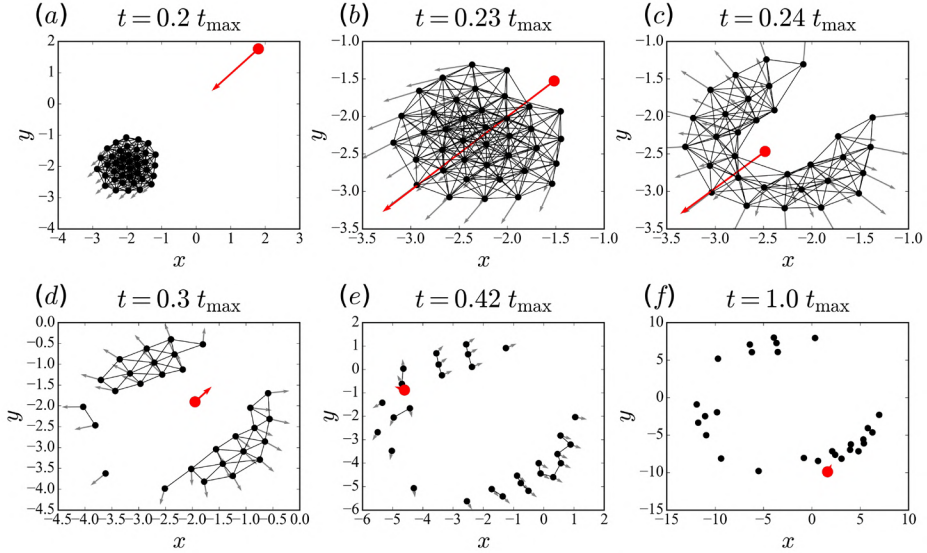


Figure 3. The results of 2D simulation for Pattern III: Scattered. The images demonstrate the behavior of the schooling prey and the predator, as well as the associated condition of  $\epsilon$ -school at: (a)  $t = 0.2t_{\max}$ , (b)  $t = 0.23t_{\max}$ , (c)  $t = 0.24t_{\max}$ , (d)  $t = 0.3t_{\max}$ , (e)  $t = 0.42t_{\max}$ , and (f)  $t = t_{\max}$ , respectively.

of prey fish maintains its unitary  $\epsilon$ -school until the end of simulation time.

Up until this point, within the context of the four observed predator-avoidance patterns, it seems that Pattern IV (Maintain Formation and Distance) provides the best protection mode for the schooling prey, since no single prey is eaten by the predator. On the other hand, Pattern III (Scattered) provides the least protection for the schooling prey (13 prey fish is eaten by the predator). Between these two extremes, Pattern I (Split and Reunion) and Pattern II (Split and Separate into Two Groups) result in a total number of 11 and 5 eaten prey fish, respectively. It is important to note, however, that as our model is stochastic, executing the simulation repeatedly with the same parameters (for the same predator-avoidance pattern) may result in a different total number of eaten prey by the predator. It is therefore crucial to take such stochastic behavior into consideration. To do so, we deliberately run the simulation 1,000 times for each of the corresponding predator-avoidance patterns. Fig. 5a presents the total number of eaten prey for each of the associated patterns. According to Fig. 5a, it is apparent that Pattern IV (Maintain Formation and Distance) is the most effective evasive mode for the schooling prey since no single prey is being eaten throughout the 1,000 simulation runs. On the other hand, the least effective anti-predation mode is displayed by Pattern III (Scattered), with a median of 13 eaten prey during the predator's attack. Such findings are consistent with observations of diverse fish species in the natural aquatic ecosystem (see, for example, Refs. 17–20).

Fig. 5b shows the average number of  $\epsilon$ -schools at each time step ( $N_{\epsilon}(t)$ ), calculated over 1,000 simulation runs for each pattern, using the same parameters as before. A careful inspection of Fig. 5b reveals that the number of  $\epsilon$ -schools increases from one to a certain value, then decrease to one (for Pattern I) or two (for Pattern II). In Pattern

#### 4 - Maintain Distance 2D.jpg

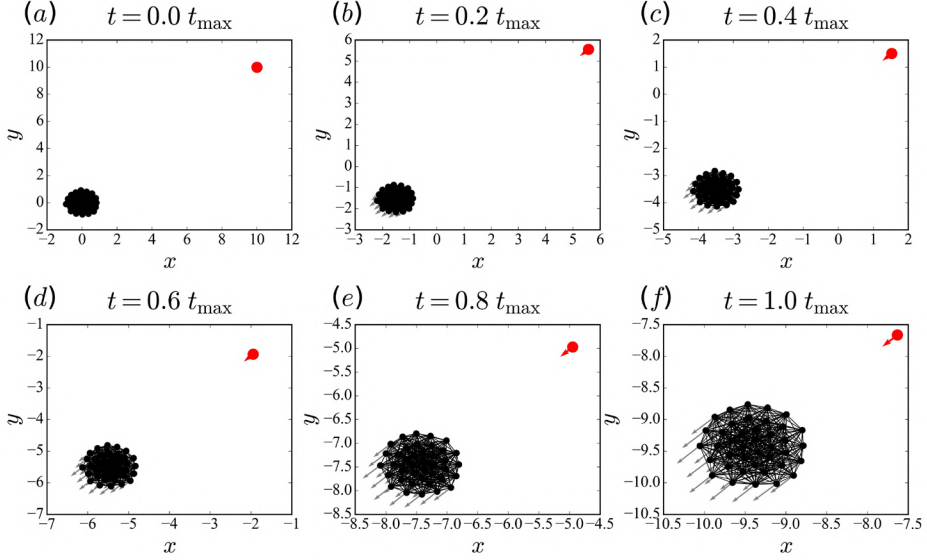


Figure 4. The results of 2D simulation for Pattern IV: Maintain Formation and Distance. The images demonstrate the behavior of the schooling prey and the predator, as well as the associated condition of  $\epsilon$ -school at: (a)  $t = 0$ , (b)  $t = 0.2t_{\max}$ , (c)  $t = 0.4t_{\max}$ , (d)  $t = 0.6t_{\max}$ , (e)  $t = 0.8t_{\max}$ , and (f)  $t = t_{\max}$ , respectively.

III, the number of  $\epsilon$ -schools increases as the school becomes more scattered, while in Pattern IV, it remains at one throughout the allotted simulation time.

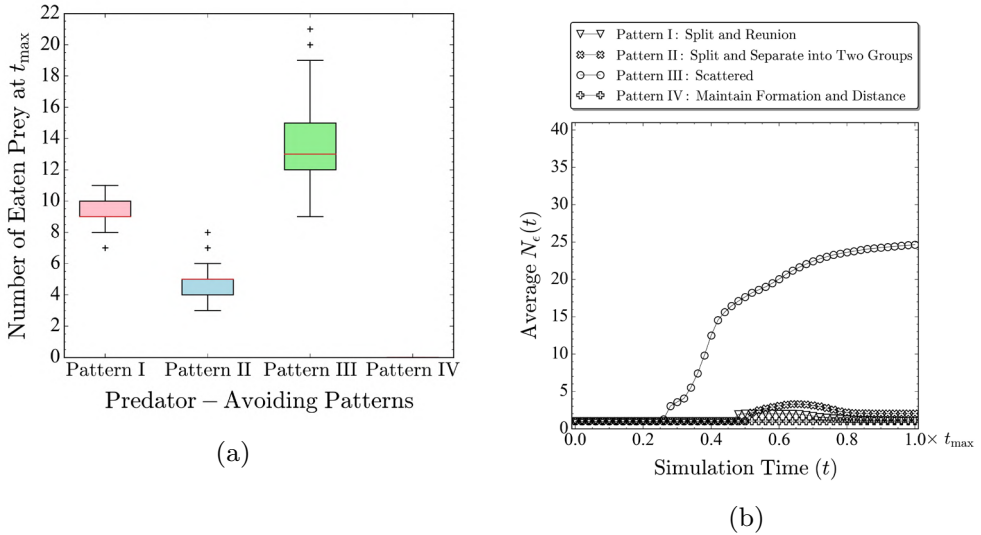


Figure 5. 2D simulation: (a) Total number of eaten prey, (b) Average number of  $\epsilon$ -schools (average  $N_{\epsilon}(t)$ ) over 1,000 simulation runs.

### 3.2 Three-dimensional space

In this subsection, we present the results of the simulation for the four predator-avoidance patterns alongside their associated  $\epsilon$ -schools in three-dimensional space. Here, the value of  $\epsilon$  is similar to the one employed in the two-dimensional case. Table 2 summarizes the adopted model parameter settings to run the three-dimensional simulations.

Table 2. Parameter settings for three-dimensional simulations of predator-avoidance fish schooling.

Pattern	Hunting Tactic	$\alpha$	$\beta$	$\delta$	$p$	$\theta_1$	$\theta_2$	$\gamma_1$	$\gamma_2$
I	II	15	0.5	1	4	1	0.5	0.08	0.1
II	I	0.36	0.5	1	4	15	1	0.1	0.1
III	II	1	0.5	5	2	1	2	1	0.1
IV	I	2	0.5	0.1	2	1	1	5	10

Figs. 6 - 9 exhibit the three-dimensional simulation results for Pattern I (Split and Reunion), Pattern II (Split and Separate into Two Groups), Pattern III (Scattered), and Pattern IV (Maintain Formation and Distance), respectively. In general, the main characteristics of  $\epsilon$ -schools for all the patterns are similar with the ones observed in the two-dimensional cases.

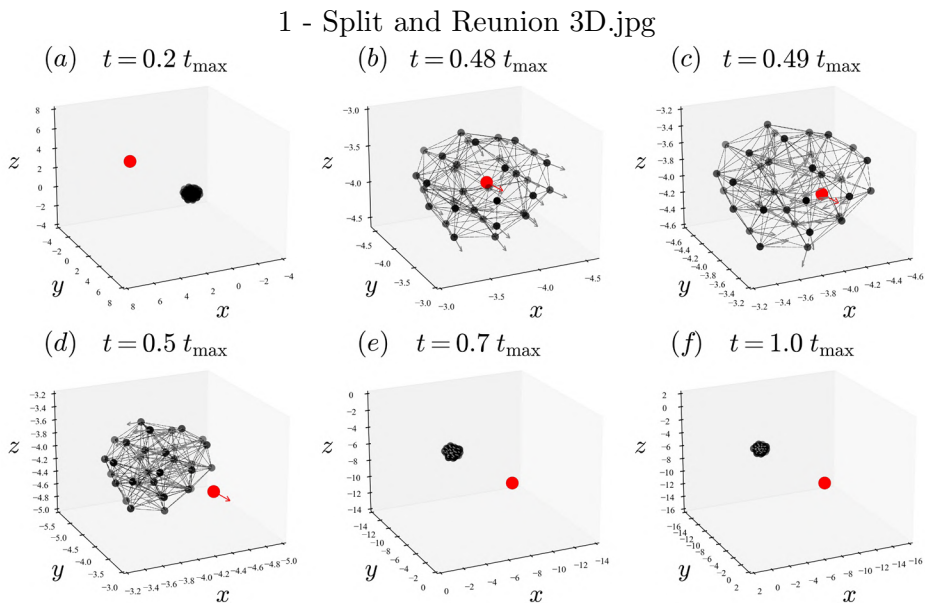


Figure 6. The results of 3D simulation for Pattern I: Split and Reunion. The images demonstrate the behavior of the schooling prey and the predator, as well as the associated condition of  $\epsilon$ -school at: (a)  $t = 0.2t_{\max}$ , (b)  $t = 0.48t_{\max}$ , (c)  $t = 0.49t_{\max}$ , (d)  $t = 0.5t_{\max}$ , (e)  $t = 0.7t_{\max}$ , and (f)  $t = t_{\max}$ , respectively.

A distinctive feature with the former two-dimensional cases, however, lies in the fact that in the three-dimensional spaces, the individual prey has more spatial flexibil-

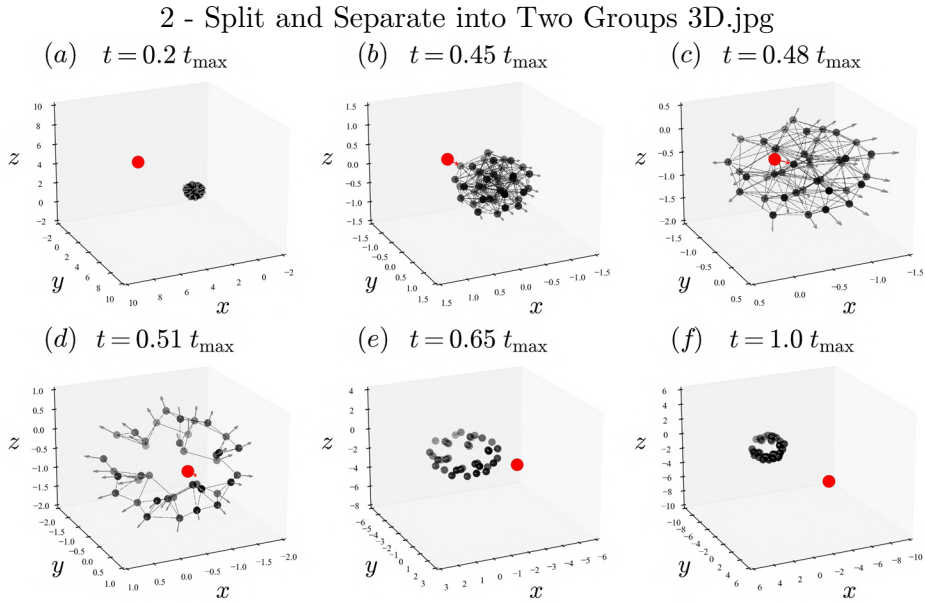


Figure 7. The results of 3D simulation for Pattern II: Split and Separate into Two Groups. The images demonstrate the behavior of the schooling prey and the predator, as well as the associated condition of  $\epsilon$ -school at: (a)  $t = 0.2t_{\max}$ , (b)  $t = 0.45t_{\max}$ , (c)  $t = 0.48t_{\max}$ , (d)  $t = 0.51t_{\max}$ , (e)  $t = 0.65t_{\max}$ , and (f)  $t = t_{\max}$ , respectively.

ity (more degrees of freedom) in its movement to avoid the approaching predator. This reflects in the fewer prey that is being eaten by the predator for each of the predator-avoidance patterns than in their corresponding two-dimensional counterparts. Fig. 10a shows the total number of eaten prey for the four predator-avoidance patterns over 1,000 simulation runs for each of the corresponding patterns. A comparison of Fig. 5a and Fig. 10a supports the erstwhile exposition: fewer prey is being eaten in the three-dimensional cases than the corresponding two-dimensional counterparts due to the higher degrees of freedom in the spatial movements of each individual prey.

Fig. 10b demonstrates the number of  $\epsilon$ -schools for the three-dimensional cases. Here again, we can observe that the  $\epsilon$ -schools structure for all of the associated predator-avoidance patterns exhibit relatively similar characteristics with their respective two-dimensional cases. Such a consistent result between the two- and three-dimensional simulations reflects the reliability and robustness of our model (1) in describing the transformation of geometrical structure of the schooling prey during predation threat of a solitary predator.

## 4 Conclusions

As a final remark, this paper extends the study of the SDE model of predator-avoidance in fish schools as presented in Ref. 15. We propose a concept of  $\epsilon$ -school as a mathematical representation of the geometrical structure of the schooling prey fish.

By analyzing four different predator-avoidance patterns in both two and three-



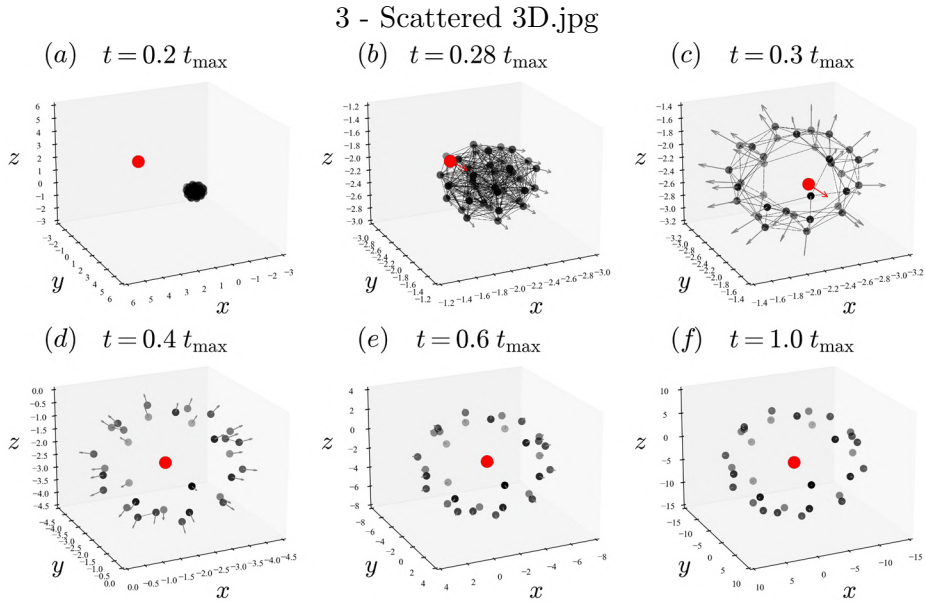


Figure 8. The results of 3D simulation for Pattern III: Scattered. The images demonstrate the behavior of the schooling prey and the predator, as well as the associated condition of  $\epsilon$ -school at: (a)  $t = 0.2t_{\max}$ , (b)  $t = 0.28t_{\max}$ , (c)  $t = 0.3t_{\max}$ , (d)  $t = 0.4t_{\max}$ , (e)  $t = 0.6t_{\max}$ , and (f)  $t = t_{\max}$ , respectively.

dimensional spaces, we found that the number of  $\epsilon$ -schools varies dynamically during the predator's approach. Generally, in the first two patterns, we observed an initial increase in the number of  $\epsilon$ -schools followed by a decrease to either one or two structures. Pattern III, however, exhibits a distinct characteristic in which the number of  $\epsilon$ -schools continued to increase until the end of the simulation. A constant unitary  $\epsilon$ -school is found in Pattern IV. These results suggest that when a predator approaches, individual fish in the school prioritize their attention to the predator rather than maintaining their formation with other schoolmates. Such a finding is consistent with real-life behavior of schooling fish in the natural aquatic ecosystem.

The results of this study contribute to a better understanding of the collective behavior of fish schools and can potentially have implications for the study of animal behavior and group dynamics in various species. Further research can be conducted to explore the impact of various parameters, such as the value of  $\epsilon$ , as well as the intensity of the noise, on the observed patterns.

## Acknowledgments

The work of the first (A.D.H.) and the second (T.V.T.) authors were supported by JSPS KAKENHI Grant Number 19K14555.

## Competing Interests

The authors declare no competing interest in this study.

#### 4 - Maintain Distance 3D.jpg

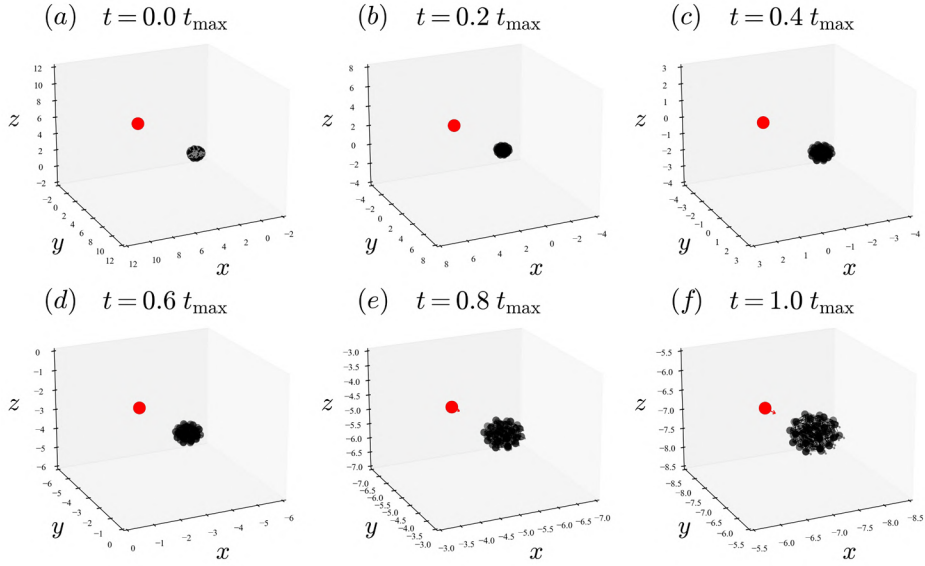


Figure 9. The results of 3D simulation for Pattern IV: Maintain Formation and Distance. The images demonstrate the behavior of the schooling prey and the predator, as well as the associated condition of  $\epsilon$ -school at: (a)  $t = 0$ , (b)  $t = 0.2t_{\max}$ , (c)  $t = 0.4t_{\max}$ , (d)  $t = 0.6t_{\max}$ , (e)  $t = 0.8t_{\max}$ , and (f)  $t = t_{\max}$ , respectively.

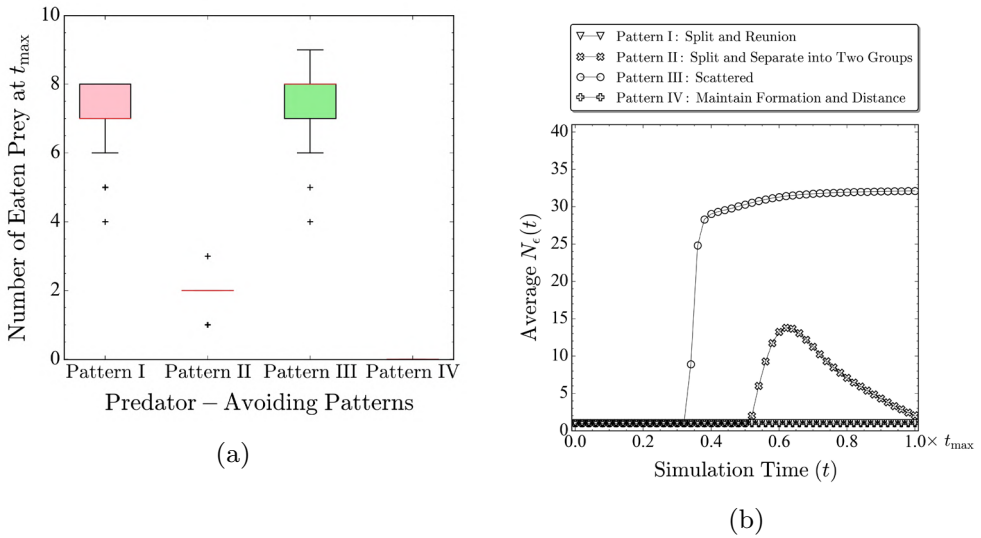


Figure 10. 3D simulation: (a) Total number of eaten prey, (b) Average number of  $\epsilon$ -schools (average  $N_{\epsilon}(t)$ ) over 1,000 simulation runs.

## Contribution

In this study, the first author (A.D.H.) contributes upon developing the computer codes used for the numerical simulations as well as writing the initial draft. The

second (T.V.T.) and the last (L.T.H.N.) authors contribute upon designing and conceptualizing the mathematical model as well as revising the initial manuscript.

## References

- [1] Aoki, I., A simulation study on the schooling mechanism in fish, *Bull. Jpn. Soc. Sci. Fish*, **48**, 8 (1982), 1081–1088, **doi:** 10.2331/suisan.48.1081
- [2] Camazine, S., Deneubourg, J., Franks, N. R., Sneyd, J., Theraula, G., and Bonabeau, E., *Self-Organization in Biological Systems*, Princeton university press, 2001
- [3] Cucker, F. and Smale, S., On the mathematics of emergence, *Jpn. J. Math.*, **2**, 1 (2007), 197–227, **doi:** 10.1007/s11537-007-0647-x
- [4] Reynolds, C. W., Flocks, herds and schools: A distributed behavioral model, *Proc. of the 14th Annual Conference on Computer Graphics and Interactive Techniques*, (1987), 25–34, **doi:** 10.1145/37401.37406
- [5] Couzin, I. D., Collective cognition in animal groups, *Trends Cognit. Sci.*, **13**, 1 (2009), 36–43, **doi:** 10.1016/j.tics.2008.10.002
- [6] Vicsek, T. and Zafeiris, A., Collective motion, *Phys. Rep.*, **517**, 3-4 (2012), 71–140, **doi:** 10.1016/j.physrep.2012.03.004
- [7] Uchitane, T., T̂a, T. V. and Yagi, A., An ordinary differential equation model for fish schooling, *Sci. Math. Jpn.*, **75**, 3 (2012), 339–350, **doi:** 10.32219/isms.75.3.339
- [8] Nguyen, L. T. H., T̂a, T. V. and Yagi, A., Quantitative investigations for ODE model describing fish schooling, *Sci. Math. Jpn.*, **77**, 3 (2015), 403–413, **doi:** 10.32219/isms.77.3.403
- [9] Nguyen, L. T. H., T̂a, T. V. and Yagi, A., Obstacle avoiding patterns and cohesiveness of fish school, *J. Theor. Biol.*, **406**, 22 (2016), 116–123, **doi:** 10.1016/j.jtbi.2016.07.017
- [10] T̂a, T. V. and Nguyen, L. T. H., A stochastic differential equation model for the foraging behavior of fish schools, *Phys. Biol.*, **15**, 3 (2018), 036007, **doi:** 10.1088/1478-3975/aab298
- [11] Pitcher, T. J., Magurran, A. E. and Winfield, I. J., Fish in larger shoals find food faster, *Behav. Ecol. Sociobiol.*, **10**, 2 (1982), 149–151, **doi:** 10.1007/BF00300175
- [12] Pitcher, T. J., Functions of shoaling behaviour in Teleosts, *The Behaviour of Teleost Fishes*, (1986), 294–337, **doi:** 10.1007/978-1-4684-8261-4\_12
- [13] Krause, J., Ruxton, G. D. and Krause, S., Swarm intelligence in animals and humans, *Trends Ecol. Evol.*, **25**, 1 (2010), 28–34, **doi:** 10.1016/j.tree.2009.06.016
- [14] Ioannou, C., Swarm intelligence in fish? The difficulty in demonstrating distributed and self-organised collective intelligence in (some) animal groups, *Behav. Process.*, **141**, (2017), 141–151, **doi:** 10.1016/j.beproc.2016.10.005
- [15] Hartono, A. D., Nguyen, L. T. H. and T̂a, T. V., A Stochastic Differential Equation Model for Predator-Avoidance Fish Schooling, *Preprint submitted*, (2022)
- [16] Rahman, Md. Saidur, *Basic graph theory*, Springer, 2017

- [17] Pavlov, D. S. and Kasumyan, A. O., Patterns and mechanisms of schooling behavior in fish: a review, *J. Ichthyol.*, **40**, 2 (2000), S163-S231
- [18] Partridge, B. L., The structure and function of fish schools, *Sci. Am.*, **246**, 6 (1982), 114–123
- [19] Potts, G. W., The schooling ethology of *Lutianus monostigma* (Pisces) in the shallow reef environment of Aldabra, *J. Zool.*, **161**, 2 (1970), 223–235, **doi**: 10.1111/j.1469-7998.1970.tb02037.x
- [20] Shaw, E., Schooling fishes: the school, a truly egalitarian form of organization in which all members of the group are alike in influence, offers substantial benefits to its participants, *Am. Sci.*, **66**, 2 (1978), 166–175

# MERGE and the role of gully erosion modelling to protect water quality on the Great Barrier Reef

Melanie E Roberts\*

Australian Rivers Institute; and School of Environment and Science, Griffith University, Gold Coast, Australia  
m.roberts2@griffith.edu.au

## 1 Introduction

Gully erosion is responsible for as much as 40% of the accelerated sediment that ultimately reaches the Great Barrier Reef (GBR) [3], contributing to poor water quality and adverse outcomes [4]. The Queensland and Australian Governments are committed to protecting the GBR, with the goal to reduce sediment transported to the reef by 25% by 2025 under the Reef 2050 Water Quality Improvement Plan [1]. As gullies are the majority source of excess sediments reaching the GBR despite occupying a small percentage of the GBR catchments, land management to slow or prevent gully erosion is receiving significant attention and investment.

Gully erosion is highly varied, affected by soil type, rainfall, catchment area, vegetation, and grazing and other land use patterns amongst other factors. The high variability in gully erosion, coupled with limited observations especially with regard to land management activities, has frustrated efforts to develop portable data-driven models [11]. Prosser [7], in a report to the Queensland Water Modelling Network, identified the need for process-based models to support gully management and remediation activities. The MERGE (modelling erosion resistance for gully erosion) gully erosion model was developed in partnership with Queensland Government and the Queensland Water Modelling Network in direct response to that call. The process-based foundation of MERGE is supported by data-driven sub-models where it is infeasible or impractical to adopt a process-based approach.

## 2 MERGE

MERGE is an event-based model for the erosion and transport of sediment within channel-like gullies. Conservation of mass for the concentration of sediment suspended in the water column, which is advected through the channel subject to deposition (sink) and entrainment (source) processes, gives the one-dimensional governing equation

$$W \frac{\partial C d}{\partial t} + \frac{\partial(CQ)}{\partial x} = \eta - \delta, \quad (1)$$

where  $C(x, t)$  [kg/m<sup>3</sup>] is the concentration,  $d(x, t)$  [m] is the flow depth,  $Q$  [m<sup>3</sup>/s] is the flow,  $\eta$  [kg/ms] is the rate of entrainment,  $\delta$  [kg/ms] is the rate of deposition,  $t$  [s] is time, and  $x$  [m] is the distance along the gully (1).

The rate of deposition is  $\delta = bCw_s$  where  $b \geq 1$  is the ratio of the average concentration  $C$  to that just above the gully floor (assumed 1 in the absence of further information), and  $w_s$  is the settling velocity. The settling velocity is a function of the particle size and density, and is typically modelled using Stokes' Equation.

The rate of entrainment  $\eta$  is determined by balancing the power required to dislodge sediment and raise it to the height  $h$  [m] against the power available from the flow. The gully is assumed to consist of a series of connected one-dimensional, homogeneous segments. The segments are classified as either 'head' or 'channel' segments. Within channel segments, the power available for entrainment is due to the stream power  $\Omega = \rho g S Q$ , where  $\rho$  [kg/m<sup>3</sup>] is the density of the water,  $g$  [m/s<sup>2</sup>] is gravitational acceleration,  $S$  is the slope of the channel, and  $Q$  [m<sup>3</sup>/s] is the flow through the channel.

Within a head segment the waterfall power must be considered together with the stream power. The waterfall power is due to the loss of potential energy as the water cascades over the gully head (or an internal step) and walls of the gully. Assuming the power is equally distributed over the head (or step) length  $L_h$  [m], the waterfall power is  $\Psi = \rho g Q (D - d) / L_h$  where  $D$  [m] is the height of the head or step, and  $d$  is the depth of the flow within the channel. To simplify the model, variation in the head height is neglected.

The stream and waterfall power is limited by the power proportion  $k < 1$ , and the carrying capacity  $C^*$ , which represents the power required to maintain the suspended sediment in the flow. The power to entrain sediment at the rate  $\eta$  [kg/ms] consists of three key components: the energy to break the cohesion of a unit mass of soil  $J$  [Joule/kg],

---

\*This research was supported by Queensland Government through the Queensland Water Modelling Network

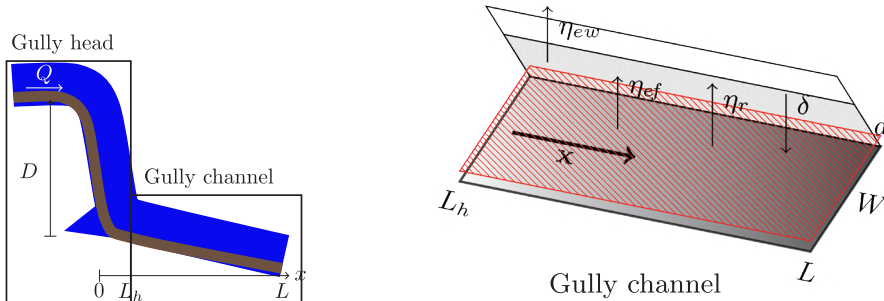


Figure 1: Geometry of the ideal gully, adapted from Roberts [8, Fig. 1]. The sediment concentration  $C(x, t)$  [kg/m<sup>3</sup>] satisfies the conservation of mass equation, which is to be solved within the bounded domain  $x \in [0, L]$ , for time  $t \geq 0$ . The gully is split into two regions for convenience, the gully head  $x \in [0, L_h]$ , and the channel  $x \in (L_h, L]$ , for time  $t \geq 0$ . The gully is of constant slope. The flow within the gully is of constant flux  $Q$  [m<sup>3</sup>/s] with depth  $d$  [m], and width  $W$  [m]. Sediment is entrained from the walls and floor at rate  $\eta_{ew}$  [kg/m s] and  $\eta_{ef}$  [kg/m s] respectively, and re-entrained at the rate  $\eta_r$  [kg/m s]. Sediment is deposited out at the rate  $\delta$  [kg/m s] forming the depositional layer (shown in red). Within the gully head a depositional layer is not formed, as deposited sediment is immediately re-entrained. Net entrainment in the gully head is at the rate  $\eta_{eh}$  [kg/m s].

the energy to overcome static friction  $F$  [Ws/kg] (assumed negligible), and the energy to lift the sediment to the height  $h$  [m], namely  $\beta = (\sigma - \rho)gh/\sigma$ , where  $\sigma$  [kg/m<sup>3</sup>] is the soil density. Thus the power required to entrain sediment at the rate  $\eta$  is  $\eta(J + F + \beta)$ . Equating the power available, limited by the power proportion and the carrying capacity, with the power required gives the rate of entrainment

$$\eta = \frac{k(\Psi + \Omega)}{J + F + \beta} \left(1 - \frac{C}{C^*}\right). \quad (2)$$

Following Hairsine and Rose [5] MERGE explicitly models the depositional layer, which forms atop the gully floor when the rate of deposition locally exceeds the rate of entrainment. It is assumed that a depositional layer cannot form in a head sector due to the higher power of the waterfall. In practice, the length of the gully head is measured as the length of the plunge pool that forms beneath the waterfall. Although smaller events may show different dynamics, which would warrant a different treatment of the depositional layer in the head, it is larger events that are the focus of the remediation modelling. The depositional layer lacks cohesion, and thus while a depositional layer is present,  $J = 0$  within the entrainment equation on the gully floor.

Under a steady flow through the gully, that is  $Q(x, t) = Q$ , the concentration profile within the gully will rapidly approach a steady profile  $C(x, t) = C(x)$ . In this case, analytical solutions to the conservation of mass equation are obtained for the head and channel sectors, with and without a depositional layer. These solutions are [8, Eqs. 12, 14 & 15]

$$\hat{C}_{SS_r} = \left( \frac{C^*(\hat{\zeta}_{ew} + \hat{\zeta}_r) - C_{Lh}}{\hat{\delta}^* + \hat{\zeta}_{ew} + \hat{\zeta}_r} \right) \left[ 1 - \exp\left(-\frac{\hat{x}}{C^*Q}(\hat{\delta}^* + \hat{\zeta}_{ew} + \hat{\zeta}_r)\right) \right], \quad (3)$$

$$\hat{C}_{SS_e} = \frac{AC^* - C_{Lh}(A + BC^*)}{A + BC^*} \left[ 1 - \exp\left(\frac{-\hat{x}}{QC^*}(A + BC^*)\right) \right], \quad (4)$$

$$\hat{C}_{SS_h} = \frac{A_2}{B} + \left(C^* - \frac{A_2}{B}\right) \left\{ \frac{A_2 - BC_0}{A_2 - BC_0 - B(C^* - C_0) \exp\left[\frac{-\hat{x}}{C^*Q}(A_2 - BC^*)\right]} \right\} \quad (5)$$

where  $\hat{\zeta}_{ew} = \frac{2d}{W+2d} \frac{k\Omega}{J+F+\beta}$ ,  $\hat{\zeta}_r = \frac{W}{W+2d} \frac{k\Omega}{F+\beta}$ ,  $A = \frac{k\Omega}{J+F+\beta}$ ,  $B = \frac{F+\beta}{J+F+\beta} Wbw_s$ , and  $A_2 = \frac{k(\Omega+\Psi)}{J+F+\beta}$ . Here the  $\hat{\cdot}$  notation indicates variables on the translated coordinate system such that the start of the sector corresponds to  $\hat{x} = 0$  and the concentration boundary condition is  $\hat{C}(\hat{x} = 0) = 0$ . Roberts [8] demonstrated that the quasi-steady solution is a good approximation to the full dynamic solution, even for a non-steady flow  $Q = Q(t)$ .

For a complete description of MERGE, and its development, refer to Roberts [8, 9].

### 3 Representing interventions

Gully erosion interventions, like gully erosion itself, are highly variable in their effectiveness. A review by Bartley et al. [2] reported intervention effectivenesses between 12 and 94%. Gully management interventions can be classified as direct and indirect. Examples of direct interventions include re-vegetation, water diversion, rock capping, roughening of the channel, porous check dams, and compacting and filling a site. Examples of indirect actions include stock

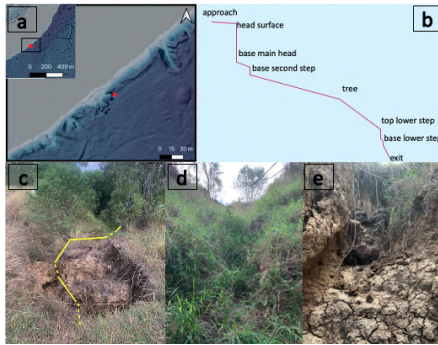


Figure 2: Case study gully showing (a) proximity to the Fitzroy River, (b) the schematic break up of the gully into head and channel sections, and photos of the gully viewed (a) from the head, (d) from the toe, and (e) the main head viewed from the first channel.

	Scenario	Manning's roughness coefficient $n$ [ $s/m^{1/3}$ ]		Flow $Q$ [ $m^3/s$ ]
		Bare soil	Vegetated	
Wet season	A	0.02	0.045	8
	B	0.02	0.045	16
Dry season	C	0.02	0.025	1.7
	D	0.02	0.025	3.5

Table 1: Case study flow and roughness scenarios

management (intensive stocking, stock reductions, stock exclusions), settling ponds, and wetlands. From a process perspective, these interventions target one of four actions, reducing flow through the gully (velocity and/or volume), increasing the erosive resistance of the soils, increasing deposition or off-site capturing of sediment. The first three actions will also reduce degradation of the site locally, while the fourth can protect receiving waters but will not reduce local erosion.

Interventions targeting the erosive resistance of the soils are modelled through the soil cohesion parameter  $J$ . Interventions that reduce the flow entering the gully are modelled through the flow  $Q$ , while interventions that modify the flow within the gully are modelled through the Manning's roughness coefficient  $n$ , which relates the flow depth  $d$  (and hence volume) to the flow  $Q$  via the data-driven Manning's Equation. Interventions that target deposition usually work to slow the flow, and hence are modelled through the Manning's roughness coefficient to affect  $Q$ .

The effects of three interventions, applied individually and in combination, on erosion at a case study gully in the Fitzroy Basin are shown here.

### 3.1 Case Study - Fitzroy Basin

The case study gully is located 2km from Rockhampton and discharges directly into the Fitzroy River. It is 21.8m from its head to mouth and consists of multiple steps (or internal heads) connected by steeply sloping channels. The gully is seasonally vegetated. In the wet season (Figure 2d) the lower reaches of the gully is vegetated with long grass, which reduces during the dry season. To apply MERGE to the case study site it was first necessary to segment the gully into distinct head and channel sections (Figure 2b). As some of the lower steps are low, they are neglected for the wet season simulations (as the water depth exceeds the step height), but are included in the dry-season simulation. Refer to Roberts [10] for a complete description of the study site, including the measurements of the various gully sectors.

Three interventions, applied in isolation and in combination, are considered. Namely roughening of the upper channel, for example as achieved through increasing ground cover, or through the introduction of branches and logs; diverting flow away from the gully, for example as achieved by reducing stocking rates in the gully catchment (which can result in increased infiltration and hence lower flow into the gully) or by building diversion bunds; and rocking the channel, which forms a protective barrier to the flow. Roughening of the channel is modelled by increasing the Manning's roughness coefficient, thereby reducing the flow  $Q$  while maintaining the flow depth  $d$ . Flow diversion is modelled by reducing the flow  $Q$  by 50%. Rocking the channel is modelled by assuming the entrainment of the underlying soil matrix is prevented, and therefore the concentration at the end of the rocked segment is that at the beginning of that segment. Table 1 shows the different flow conditions and Manning's roughness coefficients, for the different scenarios. The other parameter values were sediment density  $\sigma = 1470 \text{ kg/m}^3$ , particle size  $R = 10 \mu\text{m}$ , soil

	Scenario	Interventions applied	Sediment flux reduction (%) relative to baseline			
			Wet Season		Dry Season	
			A	B	C	D
o	Roughening of the upper channel	Roughening of the second step and channel	0.0	0.0	0.0	0.0
i	Rock upper	Rock cap the initial head and second step	41.7	41.6	34.2	34.1
io	Rock and roughen upper	Combination of (o) and (i)	41.7	41.6	34.2	34.1
ii	Rock upper and lower	Rock cap the initial head, second step, and first and second lower steps	41.7	41.6	43.2	43.3
iii	Diversion	Divert 50% of the runoff from entering the gully	49.7	50.7	49.5	49.4
iiio	Diversion & roughen	Combination of (o) and (iii)	49.7	50.7	49.5	49.4
iv	Diversion & rock upper	Combination of (i) and (iii)	70.6	71.4	66.8	67.4
ivo	Diversion & rock and roughen upper	Combination of (o) and (iv)	70.6	71.4	66.8	67.4

Table 2: Relative reduction in the sediment delivery rate [kg/s] for the different combinations of the three interventions. The sediment delivery rates without any intervention were modelled to be 5.5, 2.8, 0.8, and 0.4 m<sup>3</sup>/s for scenarios A to D respectively.

cohesion  $J = 1700$  Ws/kg, boundary concentration  $C_0 = 0$  kg/m<sup>3</sup>, carrying capacity  $C^* = 147$  kg/m<sup>3</sup>, settling velocity  $w_s = 1.07 \times 10^{-4}$  m/s, power proportion  $k = 0.005$ , concentration gradient  $b = 1$ , friction term  $F = 0$ , and gravity  $g = 9.81$  m/s<sup>2</sup>.

## 4 Results

The reduction in the total sediment delivery rate relative the the baseline (no intervention) under the different scenarios is shown in Table 2.

## 5 Discussion and Conclusions

This case study demonstrates that different interventions are variably effective, and that interventions applied in combination are not additive. These results are consistent with an earlier study applying MERGE in Prentice et al. [6], which similarly found the benefits of interventions were not additive. For this case study, diverting 50% of the runoff from entering the gully resulted in reductions in the sediment delivery rate between 49.4% and 50.7%, while rocking the main head and second step in the upper channel achieved reductions between 34.1% and 41.7%. Applying these two interventions in combination reduced delivery between 66.8% and 71.4%. This result is similar to the 56-78% reduction in erosion achieved through rock capping and vegetation in a study at Fernvale gully [6]. However, further studies in collaboration with Healthy Land and Water (as yet unpublished) demonstrated that not only do different gullies respond differently to interventions, but that the ordering of the most effective interventions will also vary.

These results highlight the importance of MERGE to explore the expected sediment reduction achieved by applying specific interventions at a specific site to support land managers. On-ground expertise remains essential for the practical application of MERGE, as expert knowledge is required to inform the exploration of interventions to ensure unfeasible options are not considered, for example where diversion would concentrate flow at a new location and trigger new gully activity, or where vegetation is unlikely to establish. Future development of MERGE is focussed on improving guidance on parameter selection, and coupling MERGE with novel data-driven modelling approaches to provide greater insight for land managers.

**Acknowledgements** This research is supported by Queensland Government through the Queensland Water Modelling Network. MERGE was developed while I was the Queensland Water Modelling Network Senior Research Fellow. The case study reported in this article received financial support from the Queensland Water Modelling Network. I acknowledge the support of the Queensland Water Modelling Network and the collaborations within it. I thank Jenny Riches, Sarah Stevens and Evan Thomas and colleagues (Queensland Department of Environment and Science) for their many contributions, which shaped MERGE.

The support of the Fitzroy Basin Association (FBA) was instrumental to the success of the case study reported in this article. FBA provided essential on-ground knowledge and relationships. I thank Daniel Boshoff for facilitating



the study and providing invaluable insights. I also thank the land holders for inviting us to undertake the reported case study on their land, and their cooperation with the project.

I also thank David Hamilton from the Australian Rivers Institute, Griffith University for many valuable conversations that shaped this project. I thank Graeme Curwen (Australian Rivers Institute) for GIS assistance.

This case study is also informed by a related case study led by Matthew Prentice (Griffith University) in collaboration with Mark Waud and Samille Loch-Wilkinson from Healthy Land and Water.

## References

- [1] Australian and Queensland Governments. Reef 2050 Water Quality Improvement Plan 2017-2022, 2018.
- [2] Rebecca Bartley, Jean Poesen, Scott Wilkinson, and Matthias Vanmaercke. A review of the magnitude and response times for sediment yield reductions following the rehabilitation of gullied landscapes. *Earth Surface Processes and Landforms*, 45(13):3250–3279, August 2020. doi:10.1002/esp.4963.
- [3] Andrew P Brooks, John Spencer, Nicholas Doriean, Tim J Pietsch, and Jorg Hacker. A comparison of methods for measuring water quality improvements from gully rehabilitation in great barrier reef catchments. In *Proceedings of the 9th Australian Stream Management Conference*, pages 1–8, Hobart, Australia, 2018.
- [4] Great Barrier Reef Marine Park Authority. Great Barrier Reef Outlook Report 2019, 2019. URL <http://hdl.handle.net/11017/3474>.
- [5] P B Hairsine and C W Rose. Modeling water erosion due to overland flow using physical principles: 1. Sheet flow. *Water Resources Research*, 28:237–243, 1992. doi:10.1029/91WR02380.
- [6] M.J. Prentice, M.W. Waud, D. P. Hamilton, and M. E. Roberts. Assessing performance of the MERGE model for simulating gully interventions. In *MODSIM2021, 24th International Congress on Modelling and Simulation*. Modelling and Simulation Society of Australia and New Zealand, December 2021. isbn:978-0-9872143-8-6. doi:10.36334/modsim.2021.L4.prentice. URL <https://mssanz.org.au/modsim2021/papers/L4/prentice.pdf>.
- [7] Ian P Prosser. Improving how gully erosion and river sediment transport processes are represented in Queensland catchment models, 2018. URL <https://www.des.qld.gov.au/science/documents/qwmn-gully-erosion-processes-report.pdf>.
- [8] M E Roberts. MERGE: modelling erosion resistance for gully erosion – a process-based model of erosion from an idealised linear gully. *Soil Research*, pages 1–16, 2020. doi:10.1071/SR20027. URL <https://doi.org/10.1071/SR20027>.
- [9] Melanie E Roberts. The erosion of an ideal gully under steady state conditions. In *23rd International Conference on Modelling and Simulation*, Canberra, Australia, 2019. doi:10.36334/modsim.2019.G1.roberts.
- [10] Melanie E Roberts. Regional pilot application of MERGE gully erosion model. Technical report, Australian Rivers Institute, Griffith University, 2022. URL <https://tinyurl.com/yrmhcc28>. A report to the Queensland Water Modelling Network.
- [11] Melanie E. Roberts, Ryan M. Burrows, Robin N. Thwaites, and David P. Hamilton. Modelling classical gullies – a review. *Geomorphology*, 407:108216, June 2022. ISSN 0169-555X. doi:10.1016/j.geomorph.2022.108216. URL <https://www.sciencedirect.com/science/article/pii/S0169555X2200109X>.

# Mathematical Modelling of nitrogen management on dairy farms

Steve Taylor, University of Auckland

Graeme Wake, Massey University,

Tony Pleasants, Al Rae Research Centre, Massey University

Andrea Babylon, Dairy NZ,

Joshua Duley, Toha.

## Basic problem

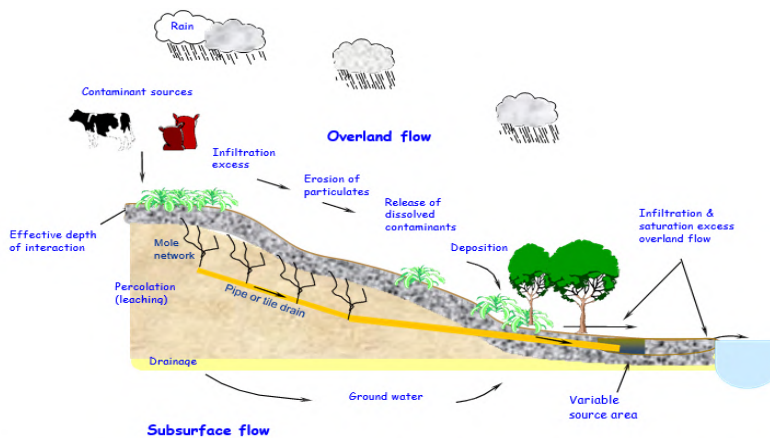


Figure 1. Schematic diagram of the typical hydrological flow paths in a catchment.

## Key points

- Grazing animals are a significant source of the contamination of rivers and streams through their deposit of dung and urine on the pasture.
- Measures to alleviate this problem are now the focus of farmers and regulatory bodies charged with addressing this problem.
- A cow typically deposits a concentration of 500 kg of nitrogen per hectare over an average area of 0.5 square meters.
- We need to understand the frequency of repeated deposits of urine at a single location.
- Efforts by farmers and regulators to manage this system are hampered by the lack of a suitable mathematical description of how this heterogeneous system evolves.



## Patch dynamics

- Let  $y$  be the uncontaminated fraction of an initially ungrazed field, so  $0 < y < 1$ .
- Let  $t$  be time measured in days and let  $y = Y(t)$  denote a realisation of the random change in  $y$ .
- We model the change in  $Y(t)$  over a small time interval  $[t, t + \Delta t]$  as

$$Y(t + \Delta t) - Y(t) = Y(t)(-\alpha \Delta t + \sigma (\Delta t)^{1/2} Z(t)),$$

where  $\alpha$  and  $\sigma$  are positive constants and  $Z(t)$  is a normal random variable with mean 0 and standard deviation 1.

## SDE approximation

$$dY = -\alpha Y dt + \sigma Y dW, \quad Y(0) = 1,$$

$$Y(t) = \exp\left(-\left(\alpha + \frac{1}{2}\sigma^2\right)t + \sigma W(t)\right).$$

This solution is obtained by setting

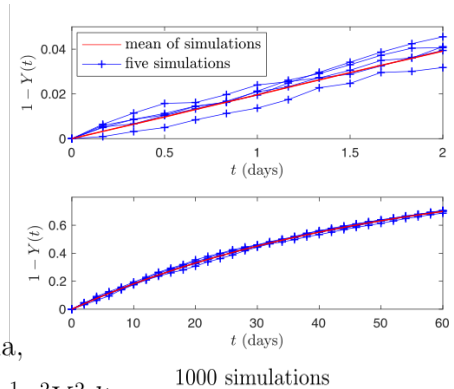
$$X = \log(Y) = g(Y).$$

Then  $X(0) = \log(Y(0)) = 0$  and by Itô's formula,

$$dX = g'(Y)dY + \frac{1}{2}\sigma^2 Y^2 g''(Y)dt = \frac{dY}{Y} + \frac{\frac{1}{2}\sigma^2 Y^2 dt}{Y^2}$$

$$= -\left(\alpha + \frac{1}{2}\sigma^2\right) dt + \sigma dW.$$

So,  $X(t) = -\left(\alpha + \frac{1}{2}\sigma^2\right)t + \sigma W(t)$ .

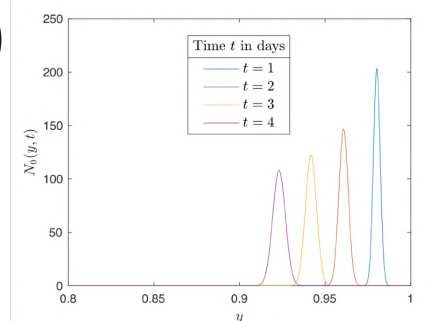


## Density function

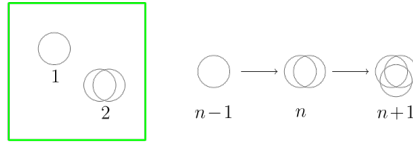
$Y(t)$ , being the exponential of a normal random variable, is a log-normal random variable with density function

$$N_0(y, t) = \frac{1}{\sigma y \sqrt{2\pi t}} \exp\left(-\frac{[(\alpha + \frac{1}{2}\sigma^2)t + \log(y)]^2}{2\sigma^2 t}\right)$$

$$\bar{Y}(t) = \mathbb{E}(Y(t)) = e^{-\alpha t}, \quad \text{var}(Y(t)) = e^{-2\alpha t} (e^{\sigma^2 t} - 1).$$



## The Multi-patch solution



The deterministic model gives an indication of what to expect...

$$\frac{dy_n}{dt} = -\alpha(y_n - y_{n-1}), \quad y_n(0) = \begin{cases} 1, & n = 0, \\ 0, & n \geq 1, \end{cases}$$

with  $y_{-1}(t) \equiv 0$ . Therefore,  $y_0(t) = e^{-\alpha t}$ .

Laplace transforms give  $y_n(t) = \frac{\alpha^n t^n}{n!} e^{-\alpha t}$ .

## Stochastic version

$$dY_n = -\alpha(Y_n - Y_{n-1})dt + \sigma(Y_n - Y_{n-1})dW, \quad n \geq 0.$$

where  $Y_{-1}(t) = 0$ ,  $W(t)$  is a Wiener process and

$$Y_n(0) = \begin{cases} 1, & n = 0, \\ 0, & \text{otherwise.} \end{cases}$$

Itô's formula leads to

$$Y_n(t) = Y_0(t) \frac{(-\log Y_0(t))^n}{n!},$$

where  $Y_0(t) = Y(t)$  is the fraction of clear field found earlier.

# Density functions

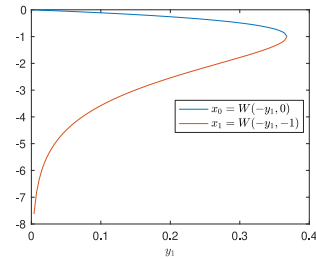
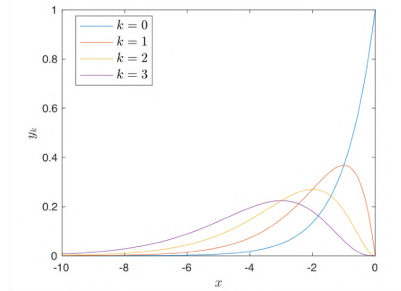
$Y_k(t)$  is related to the normal random variable  $X(t)$ :

$$Y_k(t) = \frac{(-X(t))^k}{k!} e^{X(t)}.$$

We use this to derive the density function for  $Y_k(t)$ .

This relies on the change of variable formula for density functions with variable change  $y_k = \frac{(-x)^k}{k!} e^x$ .

For  $k = 1$ , the inverses of this transformation are given by the two branches of the **Lambert  $W$  function**  
 $x_0 = W(-y_1, 0)$  and  $x_1 = W(-y_1, -1)$ .

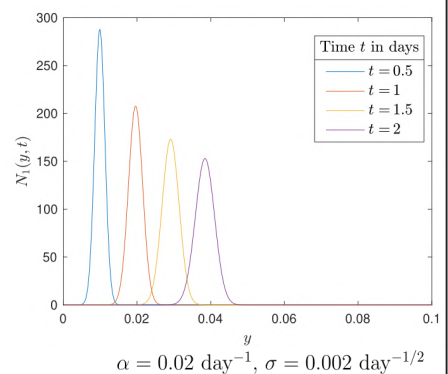


Let  $\phi(x, t)$  be the normal probability density function for  $X(t)$ :

$$\phi(x, t) = \frac{1}{\sqrt{2\pi\sigma^2 t}} \exp\left(-\frac{(x + (\alpha + \sigma^2/2)t)^2}{2\sigma^2 t}\right).$$

Let  $N_1(y_1, t)$  be the density function of  $Y_1(t)$ .

$$N_1(y_1, t) = -\phi(W(-y_1, 0), t) \frac{W(-y_1, 0)}{y_1(1 + W(-y_1, 0))} + \phi(W(-y_1, -1), t) \frac{W(-y_1, -1)}{y_1(1 + W(-y_1, -1))}.$$



Similarly,

$$N_m(y_m, t) = -\phi(x_0, t) \frac{x_0}{y_m(m+x_0)} + \phi(x_1, t) \frac{x_1}{y_m(m+x_1)}, \quad m \geq 1,$$

where  $x_0$  and  $x_1$  are given by:

$$\begin{aligned} x_0 &= mW(-(m!y_m)^{1/m}/m, 0), \\ x_1 &= mW(-(m!y_m)^{1/m}/m, -1). \end{aligned}$$

## Moments

$$\bar{Y}(t) = \mathbb{E}(Y(t)), \quad \bar{Y}_n(t) = \frac{\alpha^n t^n}{n!} e^{-\alpha t}.$$

$\text{cov}(Y_m Y_n)$  is the coefficient of  $s_1^m s_2^n$  in the expansion of

$$H(s_1, s_2, t) = \left[ e^{(s_1-1)(s_2-1)\sigma^2 t} - 1 \right] e^{(s_1+s_2-2)\alpha t}.$$

A few examples of these covariances are given below.

$$\text{var}(Y_0(t)) = e^{-2\alpha t} (e^{\sigma^2 t} - 1).$$

$$\text{var}(Y_1(t)) = te^{-2\alpha t} (e^{\sigma^2 t} (\alpha^2 t + \sigma^2(1 - 2\alpha t) + \sigma^4 t) - \alpha^2 t).$$

$$\text{cov}(Y_0(t)Y_1(t)) = te^{-2\alpha t} (\alpha (e^{\sigma^2 t} - 1) - \sigma^2 e^{\sigma^2 t}).$$

$$\text{cov}(Y_0(t)Y_2(t)) = \frac{1}{2} t^2 e^{-2\alpha t} (\alpha^2 (e^{\sigma^2 t} - 1) - 2\alpha\sigma^2 e^{\sigma^2 t} + \sigma^4 e^{\sigma^2 t}).$$

# Back to the farm...

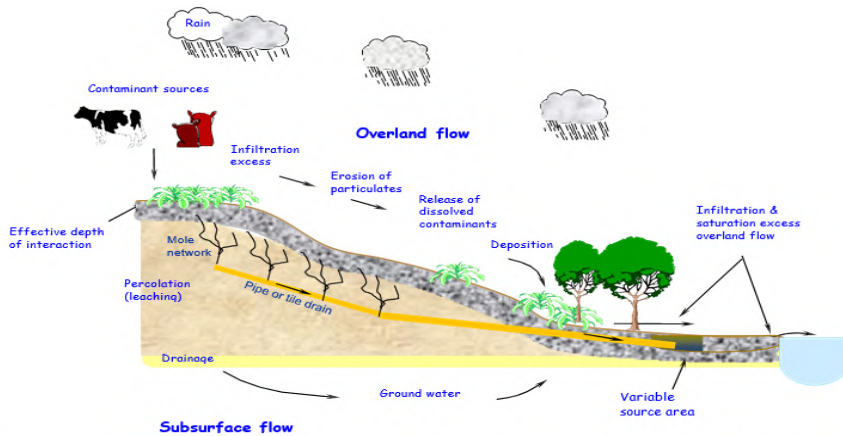
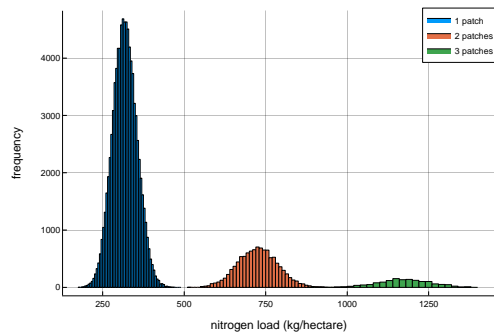


**Figure 1.** Schematic diagram of the typical hydrological flow paths in a catchment.

## Nitrogen load

The concentration of nitrogen in a urine patch has been shown to be lognormally distributed by Selbie et al. Combining this with our result gives distributions of nitrogen load across a field.



D. R. Selbie, L. E. Buckthought, M. A. Shepherd, The challenge of the urine patch for managing nitrogen in grazed pasture systems, *Advances in agronomy* 129 (2015) 229–292. doi:10.1016/bs.agron.2014.09.004.



## What happens to the nitrogen after deposition?

- Water: Rainfall, horizontal transport, transpiration.

$$\frac{dw}{dt} = R(t) - \beta(w - w_f)H(w - w_f) - PET(t)$$

- Plants: Logistic growth above wilting, grazing.

$$\frac{dP}{dt} = g \left(1 - \frac{P}{K}\right) H(w - w_w) - zN \frac{P}{P + \gamma} = f_P(P, N, w).$$

- Nitrogen: Plant uptake, catchment flow above saturation.

$$\begin{aligned} \frac{dN}{dt} &= -k_3NT(t) - k_2N\beta(w - w_f)H(w - w_f) \\ &\quad - k_1NgP \left(1 - \frac{P}{K}\right) H(w - w_w) = f_N(P, N, w) \end{aligned}$$

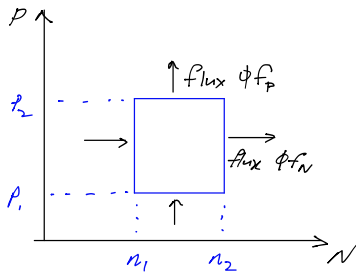
## Coupling nitrogen attenuation with the patch model?

- For rotational grazing, cows are put on a clean field for a short amount of time (1 or two days).
- In this case, attenuation and grazing are effectively not coupled. We can follow the evolution of nitrogen after the cows leave.
- What if they return? What about more general cases of grazing?
- We need to see how to couple these models.

## Need to modify the patch model

- Distribution of field fraction  $\phi = \phi(N, P, t)$ .
- Fraction of field with  $N \in (n_1, n_2)$  and  $P \in (p_1, p_2)$  is

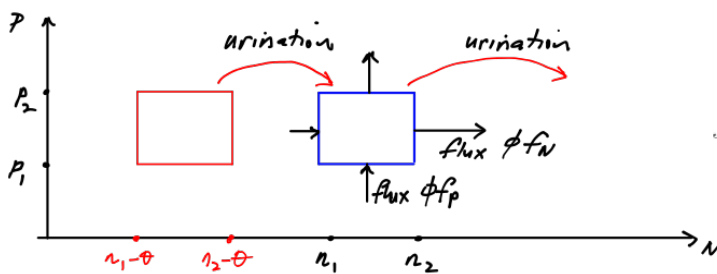
$$\int_{n_1}^{n_2} \int_{p_1}^{p_2} \phi(N, P, t) dP dN$$



$$\text{Nitrogen rate equation: } \frac{dN}{dt} = f_N(N, P), \quad (1)$$

$$\text{Biomass rate equation: } \frac{dP}{dt} = f_P(N, P). \quad (2)$$

## Conservation law



$$J = \int_{p_1}^{p_2} \int_{n_1}^{n_2} \phi(N, P, t) dN dP.$$

$$\Delta J_N = \left\{ \int_{p_1}^{p_2} f_N(n_1, P, t) \phi(n_1, P, t) dP - \int_{p_1}^{p_2} f_N(n_2, P, t) \phi(n_2, P, t) dP \right\} \Delta t,$$

$$= \Delta t \int_{p_1}^{p_2} f_N(n_1, P, t) \phi(n_1, P, t) - f_N(n_2, P, t) \phi(n_2, P, t) dP,$$

$$= -\Delta t \int_{p_1}^{p_2} \int_{n_1}^{n_2} \frac{\partial}{\partial N} [f_N(N, P, t) \phi(N, P, t)] dN dP.$$

Similarly, biomass flux is given:

$$\Delta J_P = -\Delta t \int_{p_1}^{p_2} \int_{n_1}^{n_2} \frac{\partial}{\partial P} [f_P(N, P, t)\phi(N, P, t)] dN dP.$$

Urine deposits expressed:

$$\Delta J_U = (\alpha\Delta t + \beta\Delta B) \int_{p_1}^{p_2} \int_{n_1}^{n_2} \phi(N - \theta, P, T) - \phi(N, P, t) dN dP$$

$$\frac{\partial \phi}{\partial t} = \left( \alpha + \beta \frac{\Delta B}{\Delta t} \right) [\phi(N - \theta) - \phi(N)] - \frac{\partial}{\partial N} [f_N \phi] - \frac{\partial}{\partial P} [f_P \phi].$$

For deterministic stocking rate and urination frequency this reduces to:

$$\frac{\partial \phi}{\partial t} = \alpha [\phi(N - \theta) - \phi(N)] - \frac{\partial}{\partial N} [f_N \phi] - \frac{\partial}{\partial P} [f_P \phi].$$

## Some features of this system

- The characteristic ODEs of the related first order PDE are the attenuation equations,  $\frac{dN}{dt} = f_N$ ,  $\frac{dP}{dt} = f_P$ .

- It's easy to verify that

$$\int_0^\infty \int_0^\infty \phi(N, P, t) dP dN = \text{constant} = 1.$$

- Similarly, for the nitrogen load

$$L = \int_0^\infty \int_0^\infty N \phi(N, P, t) dP dN,$$

$$\frac{dL}{dt} = \theta\alpha + \int_0^\infty \int_0^\infty f_N \phi dP dN$$

## Next steps...

- Model the flow to waterways.
- Measurements in waterways.

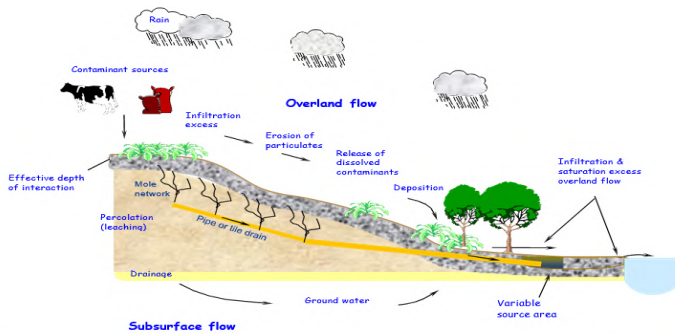
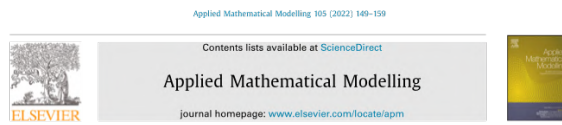


**Figure 1.** Schematic diagram of the typical hydrological flow paths in a catchment.

## Reference

Details of the first part of this talk are in...



### Modelling nutrient deposition from intensive agricultural practices

S.W. Taylor<sup>a,\*</sup>, A.B. Pleasants<sup>b</sup>, A.M. Babylon<sup>c</sup>, G.C. Wake<sup>d</sup>

<sup>a</sup>Mathematics Department, University of Auckland, Auckland, New Zealand

<sup>b</sup>AI Bar Centre for Genetics and Animal Breeding, Massey University, New Zealand

<sup>c</sup>DairyNZ Ltd, Hamilton, New Zealand

<sup>d</sup>Department of Mathematical Sciences, Auckland University of Technology, Auckland, New Zealand



This work is ongoing and is part of a team project partially supported by DairyNZ under the Project # CB1915-2020 Dynamic N Modelling & Agmardt Grant #A21048-2021. DairyNZ is an industry-led organization with head office based in Hamilton, New Zealand.

# Modelling flexural strains at the outer margins of Antarctic ice shelves caused by ocean waves

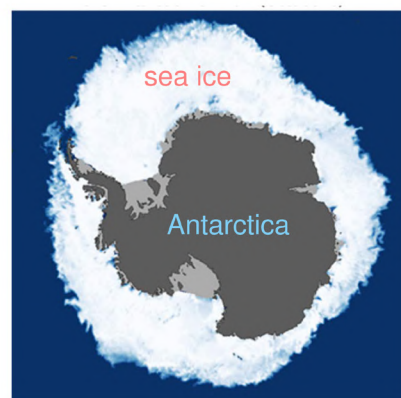
Luke Bennetts  
University of Adelaide



## Antarctic ice

### Antarctic sea ice

- Frozen ocean surface = salty
- Centimetres to metres thick
- Seasonal cycle of growth & retreat
- Doubles size of Antarctica at winter maximum



credit: NASA

## Antarctic ice

nilas



pancakes



floes

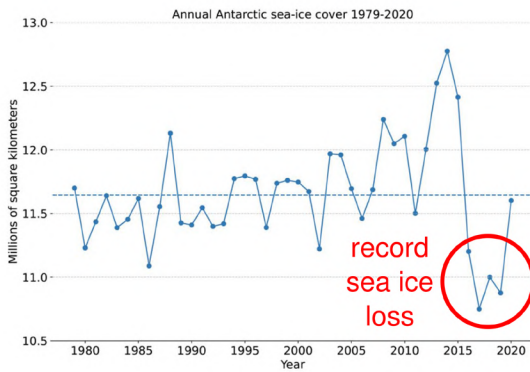


quasi-continuous



credit: NASA

## Antarctic ice



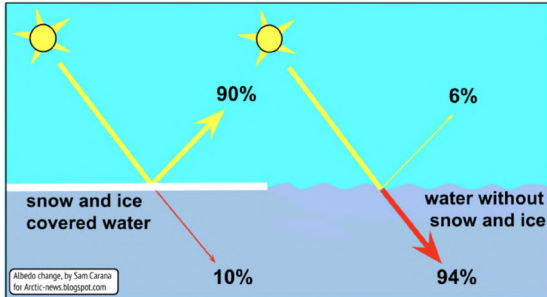
credit: C Eayrs



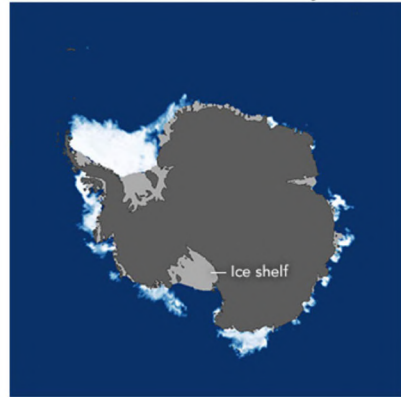
credit: NASA

## Antarctic ice

Ice albedo feedback  
less ice → warmer ocean → less ice



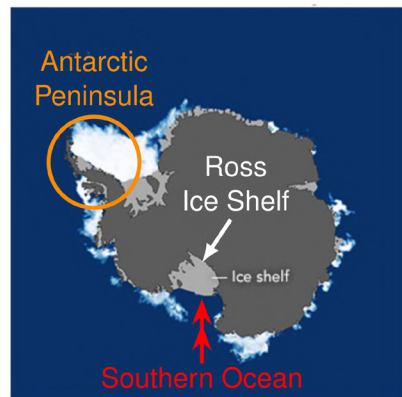
credit: S Carana



credit: NASA

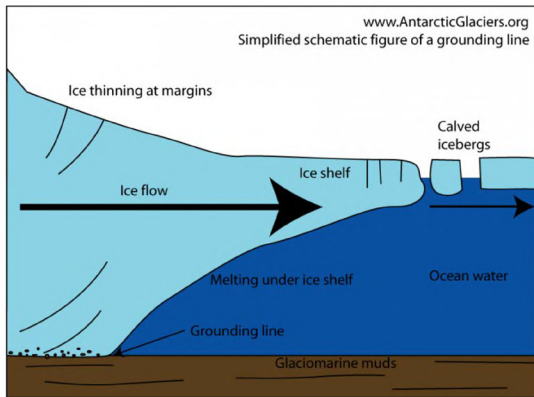
## Antarctic ice

sea ice loss also causes problems in "horizontal plane"



credit: NASA

# Antarctic ice



www.AntarcticGlaciers.org

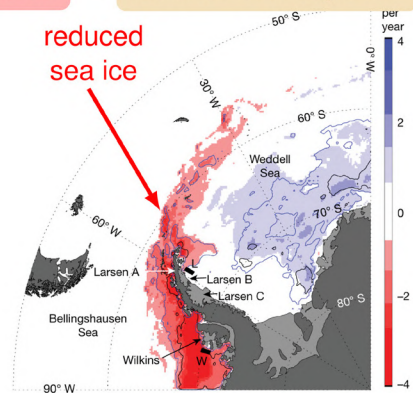
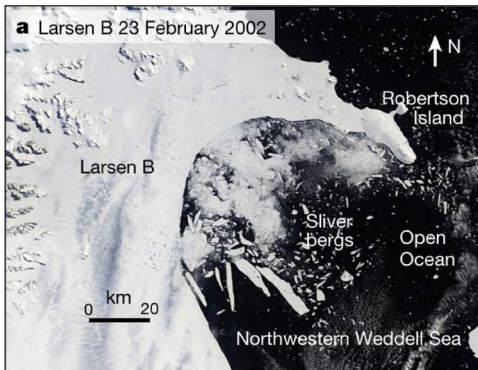
## Antarctic ice shelves

- Floating extensions of Antarctic ice sheet
- Occupy  $\approx \frac{1}{2}$  coastline
- Hundreds of metres thick
- Hundreds of kilometres long
- Moderate ice flow into ocean
- Restrain sea level rise

# Ice shelf disintegrations on Antarctic Peninsula

## Conceptual model

Reduced sea ice barrier → Swell reaches shelves → Ice shelf disintegration



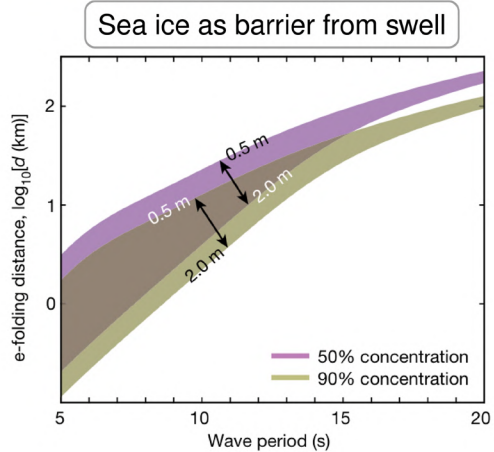
Massom et al, 2018, Nature



## Ice shelf disintegrations on Antarctic Peninsula

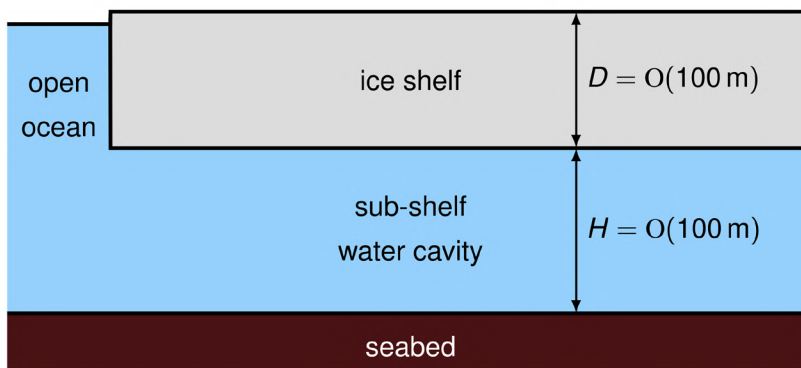
### Mathematical modelling for conceptual model

- 1 Sea ice as barrier from swell
  - Sea ice attenuates swell exponentially over distance.
  - Attenuation rate decreases with wave period and increases with ice thickness.
- 2 Wave-induced ice shelf strains
  - Waves increasingly penetrate into shelf as period increases.
  - Create flexural-gravity waves in shelf that impart strain.
  - Wavelengths increase with period = decreasing strain

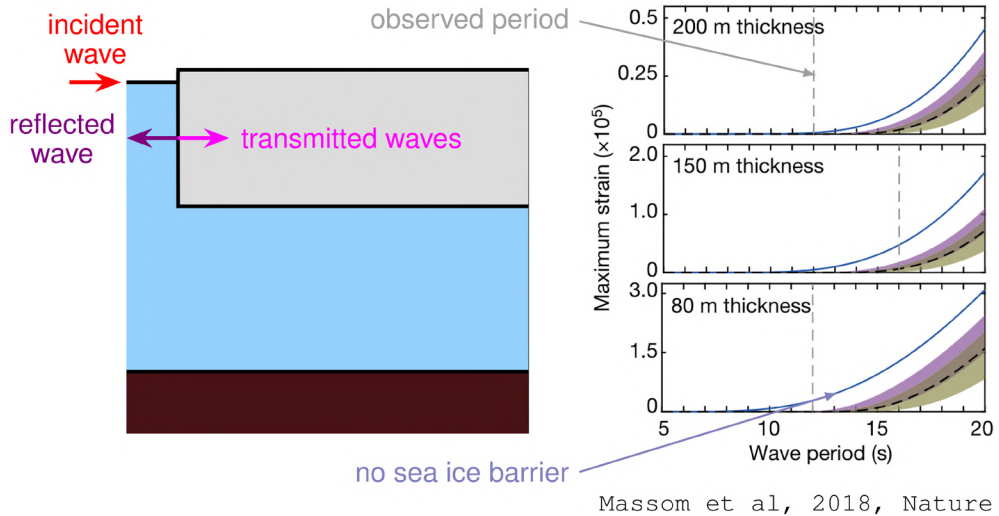


Massom et al, 2018, Nature

## Mathematical model: Wave-induced ice shelf strain



## Mathematical model: Wave-induced ice shelf strain

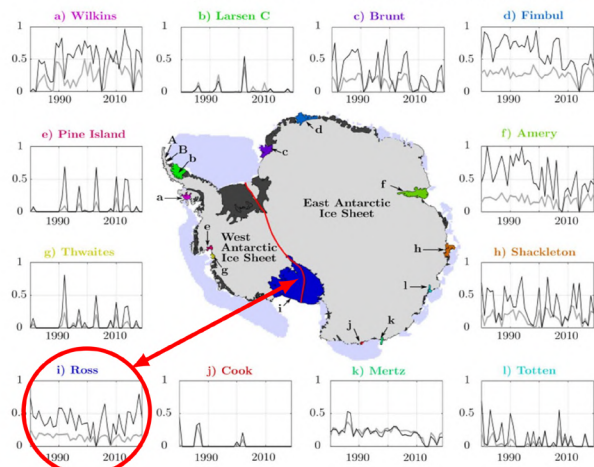


## Sea ice free corridors to ice shelves

- Sea ice free corridors allow swell to reach ice shelves unimpeded
- Developed algorithm to extract corridors
- Daily sea ice concentration data over satellite era 1979–
- Analysed 69 ice shelves around Antarctica

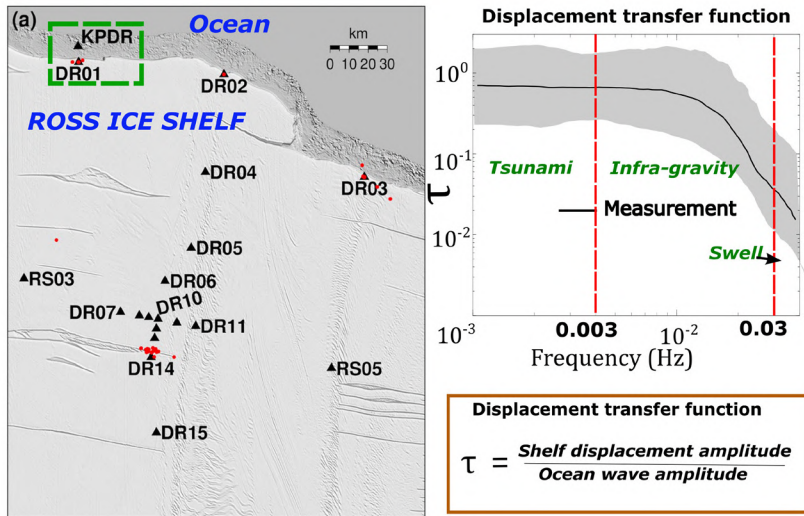
Observations of wave-induced flexure exist on Ross Ice Shelf

– Corridor days fraction – Max corridor area



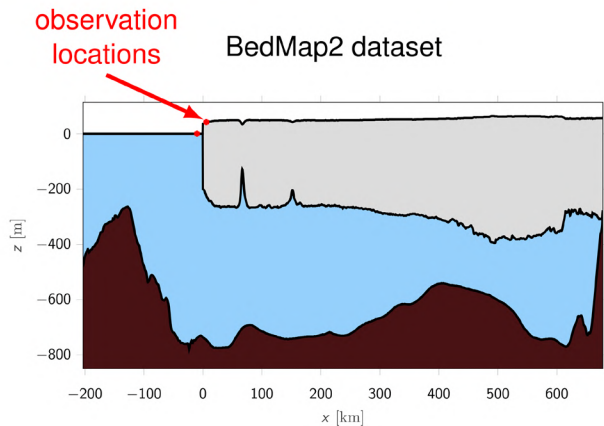
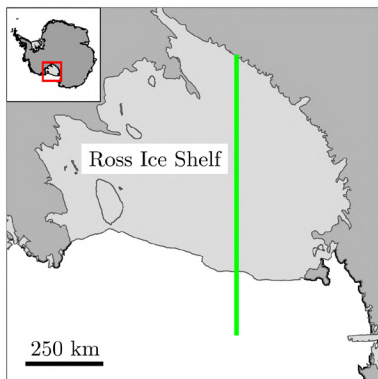
Teder et al, 2022, Env Res Lett

## Observations: Ross Ice Shelf vibrations



Chen et al, Geophys. Res. Lett., 2019

## Model validation



Fretwell et al, 2013, Cryosphere

## Model validation

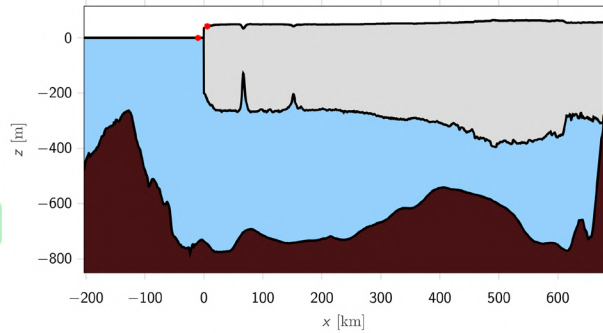
### Modelling challenges

- Coupled fluid–solid motion
- Wide frequency spectrum
- $\sim 1000$  km varying geometry = non-constant coefficients
- 100s of transects

### Approximation methods

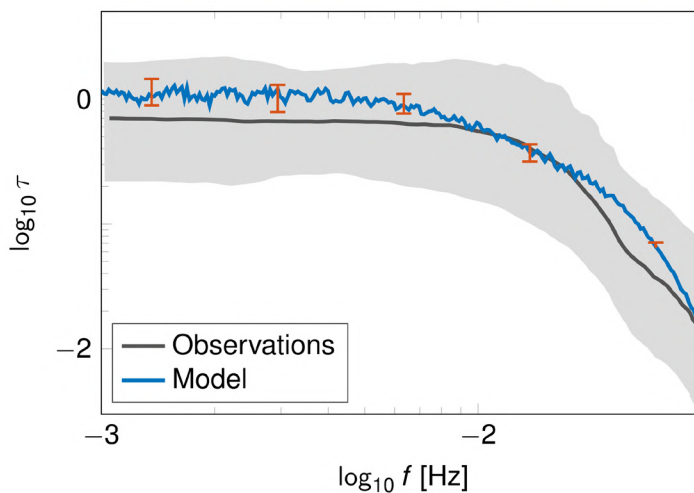
- 1 'Single mode' depth average  
⇒ ODE system
- 2 Step approximation  
⇒ Linear system  
⇒ Recursive solution

BedMap2 dataset



Fretwell et al, 2013, Cryosphere

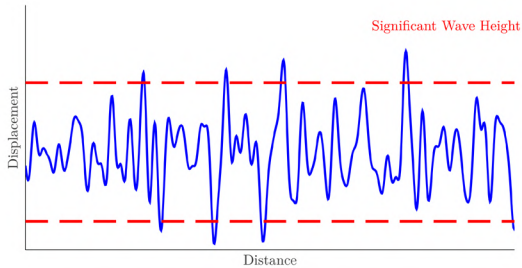
## Model validation: Displacement transfer function



Bennetts et al, 2022, Geophys Res Lett

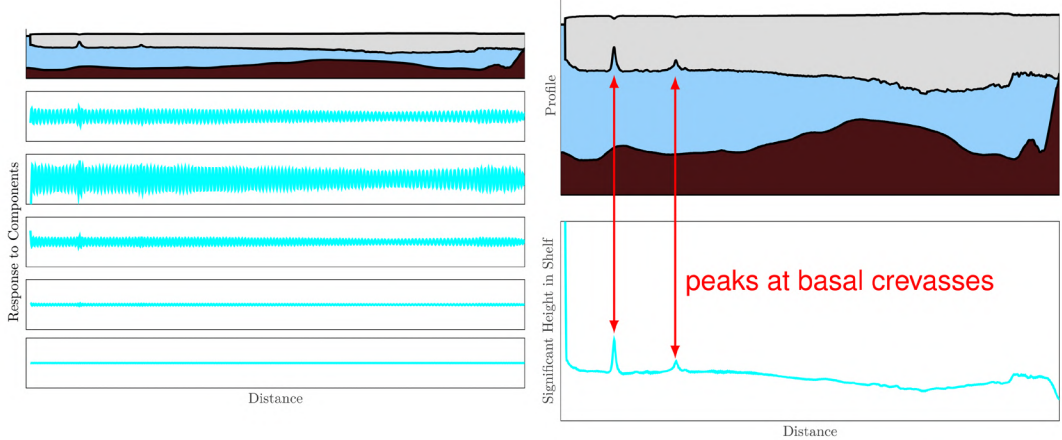
## Irregular ocean Waves

Ocean waves are irregular, i.e. not sinusoidal!!!

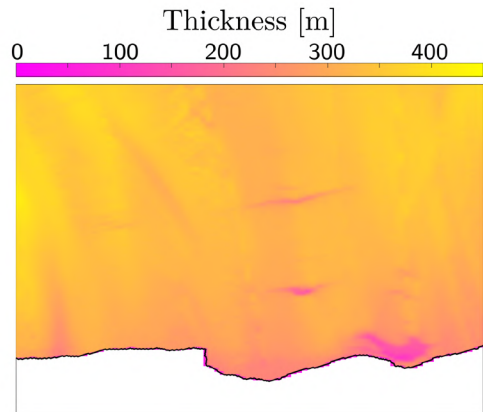
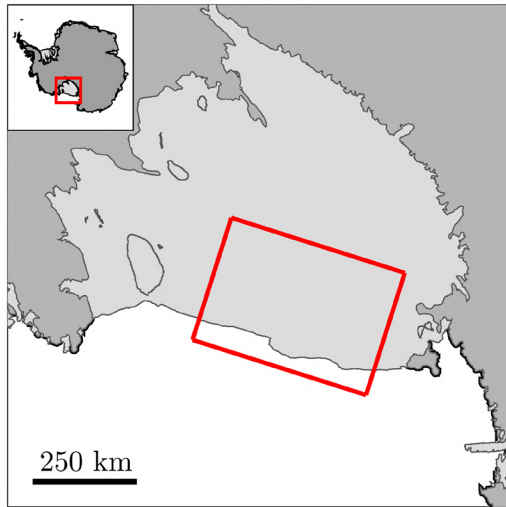


- Significant wave height
- Peak period
- (Mean wave direction)
- Superposition of spectral (frequency/period) components
- Random phase of spectral components

## Irregular ocean Waves

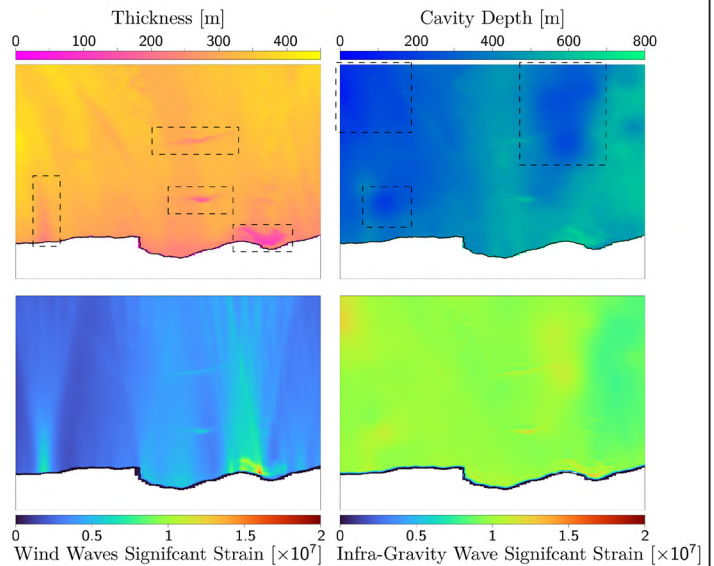


## Ross Ice Shelf



## Ross Ice Shelf strain: Swell vs IG waves

- Ice shelf crevasses = local thinning
- Seabed protrusions = local shallowing
- Swell period 13 s
- Swell height 6.7 m
- IG period 67 s
- IG height 30 mm



## What's next?

### Applications

- Quantify strains leading up to disintegration events . . .
- . . . and strains withstood by other shelves
- Link with 'glaciological factors'

### Model development

- Ice shelf grounding line condition
- Viscosity / damping
- Three-dimensionality
- Narrow features (cracks and rifts) → advanced plate models



**Mathematics: key enabling technology for scientific machine learning**

FORUM MATHEMATICS FOR INDUSTRY  
MELBOURNE, NOVEMBER 21-24, 2022

Wil Schilders, TU Eindhoven & Hans Fischer senior fellow TUM-IAS  
President-elect ICIAM

Department of Mathematics and Computer Science

**TU/e** EINDHOVEN UNIVERSITY OF TECHNOLOGY

## Happy to be at FMI again!

- Great to see that this event is continuing to be held every year, in different (and nice!) places in the Asia-Pacific region
- Fantastic that APCMfI is so successful – with similar experiences as ECMI in Europe
- Love to experience more of the beautiful city of Melbourne



2 Wil Schilders - Mathematics: key enabling technology for scientific machine learning

**TU/e**



## FMI 2022: "Mathematics of Public Health and Sustainability"

- Excellent topic for a conference; mathematics is indispensable in our complex world with the many challenges we are facing in sustainability, climate, energy transition and more
- In this context, I would like to remind you of the International Year of Basic Sciences for Sustainable Development (IYBSSD 2022) that has been initiated by the ISC
- See [www.iybssd2022.org](http://www.iybssd2022.org); suggest to mention FMI 2022 as an event here

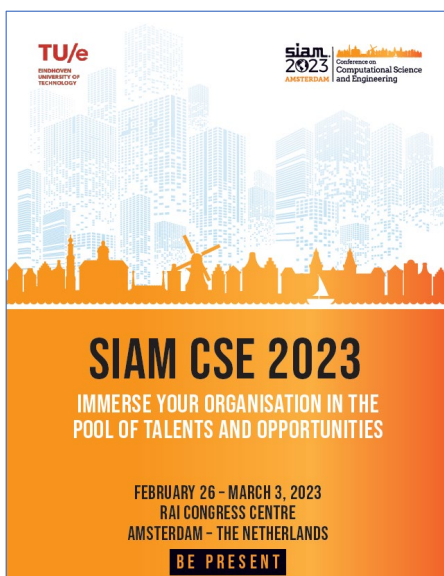


**SUSTAINABLE DEVELOPMENT GOALS**  
17 GOALS TO TRANSFORM OUR WORLD



3 Wil Schilders - Mathematics: key enabling technology for scientific machine learning

**TU/e**



## Advertisement

2200+ participants expected

8 renowned invited speakers on a variety of topics

Public event with 5 TED talks, advertising mathematics to the general public and broadcast world-wide

Hackathon in weekend before conference, with challenges from 6 major companies like Siemens, ASML (great for young talented researchers)

<https://www.siam.org/conferences/cm/conference/cse23>

Registration will open November 26

## Advertisement (2)

- ICIAM organizes a major conference on industrial and applied mathematics every 4 years
- ICIAM 2023 will be held in Tokyo, August 20-25
- You are all encouraged to submit proposals for mini-symposia!
- Hope yo see many of you in Tokyo



5 Wil Schilders - Mathematics: key enabling technology for scientific machine learning

TU/e

## Contents

- Some opening thoughts
- Artificial Intelligence, Machine Learning and Neural Networks
- Hybrid methods: combining CSE and AI methods
- Example 1: Dynamic neural networks
- Example 2: Geometric concepts and AI
- Conclusion

6 Wil Schilders - Mathematics: key enabling technology for scientific machine learning

TU/e



## But then.....

1. High Performance Computing started (again) to become important, and in fact inevitable due to the ending of Moore's Law
  - Numerical methods needed to be made parallelizable



## But then.....

1. High Performance Computing started (again) to become important, and in fact inevitable due to the ending of Moore's Law
  - Numerical methods needed to be made parallelizable
  - ICCG, for example, shows a very bad performance on current supercomputers



Rank	Site	Computer	Cores	HPL Rmax (Pflop/s)	TOP500 Rank	HPCG (Pflop/s)	Fraction of Peak
1	DOE/SC/ORNL USA	Summit, AC922, IBM POWER9 22C 3.7GHz, Dual-rail Mellanox FDR, NVIDIA Volta V100, IBM	2,397,824	148.60	1	2.926	1.5%
2	DOE/NNSA/LLNL USA	Sierra, S922LC, IBM POWER9 20C 3.1 GHz, Mellanox EDR, NVIDIA Volta V100, IBM	1,572,480	94.64	2	1.796	1.4%
3	RIKEN Advanced Institute for Computational Science Japan	K computer, SPARC64 VIIIfx 2.0GHz, Tofu interconnect, Fujitsu	705,024	10.51	18	0.603	5.3%
4	DOE/NNSA/LANL/SNL USA	Trinity, Cray XC40, Intel Xeon E5-2698 v3 16C 2.3GHz, Aries, Cray	979,072	20.16	6	0.546	1.3%
5	Natl. Inst. Adv. Industrial Sci. and Tech. (AIST) Japan	ABCI, PRIMERGY CX2570M4, Intel Xeon Gold 6148 20C 2.4GHz, Infiniband EDR, NVIDIA Tesla V100, Fujitsu	368,640	16.86	10	0.509	1.7%
6	Swiss National Supercomputing Centre (CSCS) Switzerland	Piz Daint, Cray XC50, Intel Xeon E5-2690v3 12C 2.6GHz, Cray Aries, NVIDIA Tesla P100 16GB, Cray	387,872	21.23	5	0.497	1.8%
7	National Supercomputing Center in Wuxi China	Sunway TaihuLight, Sunway MPP, SW26010 260C 1.45GHz, Sunway, NRCPC	10,649,600	93.02	3	0.481	0.4%
8	Korea Institute of Science and Technology Information Republic of Korea	Nurion, CS500, Intel Xeon Phi 7250 68C 563584C 1.4GHz, Intel Omni-Path, Intel Xeon Phi 7250, Cray	570,020	13.93	13	0.391	1.5%
9	Joint Center for Advanced High Performance Computing Japan	Oakforest-PACS, PRIMERGY CX600 M1, Intel Xeon Phi Processor 7250 68C 1.4GHz, Intel Omni-Path Architecture, Fujitsu	556,104	13.55	14	0.385	1.5%
10	DOE/SC/LBNL/NERSC USA	Cori, XC40, Intel Xeon Phi 7250 68C 1.4GHz, Cray Aries, Cray	622,336	14.02	12	0.355	1.3%

HPCG Benchmark June 2019

## But then.....

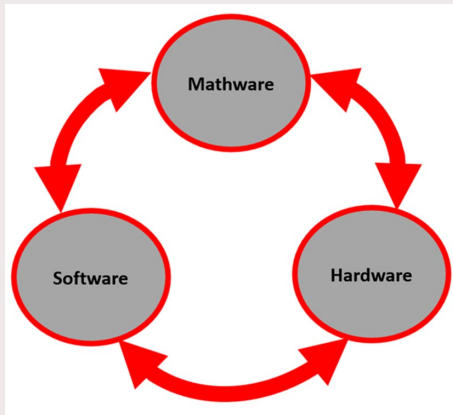
- High Performance Computing started (again) to become important, and in fact inevitable due to the ending of Moore's Law
  - Numerical methods needed to be made parallelizable
  - ICCG, for example, shows a very bad performance on current supercomputers
  - Hence, for the solution of sparse linear systems, entirely new methods need to be developed

**REVOLUTIONARY NEW IDEAS NEEDED!**

(NLAFET project of Iain Duff and Jack Dongarra)



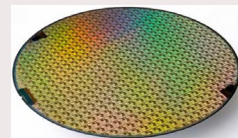
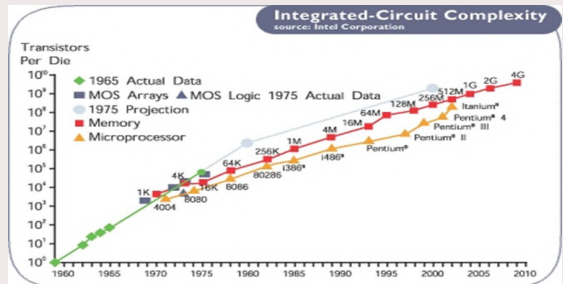
## Mathematical method development for HPC



- Mathematical method development must be distinguished from software and hardware
- **Mathware** researchers must engage in discussions with software and hardware colleagues to achieve optimal results
- Example: ease transformations between 16, 32 and 64 bit representations (using FPGA?)

## And there is Mo(o)re

The main engine behind the electronics industry is Moore's law: every 2 years the speed and density of transistors is doubled (general knowledge!)



## Mathematical methods are outperforming hardware improvements (not general knowledge!)

Mathematical method	Period (years)	Improvement hardware	Improvement mathware
Solving large linear systems	35	10.000.000	10.000.000
Linear programming	16	1600	3300
Mixed integer programming	25	6500	870.000
Particle simulations	40	100.000.000	1.000.000.000

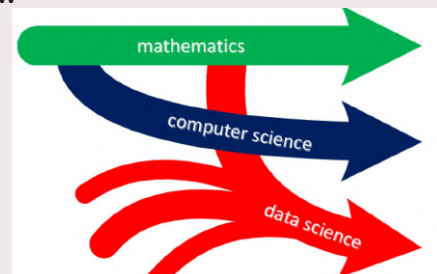
(180 years  
→ 1  
second)

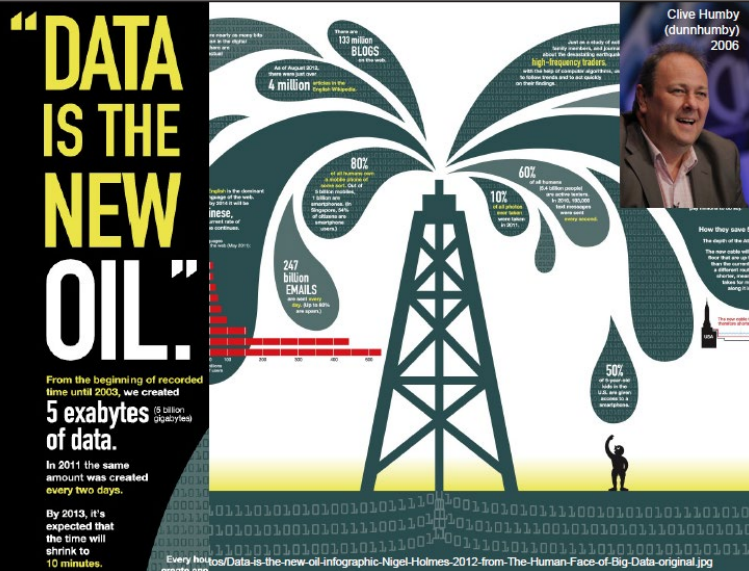
We should aim at a similar development for parallel computing!

**TU/e**

## But then.....

1. High Performance Computing started (again) to become important, and in fact inevitable due to the ending of Moore's Law
2. Data Science emerged as a discipline, and quickly became part of the curriculum at universities





PAGE 17 Wil Schilders - Mathematics: key enabling technology for scientific machine learning

- exploration (locating the data),
- extraction (how to get it),
- transform (clean and filter data)
- storage (Big Data)
- transport (getting it to the right person)
- usage (analysis, actions, etc.)



- data can be copied, oil not
- data is specific, oil is not
- if small, data storage and transport are cheap

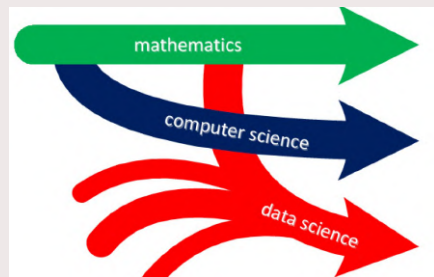
PAGE 18 Wil Schilders - Mathematics: key enabling technology for scientific machine learning



## But then.....

1. High Performance Computing started (again) to become important, and in fact inevitable due to the ending of Moore's Law
2. Data Science emerged as a discipline, and quickly became part of the curriculum at universities
  - It is an emerging discipline on the crossroads of multiple existing disciplines
  - David Donohue (Stanford): "50 years of Data Science"

**REVOLUTIONARY NEW IDEAS NEEDED!**



## But then.....

1. High Performance Computing started (again) to become important, and in fact inevitable due to the ending of Moore's Law
2. Data Science emerged as a discipline, and quickly became part of the curriculum at universities
3. Artificial Intelligence became extremely popular, with techniques for deep learning, in combination with big data

**MANY NEW CHALLENGES AHEAD!**



**Quoting Karen Willcox (Oden, Texas)**

*"It is such an exciting time to be a computational scientist. The field is in the midst of a tremendous convergence of technologies that generate unprecedented system data and enable automation, algorithms that let users process massive amounts of data and run predictive simulations that drive key decisions, and the computing power that makes these algorithms feasible at scale for complex systems and in real-time or in situ settings."*



We will concentrate on the third topic:

*Combining methods from the fields of Computational Science and Engineering (CSE) and Artificial Intelligence (AI)*

# ARTIFICIAL INTELLIGENCE, MACHINE LEARNING AND NEURAL NETWORKS

Real and Artificial Intelligence for Science and Engineering – Wil Schilders

**TU/e** EINDHOVEN  
UNIVERSITY OF  
TECHNOLOGY



## Artificial Intelligence (AI)

- The origins of AI can be traced back to the desire to build thinking machines, or electronic brains.
- In 1958, Frank Rosenblatt created the first artificial neuron that could learn by iteratively strengthening the weights of the most relevant inputs and decreasing others to achieve a desired output.

24 Wil Schilders - Mathematics: key enabling technology for scientific machine learning

**TU/e**

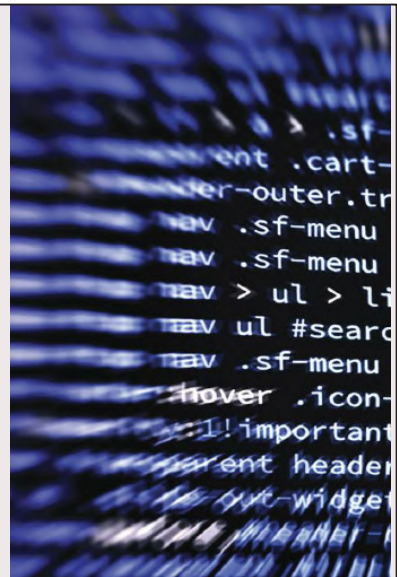
## Brain-inspired AI

- Computation in brains and the creation of intelligent systems have been studied in a symbiotic fashion for many decades.
- Europe has become a hotspot of brain-inspired computing research, the progress being accelerated by the FET flagship “Human Brain Project”.
- In technology roadmaps, brain-inspired computing is commonly seen as a future key enabler for AI on the edge.
- Researchers at INRIA have presented an interdisciplinary approach towards transferring neuroscientific findings to new models of AI. Quoting them: *“Major algorithms from artificial intelligence (AI) lack higher cognitive functions such as problem solving and reasoning.”*



## Machine Learning (ML)

- The discipline of machine learning is often conflated with the general field of AI, but machine learning specifically is concerned with the question of how to develop algorithms and program computers to automatically recognise complex patterns and make intelligent decisions based on data.
- It involves probability theory, logic, combinatorial optimization, statistics, reinforcement learning and control theory.
- Applications are ubiquitous, ranging from vision to language processing, forecasting, pattern recognition, games, data mining, expert systems and robotics.



## History of Machine Learning

- Arthur Samuels popularized the term “machine learning” in 1959; he built a checkers-playing program alongside efforts to understand the computational principles underlying human learning, in the developing field of **neural networks**.
- In the ‘90s, statistical AI emerged, formulating machine learning problems in terms of probability measures.
- Since then, the emphasis has vacillated between statistical and probabilistic learning and progressively more competitive neural network approaches.

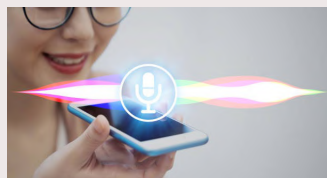


27 Wil Schilders - Mathematics: key enabling technology for scientific machine learning

TU/e

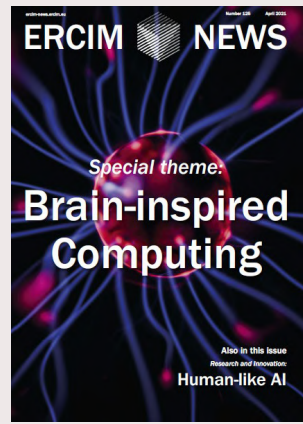
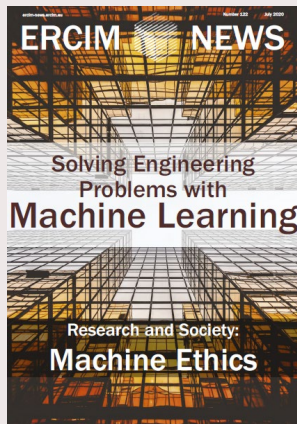
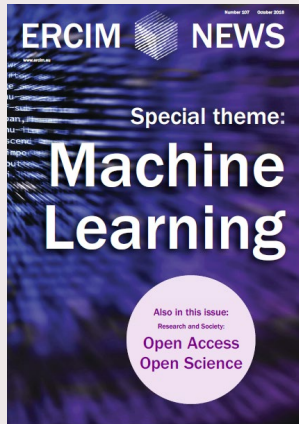
## Breakthrough in Machine Learning

- The breakthrough work by Krizhevsky, Sutskever & Hinton in 2012 has been a catalyst for AI research. They used a **deep neural network** trained exhaustively on GPUs.
- Similar advances were then quickly reported for speech recognition and later for machine translation and natural language processing.
- Companies like Google, Microsoft and Baidu established large machine learning groups.
- Since then, with the combination of big data and big computers, rapid advances have been reported, including the use of machine learning for self-driving cars, and consumer-grade real-time speech-to-speech translation.



28 Wil Schilders - Mathematics: key enabling technology for scientific machine learning

TU/e



# MACHINE LEARNING TRANSFORMING OUR WORLD

## Tackling Climate Change with Machine Learning

David Rotnick<sup>1,5</sup>, Priya L. Donti<sup>2</sup>, Lynn H. Kaack<sup>3</sup>, Kelly Kochanski<sup>4</sup>, Alexandre Lacoste<sup>5</sup>, Kris Sankaran<sup>6,7</sup>, Andrew Slavin Ross<sup>8</sup>, Nikola Milojevic-Dupont<sup>10,11</sup>, Natasha Jaques<sup>12</sup>, Anna Waldman-Brown<sup>13</sup>, Alexandra Luccioni<sup>10</sup>, Tegan Maharaj<sup>6,9</sup>, Evan D. Sherwin<sup>4</sup>, S. Karthik Mukkavilli<sup>10,7</sup>, Konrad P. Körding<sup>1</sup>, Carla Gomes<sup>14</sup>, Andrew Y. Ng<sup>14</sup>, Demis Hassabis<sup>15</sup>, John C. Platt<sup>16</sup>, Felix Creutzig<sup>10,11</sup>, Jennifer Chayes<sup>17</sup>, Yoshua Bengio<sup>6,7</sup>

<sup>1</sup>University of Pennsylvania, <sup>2</sup>Carnegie Mellon University, <sup>3</sup>ETH Zürich, <sup>4</sup>University of Colorado Boulder, <sup>5</sup>Element AI, <sup>6</sup>Mila, <sup>7</sup>Université de Montréal, <sup>8</sup>École Polytechnique de Montréal, <sup>9</sup>Harvard University, <sup>10</sup>Mercator Research Institute on Global Commons and Climate Change, <sup>11</sup>Technische Universität Berlin, <sup>12</sup>Massachusetts Institute of Technology, <sup>13</sup>Cornell University, <sup>14</sup>Stanford University, <sup>15</sup>DeepMind, <sup>16</sup>Google AI, <sup>17</sup>Microsoft Research

### Abstract

Climate change is one of the greatest challenges facing humanity, and we, as machine learning experts, may wonder how we can help. Here we describe how machine learning can be a powerful tool in reducing greenhouse gas emissions and helping society adapt to a changing climate. From smart grids to disaster management, we identify high impact problems where existing gaps can be filled by machine learning, in collaboration with other fields. Our recommendations encompass exciting research questions as well as promising business opportunities. We call on the machine learning community to join the global effort against climate change.

## Google AI Blog

The latest news from Google AI

## Using Machine Learning to “Nowcast” Precipitation in High Resolution

Monday, January 13, 2020

Posted by Jason Hickey, Senior Software Engineer, Google Research

The weather can affect a person’s daily routine in both mundane and serious ways, and the precision of forecasting can strongly influence how they deal with it. Weather predictions can inform people about whether they should take a different route to work, if they should reschedule the picnic planned for the weekend, or even if they need to evacuate their homes due to an approaching storm. But making accurate weather predictions can be particularly challenging for localized storms or events that evolve on hourly timescales, such as thunderstorms.

In “Machine Learning for Precipitation Nowcasting from Radar Images,” we are presenting new research into the development of machine learning models for precipitation forecasting that addresses this challenge by making highly localized “physics-free” predictions that apply to the immediate future. A significant advantage of machine learning is that inference is computationally cheap given an already-trained model, allowing forecasts that are nearly instantaneous and in the native high resolution of the input data. This precipitation nowcasting, which focuses on 0-6 hour forecasts, can generate forecasts that have a 1km resolution with a total latency of just 5-10

5.05433v2 [cs.LG] 5 Nov 2019

## Criticism is growing...

- The much-glorified deep learning approaches all rely on the availability of massive amounts of data, often needing millions of correctly labelled examples.
- Many domains, however, including some important areas such as health care, will never have such massive labelled datasets.
- Similarly, robots cannot be trained for millions of trials, simply because they wear out long before.
- **The question is thus how to learn more with less. Here, statistics and prior knowledge will likely play a big role.**

## Criticism is growing...

There are serious limitations to current methods, as well as to our understanding of the success of machine learning techniques such as deep neural networks.

Professor Robbert Dijkgraaf\* compares machine learning with 16<sup>th</sup> century alchemy, based on an accumulation of tricks topped with a good shot of credulity rather than on a systematic analysis.

He also quotes Ali Rahimi, a well-known researcher at Google, who last year accused the subject artificial intelligence of magical thinking.

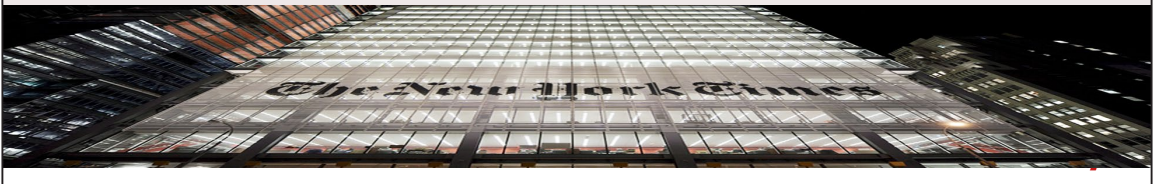


\*: Former president of Dutch Royal Academy of Sciences, former director of Princeton Institute of Advanced Studies, since a few months our new minister for Science and Education

## Criticism is growing...

The New York Times [12] goes even further, claiming that today's AI needs to do something completely different:

- “We need to stop building computer systems that merely get better and better at detecting statistical patterns in data sets – often using an approach as deep learning – and start building computer systems that from the moment of their assembly innately grasp three basic concepts: **time, space and causality**. Today's AI systems know surprisingly little about any of these concepts..... Few people working in AI are even trying to build such background assumptions into their machines.”



## Criticism is growing...

KEYWORDS: CHRISTOPHER MIMS

### Why Artificial Intelligence Isn't Intelligent

Some experts in AI think its name fuels confusion and hype of the sort that led to past 'AI winters' of disappointment



By

[Christopher Mims](#)

July 31, 2021 12:00 am ET

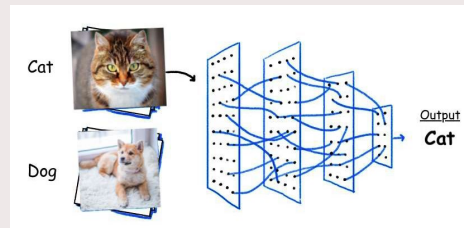
A funny thing happens among engineers and researchers who build artificial intelligence once they attain a deep level of expertise in their field. Some of them—especially those who understand what actual, biological intelligences are capable of—conclude that there's nothing “intelligent” about AI at all.

Wall Street Journal, August 4, 2021



## Image recognition

Often you see the example of a deep neural network trained to distinguish photos of cats and dogs



The network is constructed by making a long sequence of bits in the image

To me, this sounds as a very bad way of doing things.....this is absolutely not the way humans identify whether it is a cat or dog

Much better would be to use some kind of “meshing” of the objects in the photo. In this way, characteristics of the animals are captured much better. And one avoids the influence of the environment (example dogs and wolves)

## Conclusion on AI and machine learning

There is a lot of work ahead for mathematicians in the areas of artificial intelligence, machine learning and artificial neural networks (ANN)

- Understanding why methods work or do not work
- Understand the actions of the neurons (new ones?)
- Understanding on what grounds AI systems take decisions
  - In image recognition, use is made of the pixels; mathematics can provide much better methods
- How to select a good set of training data
- Using less data and prior knowledge
- Reducing the size and density of neural networks
- Predicting the topology of ANN
- .....

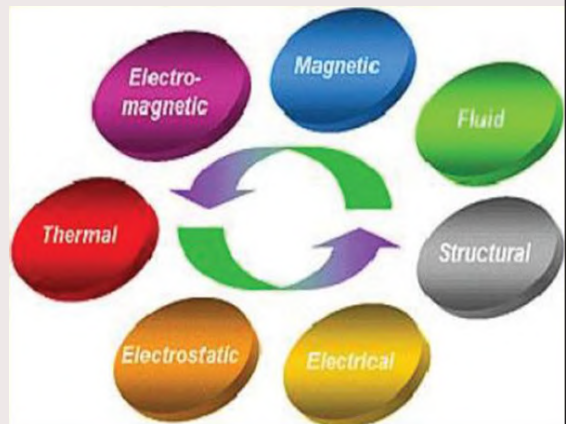
## HYBRID METHODS: COMBINING CSE AND AI

Real and Artificial Intelligence for Science and Engineering – Wil Schilders

**TU/e** EINDHOVEN  
UNIVERSITY OF  
TECHNOLOGY

### Using AI within CSE

- In recent years, researchers in the field of Computational Science and Engineering realized that they could benefit from AI methods.
- Much more accurate models and simulations, needed for example in the creation of **Digital Twins**, require much more detailed models and coupled simulations.
- Neural networks can be used for accurate models of parameters



## Going back in time: semiconductor device simulation

$$\begin{aligned}\vec{\nabla} \cdot (\varepsilon_{rel} \vec{\nabla} \phi) &= -\frac{e}{\varepsilon_0} (p - n), \\ \vec{J}_n &= -D_n \vec{\nabla} n + \mu_n n \vec{\nabla} \phi, \\ \vec{J}_p &= -D_p \vec{\nabla} p - \mu_p p \vec{\nabla} \phi, \\ \frac{\partial n}{\partial t} &= G - R - \vec{\nabla} \cdot \vec{J}_n, \\ \frac{\partial p}{\partial t} &= G - R - \vec{\nabla} \cdot \vec{J}_p.\end{aligned}$$

- Every year new models are constructed for mobility (and recombination), based upon many simulations and measurements, then using physical insight and curve-fitting
  - *Engineers and physicists provided their neural networks*
- Why not use **artificial neural networks**, based upon the abundantly available measurement and simulation data?

## Problem in this context

- Mathematicians derived conditions that mobility models must satisfy
- Peter Markowich proved that a monotonicity condition, with respect to the quasi-Fermilevel gradients, must hold
- Once the engineers at Philips presented a model that did not satisfy this condition; simulations failed at some point. They then corrected the model, satisfying the mathematical constraint
- **Obviously, models generated with neural networks should also satisfy the constraint**
- How can we achieve this???

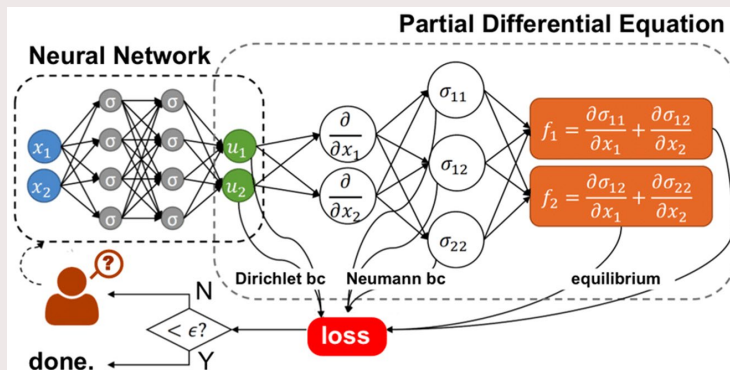
“

“The future needs Computational Science and Engineering, blending data driven and physics-based perspectives”

Karen Willcox, director Oden Institute for Computational Engineering and Sciences



## Physics Informed Neural Networks (PINNs)

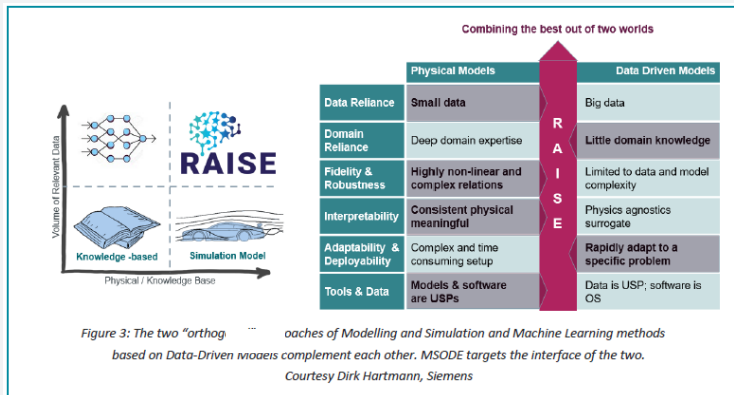


(George Karniadakis, Brown University, USA)

*I am not sure that loss functions are the way to go, it leads to many problems*

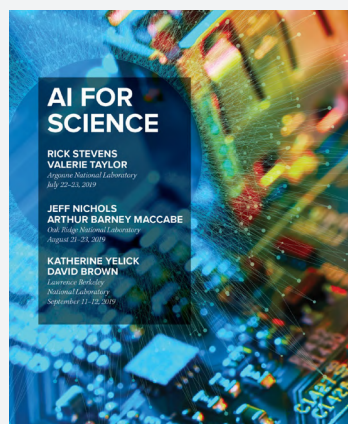
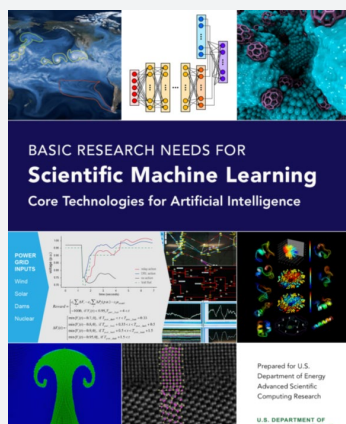
*I believe much more in hard-coded physical properties*

# Combining physics based and data-based science and engineering



Richard Feynman:  
"People who wish to analyse nature without using mathematics must settle for a reduced understanding."

# USA is front runner



## Workshop Lorentz Center (Leiden), November 1-5, 2021

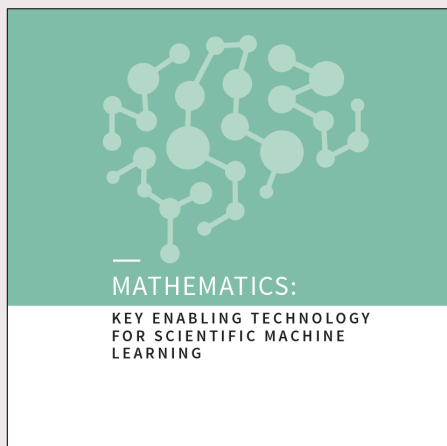
- **“Computational mathematics and machine learning”**
- Keynote speakers:
  - George Karniadakis
  - Weinan E
  - Petros Koumoutsakos
  - Carola Schönlieb
  - Stéphanie Allasonnière
  - Karen Willcox
  - Stephan Wojtowytsch
  - Paris Perdikaris
  - Erik Bekkers



45 Wil Schilders - Mathematics: key enabling technology for scientific machine learning

**TU/e**

## Booklet presented during Lorentz workshop



[https://platformwiskunde.nl/wp-content/uploads/2021/11/Math\\_KET\\_SciML.pdf](https://platformwiskunde.nl/wp-content/uploads/2021/11/Math_KET_SciML.pdf)

46 Wil Schilders - Mathematics: key enabling technology for scientific machine learning

**TU/e**

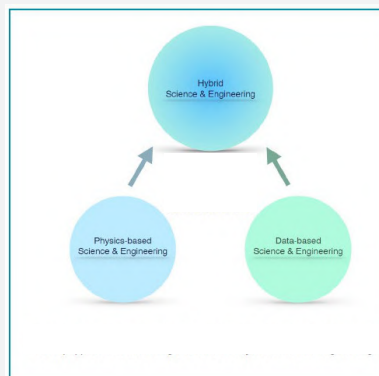
NWO XL Project UNRAVEL

# UNRAVELLING NEURAL NETWORKS

with structure-preserving computing

PAGE 47 Wil Schilders - Mathematics: key enabling technology for scientific machine learning

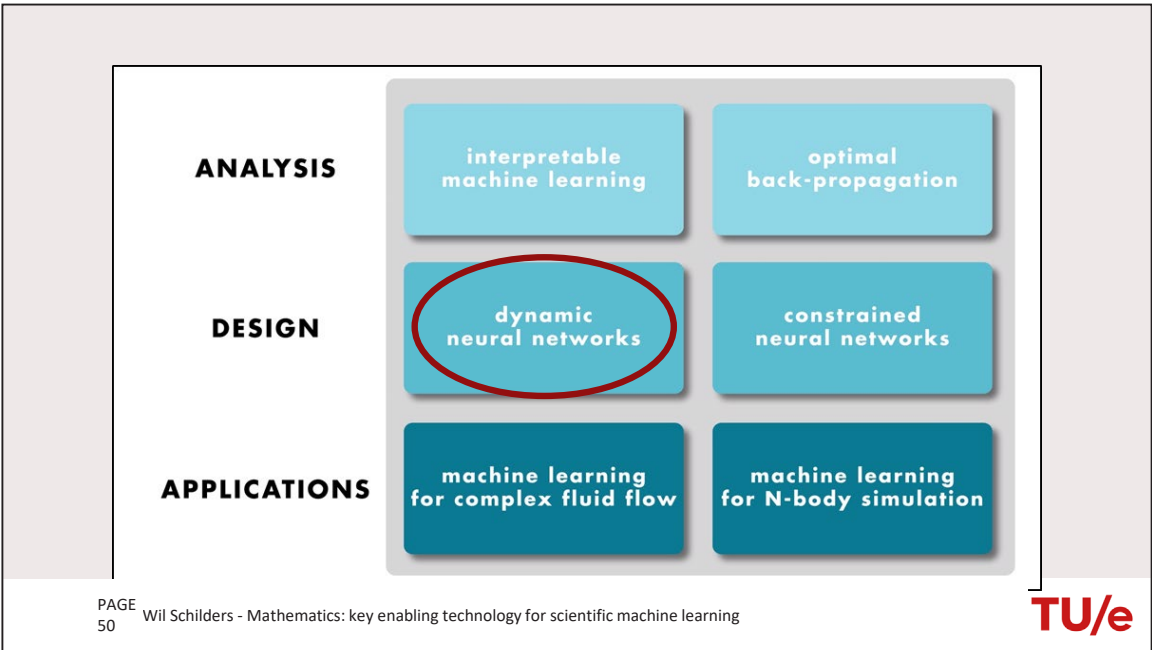
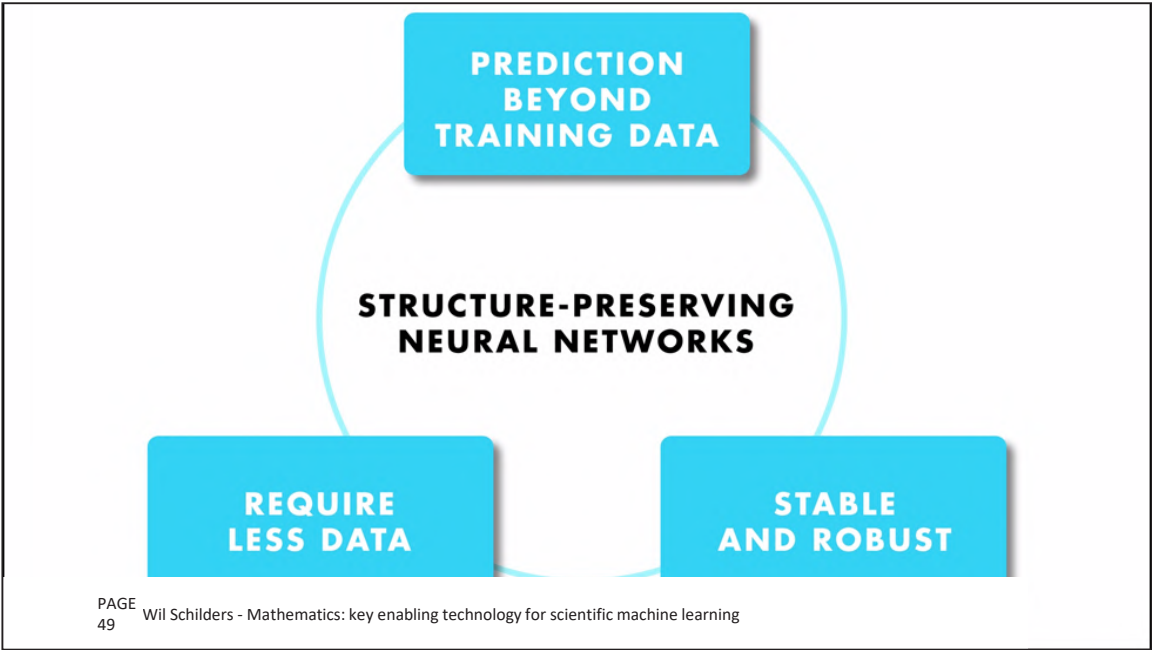
## Combining physics based and data-based science and engineering



- We aim at using so-called **mimetic methods**, i.e. methods that preserve properties of the underlying system
- How to develop mimetic neural networks or mimetic machine learning methods is an open challenge
- Such methods may need (much) less data, i.e. also work in case of “little data” rather than “big data”

48 Wil Schilders - Mathematics: key enabling technology for scientific machine learning

TU/e

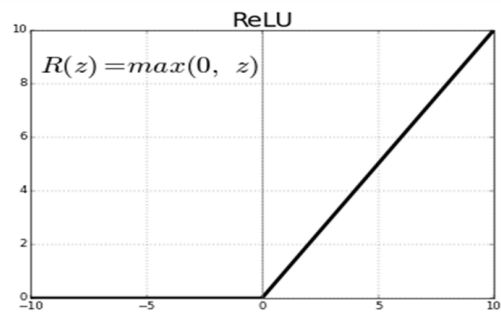
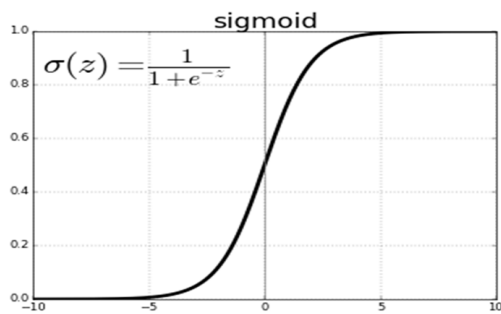




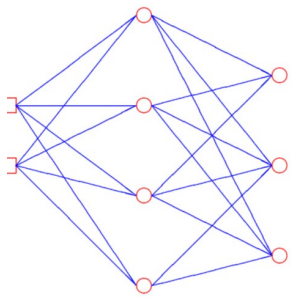
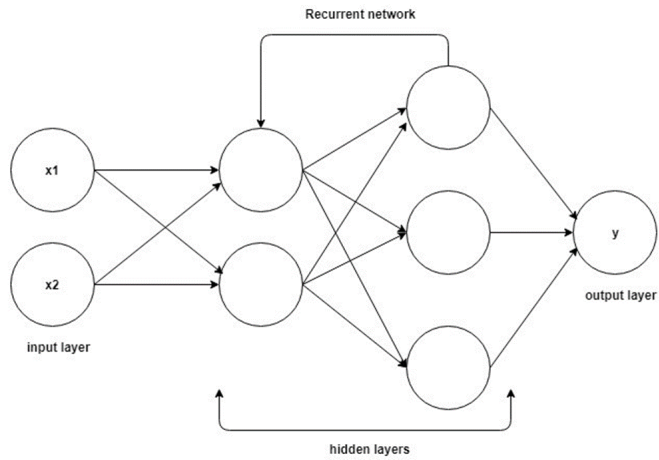
## EXAMPLE 1: DYNAMIC NEURAL NETWORKS

Real and Artificial Intelligence for Science and Engineering – Wil Schilders

Neural networks are often static, and use the following neuron  
activation functions



For dynamic situations (ODE, PDE, DAE), often recurrent neural networks are suggested



Input to neuron  $i$  in layer  $k$ :

$$s_{ik} = \sum_{j=1}^{N_{k-1}} \left( w_{ijk} y_{j,k-1} + v_{ijk} \frac{dy_{j,k-1}}{dt} \right)$$

Solve in neuron:

$$\tau_2 \frac{d^2 y_{ik}}{dt^2} + \tau_1 \frac{dy_{ik}}{dt} + y_{ik} = \mathcal{F}(s_{ik}, \delta_{ik})$$

input layer      Layer no. 1      Layer no. 2

At Philips Research, we developed truly dynamic neural networks

# Dynamic neural networks

- We were able to show that there is a 1-1 relation to state space models of the form

$$\frac{dx(t)}{dt} = Ax(t) + Bu(t),$$

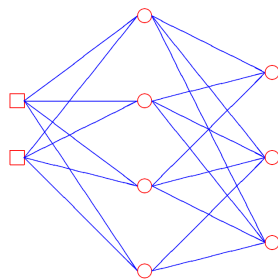
$$y(t) = Cx(t) + Du(t).$$

- Using this relation, the topology of the network can be defined (using the MOESP algorithm):
  - Number of hidden layers related to multiplicity of eigenvalues of A
  - Number of neurons related to number of complex eigenvalues
  - Real eigenvalue  $\rightarrow$  neuron with 1<sup>st</sup> order ODE
  - Complex eigenvalue(s)  $\rightarrow$  neuron with 2<sup>nd</sup> order ODE
  - Methodology involves SVD, QR, Bartels-Stewart algorithm, solving Sylvester equations

Wil Schilders - Mathematics: Key enabling technology for scientific machine learning

55

## Dynamic neural network idea



Input to neuron  $i$  in layer  $k$ :

$$s_{ik} = \sum_{j=1}^{N_{k-1}} (w_{ijk}y_{j,k-1} + v_{ijk}\frac{dy_{j,k-1}}{dt}) - \theta_{ik}$$

Solve in neuron:

$$\tau_2 \frac{d^2 y_{ik}}{dt^2} + \tau_1 \frac{dy_{ik}}{dt} + y_{ik} = \mathcal{F}(s_{ik}, \delta_{ik})$$

Input layer      Layer no. 1      Layer no. 2

The action of the first (hidden) layer in the network can be summarized as

$$T_2 x''(t) + T_1 x'(t) + x(t) = Wu(t) + Vu'(t) - \theta,$$

where  $T_1, T_2$  are **diagonal** matrices.

The MOESP algorithm results in a system of the form

$$x'(t) = \mathcal{A}x(t) + Bu(t),$$

$$y(t) = Cx(t) + Du(t).$$

Hence, we need to find  $\mathcal{Z}$  such that  $\mathcal{Z}^{-1}\mathcal{A}\mathcal{Z} = \mathcal{T}$  is block diagonal ( $1 \times 1$  and  $2 \times 2$ ).

For the construction of  $\mathcal{Z}$ , consider the **real** Schur decomposition of  $\mathcal{A}$ :

$$Q^T \mathcal{A} Q = \mathcal{R},$$

where

$$\mathcal{R} = \begin{bmatrix} \mathcal{R}_{11} & \mathcal{R}_{12} & \cdots & \mathcal{R}_{1q} \\ & \mathcal{R}_{22} & \cdots & \mathcal{R}_{2q} \\ & & \ddots & \vdots \\ & & & \mathcal{R}_{qq} \end{bmatrix}.$$

The matrices  $\mathcal{R}_{ij}$  are either  $1 \times 1$  or  $2 \times 2$  blocks, depending on whether or not the corresponding eigenvalue is complex.

The **Bartels-Stewart algorithm** can be used to find  $\mathcal{Y}$  such that

$$\mathcal{Y}^{-1} \mathcal{R} \mathcal{Y} = \mathcal{T} = \text{diag}(\mathcal{R}_{11}, \mathcal{R}_{22}, \dots, \mathcal{R}_{qq}).$$

Hence, we find the desired result:

$$\mathcal{Y}^{-1} Q^{-1} \mathcal{A} Q \mathcal{Y} = \mathcal{T}.$$

Having found  $\mathcal{Z}$  such that  $\mathcal{Z}^{-1}\mathcal{A}\mathcal{Z} = \mathcal{T}$  is block diagonal, we can translate the MOESP linear system into a neural network.

$$x'(t) = \mathcal{A}x(t) + \mathcal{B}u(t)$$

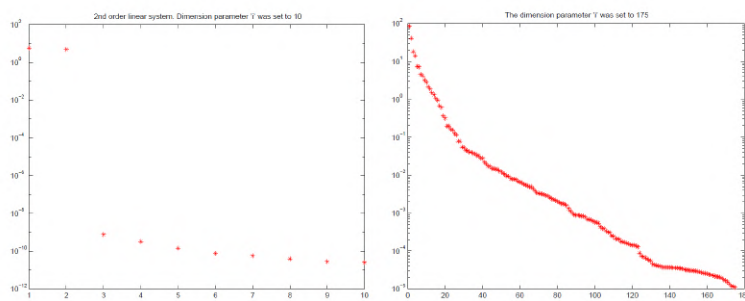
On multiplying by  $\mathcal{Z}^{-1}$ :

$$\mathcal{Z}^{-1}x'(t) = \mathcal{Z}^{-1}\mathcal{A}x(t) + \mathcal{Z}^{-1}\mathcal{B}u(t).$$

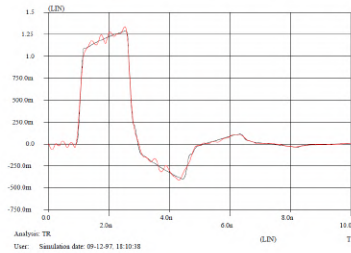
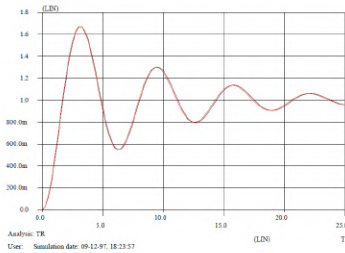
Transform to new variable  $\hat{x} = \mathcal{Z}^{-1}x$ :

$$\hat{x}'(t) = \mathcal{T}\hat{x}(t) + \mathcal{Z}^{-1}\mathcal{B}u(t).$$

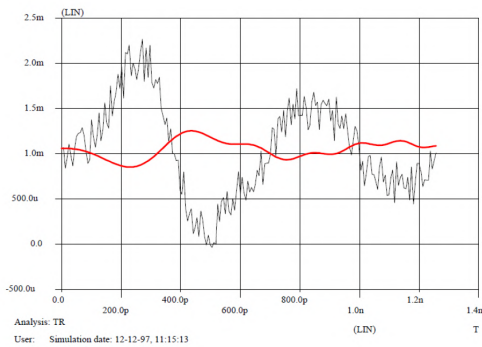
- **1 × 1 block:** 1 neuron, first order ODE
- **2 × 2 block:** 1 neuron, second order ODE



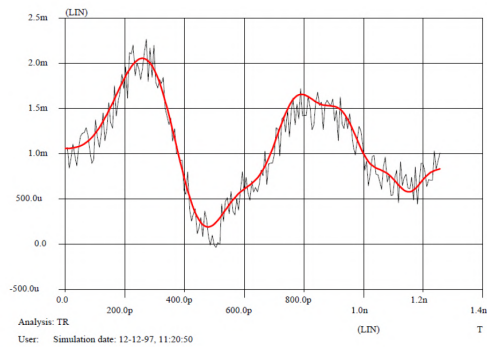
semi-logarithmic plot of singular values



Pstar analog test bench generated by NEUREKA



without MOESP preprocessing



with MOESP preprocessing

## Potential of dynamic neural networks

- We were able to predict the topology of dynamic neural networks (# hidden layers, # neurons per layer) by establishing a 1-1 correspondence with state space models
- This correspondence also opens up the way to methods for model order reduction of neural networks, translating MOR concepts for state space models
- We are currently also investigating “pruning of neural networks”, which is related to model order reduction
- Neuron action in these dynamic neural networks can be viewed as so-called high pass or low pass filters in electronics, implying that we are using electronic concepts for the construction of the networks mimicking true behaviour

## EXAMPLE 2: GEOMETRIC CONCEPTS AND AI

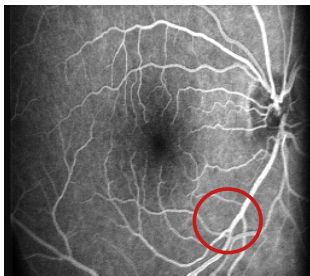
# Equivariant Deep Learning via PDEs

Remco Duits (joint work with Bart Smets & Erik Bekkers & Jim Portegies)

Applied Differential Geometry – Dep. of Mathematics and Computer Science

**TU/e** EINDHOVEN  
UNIVERSITY OF  
TECHNOLOGY

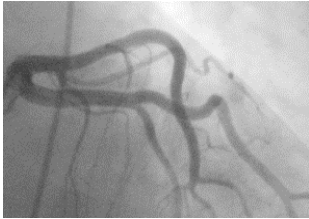
## Current image analysis methods fall short



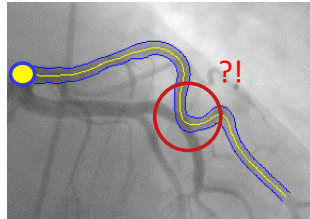
**Costly user-input to correct**



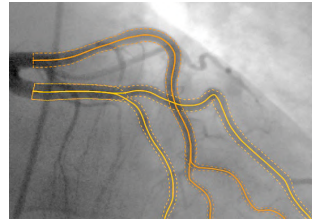
Original



Problem

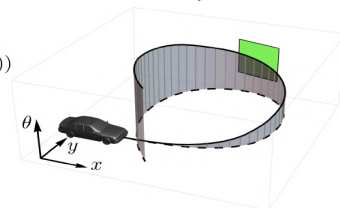
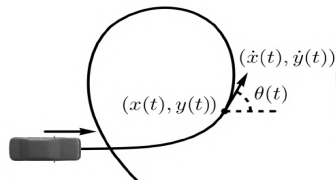
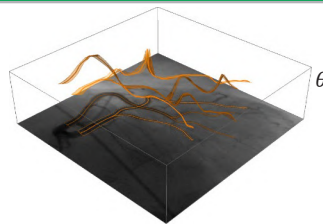
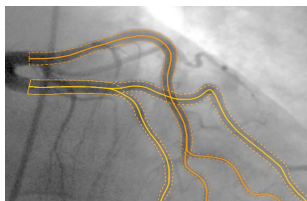


Solution



## PDE-based geometric learning

## New Dimensions



# Merge geometry and machine learning

## Geometric Image Analysis

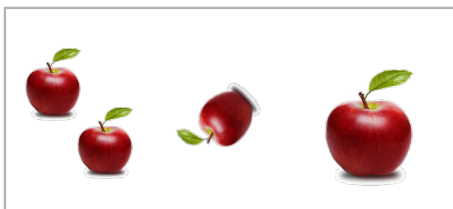
- Limited performance
- Limited scope
- **Hand-crafting**
- + **Geometric Interpretation by PDEs**
- + Low computational load
- + Few parameters
- + Little training-data

## Deep Learning

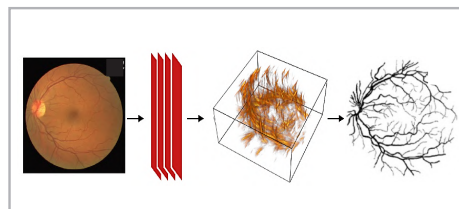
- + High performance
- + Wide scope
- + **Automatic**
- **No geometric interpretation**
- High computational load
- Too many parameters
- Huge training-data

# Geometric PDE-Based neural networks

## Reduce neural network by employing symmetry



## Learn geometry by PDEs to improve classification



## Equivariant Deep Learning via PDEs

- An exciting area of research, improving the performance of convolutional neural networks (CNN) with geometric concepts, leading to the so-called G-CNN networks
- Remco Duits has obtained a very prestigious NWO Vici grant (2.5 MEuro) to carry out this research
- For more information: <https://www.win.tue.nl/~rduits/>

## CONCLUSION

## Conclusion

- These are exciting times for researchers in the mathematical sciences, with the advent of high-performance computing, data science and artificial intelligence
- Combining “traditional” methods in Computational Science and Engineering with methods from Artificial Intelligence, Machine Learning and Neural Networks is the way forward to increase accuracy of models, as required by e.g. Digital Twinning
- **Using prior knowledge** will be key to improve the performance of neural networks
  - Increased accuracy, less data, more robustness

## Conclusion

- Expertise from numerical linear algebra and model order reduction can be used to “prune” neural networks: reducing them in size, and improving the sparsity
- Mathematics may aid in predicting the topology of neural networks, avoiding the currently employed guesswork
- The mathematical sciences are indispensable in the new multidisciplinary field of **scientific machine learning**, combining model- and data-based methods

**Real intelligence is needed to  
make artificial intelligence work**

(you may quote  
me on this)

# **POSTER SESSION**

# Quantitative Stochastic Homogenization of Parabolic Equations with Lower Order Terms

Man YANG, Graduate School of Mathematics for Innovation, Kyushu University, Email: yang.man.365@kyushu-u.ac.jp

## Introduction

According to homogenization theory, the solutions of the equation  $\nabla \cdot (\mathbf{a}(x/\epsilon)\nabla u^\epsilon) = f$  converges, as  $\epsilon \rightarrow 0$ , to the solutions of  $\nabla \cdot (\bar{\mathbf{a}}\nabla u_0) = f$  with a deterministic matrix  $\bar{\mathbf{a}}$ .

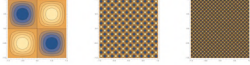


Figure: coefficients with  $\epsilon = 1/10, 1/100, 1/1000$

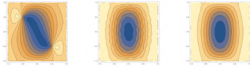


Figure: solutions with  $\epsilon = 1/10, 1/100, 1/1000$

- ▶ Stochastic homogenization: the coefficients may be periodic, or stationary. The figure on the left shows an example of periodic coefficients.
- ▶ Qualitative homogenization: proving the convergence.
- ▶ Quantitative homogenization: getting the convergence rate.

## Motivation and problem setting

♣ **Question:** How to compute homogenization for the equations with lower order terms when coefficient field is random?

♣ **Model:** To study the behavior of diffusion, let  $X_t$ :  $dX_t = D(X_t, t)dt + \sigma(X_t, t)dB_t$  and let us consider the Fokker-Planck equation,

$$\frac{\partial p(x, t)}{\partial t} = \nabla \cdot (\mathbf{a}(x, t)\nabla p(x, t)) + \mathbf{b}(x, t)(\nabla p(x, t)) + (\nabla \mathbf{b}(x, t))p(x, t),$$

where  $\mathbf{a}(x, t) = 1/2\sigma\sigma^T$  and  $\mathbf{b} = -D + \nabla \cdot \mathbf{a}$ .

Let  $\epsilon > 0$ , we study the following model,

$$\frac{\partial p^\epsilon(x, t)}{\partial t} = \nabla \cdot (\mathbf{a}^\epsilon(x, t)\nabla p^\epsilon(x, t)) + \mathbf{b}^\epsilon(x, t)(\nabla p^\epsilon(x, t)) + (\nabla \mathbf{b}^\epsilon(x, t))p^\epsilon(x, t).$$

where  $\mathbf{a}^\epsilon(x, t) := \mathbf{a}(x/\epsilon, t/\epsilon^2)$ ,  $\mathbf{b}^\epsilon(x, t) := \mathbf{b}(x/\epsilon, t/\epsilon^2)$ .

From the standpoint of homogenization, we ignore the third term on the right hand side without loss of generality.

♣ **Definition and assumption:**  $\Omega := \{(\mathbf{a}, \mathbf{b}) \mid \mathbf{a} \text{ is uniformly elliptic, } \mathbf{b} \text{ is bounded}\}$ .  $(\Omega, \mathcal{F}_{\mathbb{R}^d \times \mathbb{R}}, \mathbb{P})$ : probability space with measure  $\mathbb{P}$  which has the assumptions:

- ▶ Stationarity w.r.t  $\mathbb{Z}^d \times \mathbb{Z}$ -translation.
- ▶ Ergodicity.
- ▶ Unit range of dependence.
- $\forall U, V \in \mathbb{R}^d \times \mathbb{R}$ , if  $\text{dist}(U, V) \geq 1$ , then  $\mathcal{F}_U$  and  $\mathcal{F}_V$  are  $\mathbb{P}$ -independent.

## Main result (see [1])

Let  $U \subseteq B_1$ ,  $I \subseteq (0, 1/4)$  and set  $V := I \times U$ . Fix  $s \in (0, d)$ ,  $f \in W_{\text{par}}^{1,2+\delta}(V)$ , and let  $(p^\epsilon)_{\epsilon>0}, p_0$  be the solutions of

$$\begin{cases} \nabla \cdot (\mathbf{a}^\epsilon \nabla p^\epsilon) + \mathbf{b}^\epsilon(\nabla p^\epsilon) = \partial_t p^\epsilon & \text{in } V, \\ p^\epsilon = f & \text{on } \partial V, \end{cases}$$

and

$$\begin{cases} \nabla \cdot (\bar{\mathbf{a}} \nabla p_0) + \bar{\mathbf{b}}(\nabla p_0) = \partial_t p_0 & \text{in } V, \\ p_0 = f & \text{on } \partial V, \end{cases}$$

with deterministic matrices  $\bar{\mathbf{a}}$  and  $\bar{\mathbf{b}}$  which will be given in the following two-scale expansion.

Then the following convergence holds at least in distribution:

$$\nabla \cdot (\mathbf{a}^\epsilon \nabla p^\epsilon) + \mathbf{b}^\epsilon(\nabla p^\epsilon) - \partial_t p^\epsilon \rightarrow \nabla \cdot (\bar{\mathbf{a}} \nabla p_0) + \bar{\mathbf{b}}(\nabla p_0) - \partial_t p_0.$$

Moreover, there exist  $\beta > 0$ ,  $C(\delta, s, d, \Lambda, U) < \infty$  and a random variable  $\mathcal{X}$  satisfying  $\mathbb{E}[\exp((\theta^{-1}\mathcal{X}_+)^s)] \leq 2$ , s.t. the following estimate holds

$$\|p^\epsilon - p_0\|_{L^2(V)} \leq C\|f\|_{W_{\text{par}}^{1,2+\delta}(V)} (\epsilon^{\beta(d-s)} + \mathcal{X}\epsilon^s).$$

★ **Point of innovation:** Extending the result of [4] which studied the problem without the lower order term  $\mathbf{b}^\epsilon(\nabla p^\epsilon)$ .

★ Idea of the proof:

- Two-scale expansion  $\implies$  The first-corrector and homogenized coefficients;
- Generalized Meyer result  $\implies$  Transfer the question to the first-order corrector;
- Energy quantities  $\implies$  Transfer the information from  $\mathbf{a}$  to the solution.

## A generalization of Meyer estimate (see [1])

**Theorem:**

Fix  $p \geq 2$ ,  $f \in W_{\text{par}}^{1,q}(V)$  and suppose that  $p(x, t)$  is the unique solution to

$$\begin{cases} \partial_t p - \nabla \cdot (\mathbf{a}\nabla p) - \mathbf{b}\nabla p = 0 & \text{in } V, \\ p = f & \text{on } \partial V. \end{cases}$$

Then there exist  $\delta > 0$  and  $C < \infty$  s.t.  $p \in W_{\text{par}}^{1,2+\delta}(V)$  and

$$\|\nabla p\|_{L^{2+\delta}(V)} \leq C\|f\|_{W_{\text{par}}^{1,2+\delta}(V)}.$$

{ Generalized Caccioppoli inequality  $\implies$  Generalized Meyer estimate.  
Generalized weak formulation

★ Key of this extension: the boundedness of  $\mathbf{b}$ .

## Tools in the proof

♣ **Two-scale expansion:** [2] Classical technique for homogenization.

The solution  $p^\epsilon$  is a series, as  $\epsilon \rightarrow 0$ :  $p^\epsilon(x, t) = \sum_{i=0}^{\infty} \epsilon^i p_i(x, \frac{x}{\epsilon}, t, \frac{t}{\epsilon^2})$ .

◊ The first-order corrector  $\phi$ :

$$\partial_{t_2} \phi(y, t_2) = \nabla_{y'} \cdot (\mathbf{a}^\epsilon(e + \nabla_y \phi(y, t_2))).$$

(Information:  $\phi$  only depends on  $\mathbf{a}$ , and independent of  $\mathbf{b}$ )

◊ The homogenized coefficients:

$$\begin{cases} \bar{\mathbf{a}}\mathbf{e} := \mathbb{E}_{\mathfrak{a}} \left[ \int_{\mathbb{C}_0} \mathbf{a}(e + \nabla \phi) dx dt \right] \\ \bar{\mathbf{b}}\mathbf{e} := \mathbb{E}_{\mathfrak{b}} \left[ \int_{\mathbb{C}_0} \mathbf{b}(e + \nabla \phi) dx dt \right] \end{cases} \implies \begin{cases} \mathbf{a}^\epsilon(e + \nabla \phi) \rightharpoonup \bar{\mathbf{a}}\mathbf{e} \\ \mathbf{b}^\epsilon(e + \nabla \phi) \rightharpoonup \bar{\mathbf{b}}\mathbf{e}. \end{cases}$$

(Ergodicity and stationarity  $\implies$  weak convergence in  $L^2(\square_0)$  as  $\epsilon \rightarrow 0$ .)

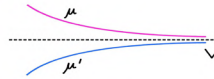
♣ **H-convergence:** Test function method; First introduced by TarTar [5].

◊ The test function:  $w^\epsilon := p_0 + \eta_\epsilon \sum_{i=1}^d \frac{\partial p_0}{\partial x_i}(x, t) \phi_i(\frac{x}{\epsilon}, \frac{t}{\epsilon^2})$ .

◊  $p^\epsilon \rightharpoonup w^\epsilon$ :  $w^\epsilon$  act as a bridge by using the triangle inequality and the generalized Meyer estimate to connect  $p^\epsilon$  and  $p_0$ .

♣ **Energy quantities:** First established by Dal Maso.

- ◊ Subadditive quantity  $\mu$  [3]: Prove the convergence.
- ◊ Superadditive quantity  $\mu'$  [4]: Get the convergence speed.



- Estimation of the difference.
- The convergence rate.

• Transfer the properties of the coefficients to the energy quantity and then to the solution.

## Future works

♣  $dX_t = D(X_t)dt + \sigma(X_t)dB_t + dY_t$ , ( $Y_t$ : Lévy motion) with generator

$$\begin{aligned} \mathcal{L}g(x) &= \sum_{i=1}^d D_i(x) \frac{\partial}{\partial x_i} g(x) + \frac{1}{2} \sum_{i=1}^d \sum_{j=1}^d \mathfrak{a}_{ij}(x) \frac{\partial^2}{\partial x_i \partial x_j} g(x) \\ &\quad + \int_{\mathbb{R}^d \setminus \{0\}} [g(x+y) - g(x) - I_{(|y|<1)} y_i \frac{\partial}{\partial x_i} g(x)] \nu(dy). \end{aligned}$$

- To study the Fokker-Planck equation for  $X_t$  by using homogenization.
- To consider the case of time-dependent coefficients.

## References

- [1] Man Yang (Preprint) Quantitative Stochastic Homogenization of Parabolic Equations with Lower Order Terms.
- [2] Alain Bensoussan, Jacques-Louis Lions, and George Papanicolaou (2011) Asymptotic analysis for periodic structures.
- [3] Gianni Dal Maso and Luciano Modica (1986) Nonlinear stochastic homogenization.
- [4] Scott N Armstrong and Charles K Smart (2016) Quantitative stochastic homogenization of convex integral functionals.
- [5] Murat, F., and Tartar, L., (1997) H-convergence.

## Acknowledgements

This work was supported by WISE program (MEXT) at Kyushu University.

# The critical points of the elastic energy among curves pinned at endpoints

Kensuke Yoshizawa (Institute of Mathematics for Industry, Kyushu University), email: k.yoshizawa@mi.kyushu-u.ac.jp.

## Overview

This poster is based on [4] and it is devoted to the presentation of **optimal shapes of elastic rods whose endpoints are fixed** (up to zeroth order). The mathematical analysis corresponds to the following variational problem.

- $\gamma : [0, 1] \rightarrow \mathbf{R}^2$ ; planar curve
  - Length  $\mathcal{L}(\gamma)$ , endpoints  $\gamma(0), \gamma(1)$ : fixed
  - Minimize the **elastic energy**:  $\mathcal{B}(\gamma) = \int_{\gamma} |x'|^2 ds$
- $x$ : signed curvature,  $s$ : arclength parameter

## History: once upon a time, Euler suggested...

- 1744: Euler [3] suggested that ideal elastic rods are characterized as a **minimizer of the elastic energy  $\mathcal{B}$  under the condition which fixes the length of curves and fixes endpoints up to first order**. He also gave a classification of candidates of minimizers (Fig. 1).
- 1906: Max Born [2] did an experiment to deduce the shape of an elastic rod (Fig. 2). He also investigated stability of elastic rods.
- 2020: Arroyo-Garay-Pámpano [1] showed numerical procedures to obtain critical points of  $\mathcal{B}$  in  $\mathcal{A}_L$ .
- Today: It is still difficult to obtain
  - explicit formulae of all critical points of  $\mathcal{B}$  under boundary conditions;
  - uniqueness of global minimizers.

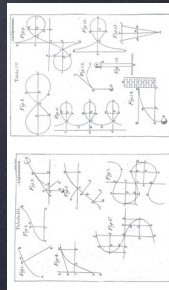


Figure 1: Euler

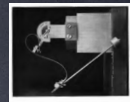


Figure 2: Born



Figure 3: Arroyo et al.

## Problem

Find all critical points of  $\mathcal{B}$  in

$$\mathcal{A}_L := \left\{ \gamma \in C^\infty([0, 1]; \mathbf{R}^2) \mid \gamma(0) = (0, 0), |\gamma'| > 0, \gamma(1) = (1, 0), \mathcal{L}(\gamma) = L \right\}.$$

Determine minimizers of  $\mathcal{B}$  in  $\mathcal{A}_L$ .

## Theorem (14), Explicit formulae

The set of all critical points of  $\mathcal{B}$  in  $\mathcal{A}_L$  is

$$\left\{ \gamma \in \mathcal{A}_L \mid \tilde{\gamma}_n \text{ are length parameterizations of } \gamma, \text{ is } \left. \begin{array}{l} \tilde{\gamma}_n^+, \tilde{\gamma}_n^-, \tilde{\gamma}_n^+, \text{ or } \tilde{\gamma}_n^- \text{ for } n \in \mathbb{N} \end{array} \right\}.$$

Type I:  $\tilde{\gamma}_n^\pm(s) := (\tilde{X}_n(s), \pm \tilde{Y}_n(s))$ ,  $s \in [0, L]$ ,

$$\tilde{X}_n(s) := 2\tilde{p}^2 \int_0^s \operatorname{cn}\left(\frac{2nK(\tilde{p})}{L}t + K(\tilde{p}), \tilde{p}\right)^2 dt + (1 - 2\tilde{p}^2)s,$$

$$\tilde{Y}_n(s) := -\frac{\tilde{p}L}{nK(\tilde{p})} \operatorname{cn}\left(\frac{2nK(\tilde{p})}{L}s + K(\tilde{p}), \tilde{p}\right),$$

where  $\tilde{p}$  is a unique solution of  $2E(\tilde{p})/K(\tilde{p}) - 1 = 1/L$ .

Type II:  $\tilde{\gamma}_n^\pm(s) := (\tilde{X}_n(s), \pm \tilde{Y}_n(s))$ ,  $s \in [0, L]$ ,

$$\tilde{X}_n(s) := -2\tilde{p}^2 \int_0^s \operatorname{cn}\left(\frac{2nK(\tilde{p})}{L}t - K(\tilde{p}), \tilde{p}\right)^2 dt - (1 - 2\tilde{p}^2)s,$$

$$\tilde{Y}_n(s) := -\frac{\tilde{p}L}{nK(\tilde{p})^2} \operatorname{cn}\left(\frac{2nK(\tilde{p})}{L}s - K(\tilde{p}), \tilde{p}\right),$$

where  $\tilde{p}$  is a unique solution of  $-2E(\tilde{p})/K(\tilde{p}) + 1 = 1/L$ .

•  $K(\tilde{p})$  (resp.  $E(\tilde{p})$ ): the complete elliptic integral of the first (resp. second) kind  
 •  $\operatorname{cn}(\cdot, \tilde{p})$ : the elliptic cosine function with modulus  $\tilde{p} \in [0, 1]$

## Strategy: solve the corresponding ODE

Formulation:  $\gamma$  is a critical point of  $\mathcal{B}$  in  $\mathcal{A}_L$

$\iff \exists \lambda \in \mathbf{R}$  s.t. the signed curvature  $\kappa$  satisfies

$$2\tilde{p}^2\kappa + \kappa^3 + \lambda\kappa = 0 \quad \text{in } (0, L) \quad (\star)$$

under the same boundary condition.

• Boundary value problem for ODE

•  $(\star)$  is of higher order ( $\tilde{p}^2\kappa \sim \gamma''''$ ), and includes a multiplier  $\lambda \in \mathbf{R}$

• Key method: shooting method

## Application

Explicit formulae show the "shapes" of  $\tilde{\gamma}_n^+$  and  $\tilde{\gamma}_n^-$ .



E.g.,  $\tilde{\gamma}_n^+$  has a "loop" in view of  $\tilde{X}_n(L/2) < 0$ ,  $\tilde{\gamma}_n^-$  has no loop since  $\tilde{X}_n$  is monotone.

Similarity & (axial) symmetry:

- $\tilde{\gamma}_n^+(s) = \frac{1}{n} \tilde{\gamma}_1(ns)$ ,  $s \in [0, \frac{L}{n}]$  (Similarity)
- $\tilde{X}_n(s) + \tilde{X}_n(L-s) = 1$ ,  $\tilde{Y}_n(s) = \tilde{Y}_n(L-s)$ ,  $s \in [0, L]$  (Symmetry)

Quantitative comparison of the bending energy of all critical points. By explicit formulae,

$$\mathcal{B}(\tilde{\gamma}_n^+) = \frac{16r^2}{L} K(\tilde{p}) \left( \tilde{p}^2 K(\tilde{p}) - K(\tilde{p}) + E(\tilde{p}) \right) = n^2 \mathcal{B}(\tilde{\gamma}_1^+)$$

(The left-hand side becomes  $\mathcal{B}(\tilde{\gamma}_n^+)$  if we replace  $\tilde{p}$  with  $\tilde{p}$ ).

This together with fundamental properties of  $K(\cdot)$ ,  $E(\cdot)$  yields  $\mathcal{B}(\tilde{\gamma}_1^+) < \mathcal{B}(\tilde{\gamma}_1^-)$ .

## Theorem (Uniqueness of global minimizers)

Global minimizers of  $\mathcal{B}$  in  $\mathcal{A}_L$  are nothing but  $\tilde{\gamma}_1^+$  and  $\tilde{\gamma}_1^-$ .

## Reference

- [1] J. Arroyo, O. J. Garay, and Á. Pámpano, *Boundary value problems for Euler-Bernoulli planar elastica. A solution construction procedure*, J. Elasticity **139** (2020), 389–388.
- [2] M. Born, *Untersuchungen über die Stabilität der elastischen Linie in Ebene und Raum, unter verschiedenen Grenzbedingungen*, PhD thesis, University of Göttingen (1906).
- [3] L. Euler, *Méthodus inveniendi lineas curvas maximi minimive proprietate gaudentes, sive solutio problematis isoperimetrici latissimo sensu accepti*, Marcum-Michaellem Bousquet & socios, Lausanne, Geneva (1744).
- [4] K. Yoshizawa, *The critical points of the elastic energy among curves pinned at endpoints*, Discrete Contin. Dyn. Syst. **42** (2022), 403–423.

# Expected number of zeros for Gaussian analytic function with finitely dependent Gaussian coefficients

Kohei Noda<sup>1</sup>, Tomoyuki Shirai<sup>2</sup>

<sup>1</sup>Graduate School of Mathematics and Joint Graduate School of Mathematics for Innovation, Kyushu University. e-mail:noda.kohei.721@s.kyushu-u.ac.jp  
<sup>2</sup>Institute of Mathematics for Industry, Kyushu University.

## Introduction

- How do the random coefficients of a power series affects its zeros?
- The history of random power series could be traced back to the studies of Paley, Zygmund and Wiener. It is still a hot topic in probability theory.
- Peres and Virág [3] studied the zeros of random power series

$$f_{PV}(z) = \sum_{n=0}^{\infty} \zeta_n z^n$$

where  $\{\zeta_n\}_n$  is independent, identically distributed (i.i.d.) complex Gaussian random variables.

- In our work [1], we replace  $\{\zeta_n\}_n$  with finitely dependent stationary Gaussian coefficients  $\{\xi_k\}_k$ , and then, we show that the degeneracy of zeros of spectral density of  $\{\xi_k\}_k$  sensitively affects zeros of  $f(z) := \sum_{k=0}^{\infty} \xi_k z^k$  from the point of view of the expected number of zeros of  $f(z)$ .

## Gaussian analytic function (GAF): Examples and properties

- Gaussian analytic function is a holomorphic function-valued Gaussian process on a domain contained in  $\mathbb{C}$ .
- One of the key quantities for zeros process of GAFs is the number of zeros:  $N_f(r) = \#\{z \in \mathbb{C} : f(z) = 0, |z| \leq r\}$  for GAF  $f(z)$ .
- Peres and Virág showed that zeros process of  $f_{PV}(z)$  is the determinantal point process. In particular,  $\mathbb{E}N_{f_{PV}}(r) = \frac{r^2}{1-r^2}$ .

There are well-known three invariant Gaussian analytic functions:

- Entire GAF: For  $L > 0$ ,  $f_L^{\text{Ent}}(z) = \sum_{n=0}^{\infty} \sqrt{\frac{L^n}{n!}} \zeta_n z^n$ .
- Hyperbolic GAF: For  $L > 0$ ,  $f_L^{\text{Hyp}}(z) = \sum_{n=0}^{\infty} \sqrt{\frac{\Gamma(L+n)}{\Gamma(L)n!}} \zeta_n z^n$ .
- Spherical GAF: For  $L \in \mathbb{N}$ ,  $f_L^{\text{Sph}}(z) = \sum_{n=0}^L \sqrt{\binom{L}{n}} \zeta_n z^n$ .

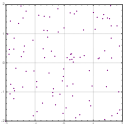


Figure 1 – Entire GAF.

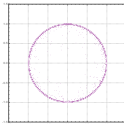


Figure 2 – Hyperbolic GAF.

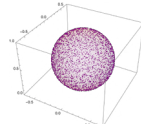


Figure 3 – Spherical GAF.

## GAF with finitely dependent stationary Gaussian process coefficients and our methods

- Let  $\{\xi_n\}_n$  be mean 0, variance 1, and complex finitely dependent stationary Gaussian processes with the covariance function  $\gamma(k) = \mathbb{E}[\xi_n \overline{\xi_{n+k}}]$ .
- Our model is  $f(z) := \sum_{k=0}^{\infty} \xi_k z^k$ . Our key quantity is  $\Theta(r, z) = \sum_{k \in \mathbb{Z}} \gamma(k) r^{|k|} z^k$ , whose zeros determine the asymptotic behavior of zeros of  $f(z)$ .
- 2-dependent case:  $f_{a,b}(z) = \sum_{k=0}^{\infty} \xi_k z^k$  with 2-dependent Gaussian process  $\{\xi_n\}_n$  with the covariance function  $\gamma_{a,b}(k) = \delta_{k,0} + a\delta_{k,\pm 1} + b\delta_{k,\pm 2}$ ,  $\Theta(r, z) = 1 + ar(z + z^{-1}) + br^2(z^2 + z^{-2})$ .
- n-dependent case:  $f_n(z) = \sum_{k=0}^{\infty} \xi_k z^k$  with n-dependent Gaussian process  $\{\xi_n\}_n$  with covariance function  $\gamma_n(k) = \begin{cases} \binom{2n}{n+k} \binom{2n}{n}^{-1} & (|k| = 0, 1, 2, \dots, n), \\ \text{else,} & \end{cases}$ ,  $\Theta(r, z) = \binom{2n}{n}^{-1} z^{-n} (z+1)^{2n}$ .

- Key tool is the Edelman-Kostlan formula in the case of dependent coefficients:

$$\mathbb{E}N_f(r) = \frac{r^2}{1-r^2} - \frac{r}{2\pi i} \oint_{\partial \mathbb{D}} \frac{G'(rz)}{\Theta(r, z)} dz, \quad G(z) = \sum_{n=1}^{\infty} \overline{\gamma(n)} z^n.$$

- Our strategies are:
  1. Residue calculus and asymptotic behavior of zeros of  $\Theta(r, z)$  as  $r \rightarrow 1$ .
  2. Newton polygon method (n-dependent model).

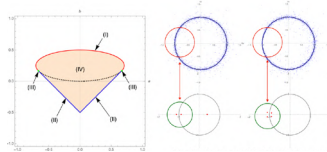


Figure 4 – The left figure is the region of positive definiteness of  $\gamma_{a,b}(k)$ , and the right two figures are the behaviors of zeros  $z(r)$  of  $\Theta(r, z) = 0$  as  $r \rightarrow 1$ . Plots for  $a = 1/4, b = -1/4$  (middle) and  $a = 2/3, b = 1/6$  (right). The multiplicity of zeros affects on zeros of  $f_{a,b}(z)$ .

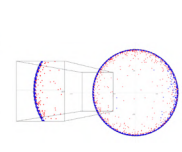


Figure 5 – Superposition of zeros of Peres-Virág GAF (Red) and  $f_{a,b}(z)$  (Blue).

## Main results [1]

Consider GAF  $f(z) = \sum_{k=0}^{\infty} \xi_k z^k$ .

- The spectral density of finitely dependent stationary Gaussian process  $\Xi = \{\xi_k\}_k$ ,  $\Theta(1, z) = \sum_{k \in \mathbb{Z}} \gamma(k) z^k$  of  $\Xi$  has zeros  $\theta_j$  of multiplicity  $2k_j$  for  $j = 1, 2, \dots, p$ .
- Put  $\alpha = (2k - 1)/(2k)$  with  $k = \max_{1 \leq j \leq p} k_j$ ;  $\alpha = 0$  otherwise.

Then,  $\exists C_{\Xi} > 0$  s.t.

$$\mathbb{E}N_f(r) = \frac{r^2}{1-r^2} - C_{\Xi}(1-r^2)^{-\alpha} + o((1-r^2)^{-\alpha}), \quad \text{as } r \rightarrow 1.$$

In general,  $\mathbb{E}N_f(D) \leq \mathbb{E}N_{f_{\text{PV}}}(D)$  for GAF  $f$  with stationary Gaussian process coefficients and a domain of  $\mathbb{D}$ . Hence, a negative term of slower growth appears.

♣ 2-dependent case: On each region (I), (II), (III), and (IV), as  $r \rightarrow 1$ ,

$$\begin{aligned} \text{(I)} \quad \mathbb{E}N_{f_{a,b}}(r) &= \frac{r^2}{1-r^2} - \sqrt{\frac{2b}{6b-1}} \frac{1}{(1-r^2)^{1/2}} + O(1), & \text{(II)} \quad \mathbb{E}N_{f_{a,b}}(r) &= \frac{r^2}{1-r^2} - \frac{1}{2} \sqrt{\frac{1-2b}{1-6b(1-r^2)^{1/2}}} + O(1), \\ \text{(III)} \quad \mathbb{E}N_{f_{a,b}}(r) &= \frac{r^2}{1-r^2} - \frac{1}{2^{5/4}} \frac{1}{(1-r^2)^{3/4}} + O(1), & \text{(IV)} \quad \mathbb{E}N_{f_{a,b}}(r) &= \frac{r^2}{1-r^2} - C(a, b) + O(1-r^2), \text{ where } C(a, b) \geq 0. \end{aligned}$$

♣ n-dependent case:

$$\mathbb{E}N_f(r) = \frac{r^2}{1-r^2} - D_n(1-r^2)^{-\frac{2n-1}{2n}} + O((1-r^2)^{-\frac{2n-1}{2n}}), \quad \text{as } r \rightarrow 1, \quad \text{where } D_n = \frac{1}{2n \sin \frac{\pi}{2n}} \left\{ \binom{2(n-1)}{n-1} \right\}^{\frac{1}{2n}}.$$

## Conclusions

1. If we consider the fractional Gaussian noise  $\{\xi_n^H\}_n$  with  $\mathbb{E}[\xi_n^H \overline{\xi_{n+k}^H}] = \frac{1}{2} |k+1|^{2H} + \frac{1}{2} |k-1|^{2H} - |k|^{2H}$  [2], then  $\Theta(r, z)$  becomes the infinite series. Hence, we need to develop a new tool to let information of zeros of infinite series with covariance function coefficients.

2. We would like to establish a variance formula of  $N_f(r)$  for GAF with dependent Gaussian coefficients and develop an algorithm as we have done in the case of the expected number of zeros.

## References

- [1] Kohei, N. and Tomoyuki, S.: Expected number of zeros of random power series with finitely dependent Gaussian coefficients, to appear in *Journal of Theoretical Probability*.
- [2] Mukeru, S., Muliyil, M. P., Nizabanita, J., and Mqanda, M. M.: Zeros of Gaussian power series with dependent random variables. *Illinois J. Math.* **64**, no. 4 (2020), 569–582.
- [3] Peres, Y. and Virág, B.: Zeros of the i.i.d. Gaussian power series: a conformally invariant determinantal process. *Acta Math.* **194**, no. 1 (2005), 1–35.

## Acknowledgments

This work was supported by Japan Society for the Promotion of Science (JSPS) KAKENHI [JP18H01124] and partially supported by KAKENHI [JP16H06338, JP20H00119, JP20K20884 to T.S.], and K.N. was supported by WISE program (MEXT) at Kyushu University.



# Study on recurrences of random walks on growing k-ary trees

Shuma Kumamoto<sup>1</sup>, Shuji Kijima<sup>2</sup>, Tomoyuki Shirai<sup>3</sup>

- 1, Graduate School of Mathematics, Kyushu University, e-mail :kumamoto.shuma.693@s.kyushu-u.ac.jp
- 2, Faculty of Data Science, Shiga University
- 3, Institute of Mathematics for Industry, Kyushu University

## Background

- Kijima et al. investigated the number of vertices unvisited by a random walk on a growing network, which is interesting in network science/engineering [2].
- Random walk is also important in machine learning [4].
- Dembo et al. investigated the condition that the origin becomes **recurrent/transient** by a random walk on a growing region in lattice [1].

There is a lot of variants of random walks on growing regions, nevertheless, a little is known about it.

It is known that the random walk on infinite k-ary tree (fig 1) is transient at the root [5]. This work investigates conditions that a random walk on a growing k-ary tree (fig 2) becomes recurrent/transient.

### Recurrent/Transient

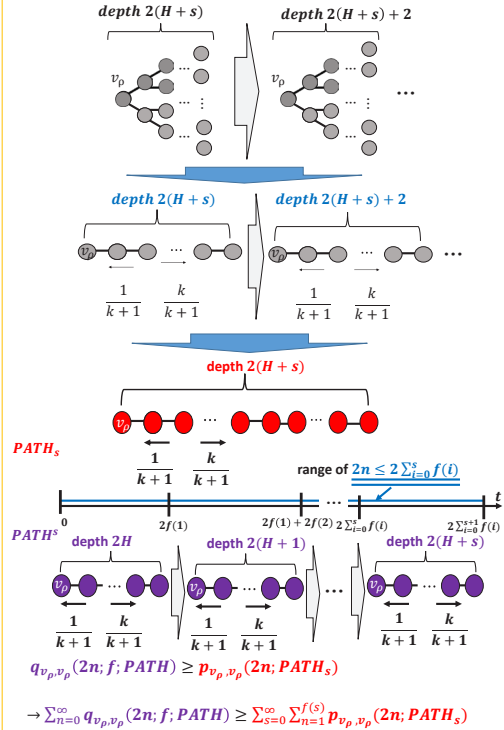
A vertex  $v$  is called **recurrent/transient** if the following equation holds:

$$\sum_{n=0}^{\infty} P_{v,v}(2n) = +\infty/\text{constant}.$$

## Theorem

- (i) If  $\sum_{b=0}^{+\infty} \frac{f(h+b)}{k^{2(h+b)}} = +\infty$  then  $v_p$  is recurrent.
- (ii) Otherwise (if  $\sum_{b=0}^{+\infty} \frac{f(h+b)}{k^{2(h+b)}} = \text{constant}$  then)  $v_p$  is transient.

## Sketch of proof (i) (proof (ii) is similar)



## Preliminary

### Growing k-ary tree (see figure 2)

$TREE_s := (V_s, E_s)$ : Tree of depth  $2(h+s)$

$TREE^s := TREE_0, TREE_1, \dots, TREE_s$

$f(s) := \frac{1}{2}$  duration of  $TREE^s \rightarrow TREE^{s+1}$

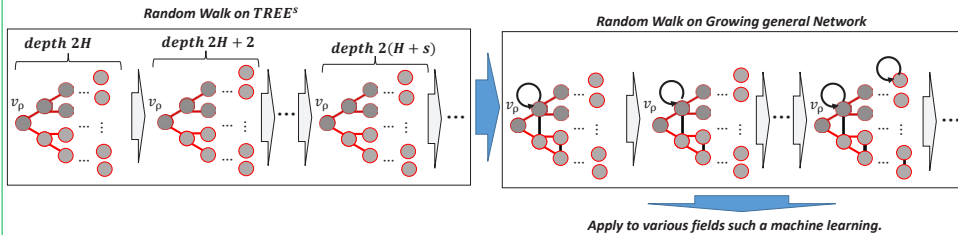
$TREE := \lim_{s \rightarrow \infty} TREE_s$  (Figure 1)

### Probabilities

$q_{x,y}(2n; f; TREE^{s(n)})$ : probability of going  $2n$  steps from  $x$  to  $y$  on  $TREE^{s(n)}$

$p_{x,y}(2n; TREE_s)$ : probability of going  $2n$  steps from  $x$  to  $y$  on  $TREE_s$

## Future work



## Reference

- [1] A. Dembo, R. Huang, V. Sidoravicius. Walking within growing domains: recurrence versus transience. Electronic Journal of Probability. 19, 1-20. (2014).
- [2] S. Kijima, N. Shimizu, T. Shiraga: How Many Vertices Does a Random Walk Miss in a Network with Moderately Increasing the Number of Vertices? SODA 2021: 106-122
- [3] D. A. Levin, Y. Peres: Markov chains and mixing times. American Mathematical Soc., 2017.
- [4] J. Li, L. Wu, R. Hong, J. Hou: Random walk based distributed representation learning and prediction on Social Networking Services. Inf. Sci. 549: 328-346 (2021)
- [5] R. Lyons, R. Pemantle, Y. Peres: Unsolved problems concerning random walks on trees. In K. B. Athreya, P. Jagers (Eds.) Classical and modern branching processes. Springer, New York, NY, 1997. 223-237.

Kentaro Yonemura<sup>1</sup>

<sup>1</sup>Faculty of Mathematics, Kyushu University, Japan

## Introduction

A *quandle* is an algebraic system introduced by D.Joyce [3] and S.V.Matveev [4] in 1982. This poster is based on the work reported in [5], which studies spherical quandles.

**Conjecture** For any algebraically connected smooth quandle  $X$ , there is a Lie group  $G$  and an embedding  $\iota : X \rightarrow \text{Conj } G$  as manifold and quandle homomorphism.

We prove the conjecture for spherical quandles

## Why we study quandles

To make knot theory useful to the society as a whole. I consider quandle theory to be a unifying reconstruction of knot theory.

It is difficult to understand the whole picture of knot theory. A book [1] outlining knot theory in various fields has been published recently and the thickness of book is almost the width of iPhone 12 Pro.



Figure 1: Thickness of [1] vs. the width of iPhone 12 Pro

## Quandle basics

A quandle is an algebraic system  $(X, \triangleright)$  satisfying the following three conditions:

- 1  $\forall x, y \in X, x \triangleright x = x,$
- 2  $\forall y, \text{ the map } S_y : X \rightarrow X; x \mapsto x \triangleright y \text{ is a bijection,}$

$$\forall x, y, z, (x \triangleright y) \triangleright z = (x \triangleright z) \triangleright (y \triangleright z).$$

The quandle conditions are often interpreted as an abstraction of Reidemeister moves.

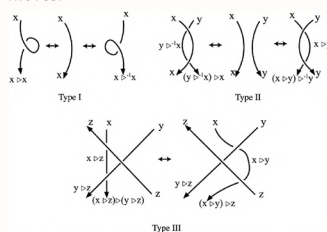


Figure 2: Geometric interpretation of quandle operations

**Definition** For a group  $G$ , suppose  $x \triangleright y = y^{-1}xy$  for  $x, y \in G$ , we get a quandle  $(G, \triangleright)$  called *conjugacy quandle*. We denote this quandle by  $\text{Conj } G$ .

**Definition** Suppose  $S^n$  be an  $n$ -sphere  $\{(x_1, \dots, x_{n+1}) \in \mathbb{R}^{n+1} \mid \sum_{k=1}^n x_k^2 = 1\}$  and  $x \triangleright y = 2\langle x, y \rangle y - x$  for  $x, y \in S^n$ , where  $\langle -, - \rangle$  is the Euclidean inner product. Then,  $(S^n, \triangleright)$  is a quandle called *spherical quandle*. We denote this quandle by  $S^n_{\mathbb{R}}$ .

## Embedding spherical quandles in pin groups

If a quandle is embedded in a conjugacy quandle of a group, the structure of the quandle will be easy to deal with using knot theory. We sketch the proof of embedding of spherical quandles  $S^n_{\mathbb{R}}$  into spin groups. The embedding is stated by M.Eisermann [2] without proof.

### Main result

Suppose  $n$ -sphere  $S^n$  has the spherical quandle structure and projective space  $\mathbb{R}P^n$  has the induced smooth quandle structure. There are embedding  $\iota : S^n \rightarrow \text{Pin}(n+1)$  and  $i : \mathbb{R}P^n \rightarrow O(n+1)$  and

the following diagram is commutative:

$$\begin{array}{ccc} S^n & \hookrightarrow & \text{Pin}(n+1) \\ \pi \downarrow & & \downarrow \text{Ad} \\ \mathbb{R}P^n & \xrightarrow{i} & O(n+1) \end{array}$$

where  $\pi$  is the natural covering map and  $\text{Ad}$  is the adjoint representation. Especially, the images of  $\iota$  and  $i$  are involved in  $\text{Spin}(n+1)$  and  $\text{SO}(n+1)$  respectively if  $n$  is even.

### Sketch of proof

**Step 1** Lift the action of  $\text{SO}(n+1)$  on  $\mathbb{R}P^n$  to the action of  $\text{Spin}(n+1)$  on  $S^n$  using the covering  $\pi$ .

**Step 2** Construct the embedding  $i : \mathbb{R}P^n \rightarrow O(n+1)$  using the inner automorphism of quandles.

**Step 3** See that the universal covering of  $\text{Im } i$  is the conjugacy class of  $\text{Pin}(n+1)$  and the induced diffeomorphism from  $S^n$  to the conjugacy class is a quandle homomorphism.

### Application of the result

The result helps to concisely rewrite the two-knot invariants, the longitudinal mapping and the Chern-Simons invariant with respect to principal  $\text{SU}(2)$  or  $\text{Spin}(n+1)$  bundles.

**Acknowledgments** This work was supported by JST SPRING, Grant Number JPMJSP2136.

### References

- [1] C. Adams et al, Encyclopedia of Knot Theory, Chapman and Hall/CRC, 2021.
- [2] M. Eisermann, Quandle coverings and their Galois correspondence, *Fundamenta Mathematicae* 225 (2014), 103-167.
- [3] D. Joyce, A classifying invariant of knots, the knot quandle, *J. Pure Appl. Algebra* 23 (1982), no. 1, 37-65.
- [4] S.V. Matveev, Distributive groupoids in knot theory, (*Russian*) *Mat. Sb. (N.S.)* 119(161) (1982), no. 1, 78-88, 160.
- [5] K. Yonemura, Note on spherical quandles, preprint.

# Lyapunov Regularity for Planar Piecewise Expanding Maps

Kodai Yamamoto

Joint Graduate School of Mathematics for Innovation, Kyushu University,  
yamamoto.kodai.508@s.kyushu-u.ac.jp

## Introduction

Dynamical systems is a field of mathematics that describes time evolution according to certain rules.

Here we consider iterations of maps with some smoothness as dynamical systems.

**Lyapunov exponents** are one of important characteristics in analyzing dynamical systems.

Let  $D \subset \mathbb{R}^2$  be an open rectangle and  $f : D \rightarrow D$  be a differentiable map.

We write  $Df^n(x) : \mathbb{R}^2 \rightarrow \mathbb{R}^2$  for the derivative of  $n$  iterate of  $f$  with respect to  $x$  and  $T_x D$  the tangent space.

A point  $x \in D$  is said to be **Lyapunov regular** if there exists

$\lambda(x, v) = \lim_{n \rightarrow \infty} \frac{1}{n} \log \|Df^n(x)v\|$  for some non-zero vector  $v \in T_x D$ .

$\lambda(x, v)$  is called the Lyapunov exponent.

The Lyapunov exponent is an important characteristics of a smooth dynamical systems that measure how much the vector  $v$  is expanded in average.

If the Lyapunov exponent is positive, that is one indicator of chaos.

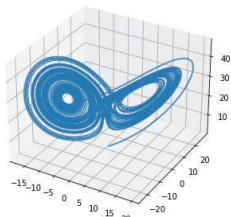


Figure: Chaos

A map  $f : D \rightarrow D$  is said to be a **piecewise  $C^r$  expanding map** if there exists a constant  $\lambda > 1$  and regions  $D_i \subset D$ ,  $1 \leq i \leq k$  with the following conditions:

(i) Each region  $D_i$ ,  $1 \leq i \leq k$ , has piecewise  $C^r$  boundary and  $\bigcup_{i=1}^k D_i = \overline{D}$ .

(ii) The restriction  $f|_{D_i}$  is extended to a neighborhood of  $\overline{D_i}$  as a  $C^r$  diffeomorphism  $f_i : \mathcal{N}(D_i) \rightarrow \mathbb{R}^2$  such that  $\|Df_i(x)v\| \geq \lambda\|v\|$  for any  $x \in \mathcal{N}(\overline{D_i})$  and tangent vector  $v \in T_x \mathcal{N}(\overline{D_i})$ .

## Introduction

We are interested in whether most of the points with respect to Lebesgue measure are Lyapunov regular or not.

In the case of an expanding map, almost every point is Lyapunov regular from Oseledets's theorem.

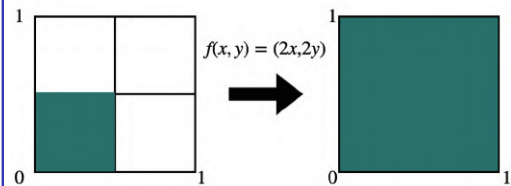


Figure: Piecewise expanding map

Question: What happens in the case of a piecewise expanding map?

## Main Result

(i) Let  $F : D \rightarrow D$  be a 2-dimensional piecewise real analytic expanding map. Then almost every point is Lyapunov regular.

(ii) For any integer  $r$  with  $1 \leq r < \infty$ , there exists a one-parameter family  $F_\sigma$  ( $0 < \sigma < 1$ ) of 2-dimensional piecewise  $C^r$  expanding maps such that almost every point is not Lyapunov regular.

This result shows that the piecewise expanding map may cause different behavior.

Also, in (i), the Lyapunov regular set has positive Lebesgue measure.

In (ii), the Lebesgue measure is zero.

More details can be seen at Y. Nakano, T. Soma and K. Yamamoto, Observable Lyapunov irregular sets for planar piecewise expanding maps, under review. <https://arxiv.org/abs/2206.09508>

## References

- [1] M. Tsujii, Piecewise expanding maps on the plane with singular ergodic properties, *Ergodic Theory Dynam. Sys.* **20** (2000) 1851-1857.
- [2] J. Buzzi, Absolutely continuous invariant probability measures for arbitrary expanding piecewise  $\mathbb{R}$ -analytic mappings of the plane, *Ergodic Theory Dynam. Sys.* **20** (2000) 697-708.

# Model Selection in Statistical Learning Theory

Naoki Nakamura

Graduate School of Mathematics, Kyushu University  
nakamura.naoki.331@s.kyushu-u.ac.jp

## 1 Rashomon Effect

Rashomon is a movie with several different explanations for the crime. [2] used the Rashomon to characterize this problem because the same phenomenon occurs in machine learning. Strictly speaking, for the same data, there exists many different accurate machine learning models. This phenomenon is called Rashomon effect.

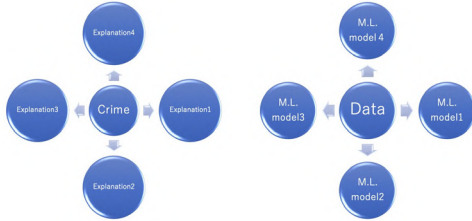


Figure 1: Rashomon Effect

## 2 Introduction

The following is the flow that engineers consider when modeling (see Figure 2). From 4, the practitioner does not try for searching simpler models. Therefore, we want to answer the following question: can we show an accurate-simpler model exists without the running machine learning algorithms?

- Occam's Razor:** We should not assume too much when explaining things.
- Accurate-Simplest Model:** Accurate model with the smallest number of parameters
- How difficult search accurate-simpler model?**
- NP-hard:** In general, the optimization problem for finding sparse simpler accurate model is NP-hard.
- Accurate-Complex Model:** Accurate model with a lot of parameters.

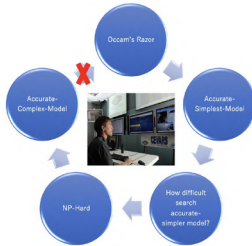


Figure 2: Practitioners don't try searching simpler models

## 3 Rashomon Ratio

If the Rashomon ratio is large means that there are many simple-accurate models in the Rashomon set.

## Rashomon set:

$$\hat{R}_S(\mathcal{F}_0, \theta) := \{f \in \mathcal{F}_0 : L(\hat{f}) \leq L(\hat{f}) + \theta\}$$

where  $\hat{f} \in \text{argmin}_{f \in \mathcal{F}} L(f)$ : The empirical risk minimizer,  $\theta$ : Rashomon parameter.

**Rashomon ratio:** Assume that  $\rho^*(\mathcal{F}_0) < \infty$  ( $\mathcal{F}_0 \subset \mathcal{F}$ ).

$$\hat{R}_{S,ratio}(\mathcal{F}_0, \theta) = \int_{f \in \mathcal{F}_0} 1_{f \in \hat{R}_S(\mathcal{F}_0, \theta)} \frac{\rho(df)}{\rho(\mathcal{F}_0)}$$

where  $\rho^*$  is prior distribution,  $\rho(df) = \frac{\rho^*(df)}{\rho^*(\mathcal{F}_0)}$ ,  $\rho(\mathcal{F}_0) = \frac{\rho^*(\mathcal{F}_0)}{\rho^*(\mathcal{F}_0)}$ .



Figure 3: Rashomon Ratio

## 4 Existence of accurate-simpler model

### Setting

- $\mathcal{F}_1$  is lower-complexity space than  $\mathcal{F}_2$ , and approximating set for the  $\mathcal{F}_2$ . (i.e.  $\mathcal{F}_1 \subset \mathcal{F}_2$ ).
- Complexity of  $\mathcal{F}_1$  and  $\mathcal{F}_2$  is decided by covering number or VC dimension.

In [1], we answer the following questions.

- Is there a guarantee that a model using the simpler function class  $\mathcal{F}_1$  will have test performance similar to the best model in  $\mathcal{F}_2$ ?

### Answer:

$$L(f_2^*) - c \sqrt{\frac{\log \#\mathcal{F}_1 + \log 2/\epsilon}{2n}} \leq L(\hat{f}_1) \leq L(f_2^*) + \delta + c \sqrt{\frac{\log 1/\epsilon}{2n}}$$

where  $\hat{f}_1 \in \text{argmin}_{f_1 \in \mathcal{F}_1} L(f_1)$ ,  $f_2^* \in \text{argmin}_{f_2 \in \mathcal{F}_2} L(f_2)$ .

- When the Rashomon set is large?

### Answer:

For simple data such as binary classification, an appropriate hypothesis space  $\mathcal{F}_1$  can be set up. In this case, we can check empirically.

## 5 Future Research

For complex data such as image data, the size of the Rashomon set cannot be generally understood because the configuration of the appropriate hypothesis space  $\mathcal{F}_1$  is not known.

- Given complex data and  $\mathcal{F}_2$  (complex neural network), can we construct  $\mathcal{F}_1$  (simple neural network)?
- Can we completely enumerate the Rashomon set for  $\mathcal{F}_1$  (simple neural network)?

## References

- [1] Leisa Semenova, Cynthia Rudin, and Roland Parr. On the Existence of Simpler Machine Learning Models. arXiv:1908.01755v4[cs.LG] 12 May 2022.
- [2] Leo Breiman et al. 2001. Statistical Modeling: The Two Cultures. Statistical Science, Vol. 16, No. 3 (Aug., 2001), pp. 199-215.

# Multiple Zeta Values and Euler's reflection formula for the Gamma function

Karin Ikeda, Kyushu University, Japan  
E-mail: ikeda.karin.236@s.kyushu-u.ac.jp



## Background

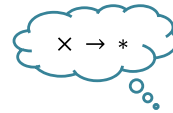
### Gamma Function

- $\Gamma(1+z) = z\Gamma(z)$
- $\Gamma(z)\Gamma(1-z) = \frac{\pi}{\sin \pi z}$



### Multiple Zeta Value

- $\zeta(2, 2, \dots, 2) = \frac{\pi^{2n}}{(2n+1)!}$
- $(\Gamma(1+x)e^{yx})^{-1} = 1 + \sum_{k=2}^{\infty} (-1)^k S(k)x^k$



$$\sum_{n=0}^{\infty} (-1)^n \zeta(\underbrace{2, \dots, 2}_n) x^{2n} = \left( 1 + \sum_{k=2}^{\infty} (-1)^k S(k)x^k \right) \times \left( 1 + \sum_{l=2}^{\infty} S(l)x^l \right)$$

This equation is correct !!

## Problem

We want to show the equality

$$\sum_{n=0}^{\infty} (-1)^n \zeta(\underbrace{2, \dots, 2}_n) x^{2n} = \left( 1 + \sum_{k=2}^{\infty} (-1)^k S(k)x^k \right) * \left( 1 + \sum_{l=2}^{\infty} S(l)x^l \right)$$

purely algebraically

$$S(k) = \sum_{\substack{k_1 + \dots + k_r = k \\ r > 1, \forall k_i \geq 2}} (-1)^r \prod_{j=1}^r \frac{(k_j - 1)}{k_j!} \zeta(k_1, k_2, \dots, k_r) \quad * : \text{Harmonic Product}$$

## Preparation

### Multiple Zeta Value

#### Definition

Let,  $k_1, \dots, k_r$  are positive integers and  $k_r > 1$ .

The multiple zeta value (MZV)  $\zeta(k_1, \dots, k_r)$  is defined by

$$\zeta(k_1, \dots, k_r) = \sum_{0 < m_1 < \dots < m_r} \frac{1}{m_1^{k_1} \dots m_r^{k_r}}$$

Depth:  $r$  Weight:  $k_1 + \dots + k_r$

#### Example

$$\zeta(2, 3) = \sum_{0 < m_1 < m_2} \frac{1}{m_1^2 m_2^3} = \frac{1}{1^2 2^3} + \frac{1}{1^2 3^3} + \frac{1}{2^2 3^3} + \frac{1}{1^2 4^3} + \frac{1}{2^2 4^3} + \dots$$

### Harmonic Product

#### What is the harmonic product

The harmonic product is a rule for expressing the product of multiple zeta values as a sum using a series representation.

#### Example

$$\begin{aligned} \zeta(p) * \zeta(q) &= \sum_{0 < m_1} \frac{1}{m_1^p} \times \sum_{0 < m_2} \frac{1}{m_2^q} \\ &= \left( \sum_{0 < m_1 < m_2} + \sum_{0 < m_1 < m_2} + \sum_{0 < m_2 < m_1} \right) \frac{1}{m_1^p m_2^q} \end{aligned}$$

## Strategy

### In the case of depth 1

#### Coefficients of $\zeta(k)$

LHS  $(-1)^1 \zeta(2)$

$$\begin{aligned} \text{RHS } 1 \times (-1)^1 \frac{k-1}{k!} \zeta(k) + 1 \times (-1)^k (-1)^1 \frac{k-1}{k!} \zeta(k) \\ + \sum_{m=2}^{k-2} \left( (-1)^m (-1)^1 \frac{m-1}{m!} \times (-1)^1 \frac{k-m-1}{(k-m)!} \right) \zeta(k) \end{aligned}$$

Thus, We will show this equation

$$\sum_{m=2}^{k-2} \left( (-1)^m \frac{(m-1)(k-m-1)k!}{m!(k-m)!k!} \right) - (1 + (-1)^k) \frac{k-1}{k!} = \begin{cases} -1 & k=2 \\ 0 & k \geq 3 \end{cases}$$

#### Proof Overview

$$\sum_{m=2}^{k-2} \left( (-1)^m \binom{k}{m} \frac{(m-1)(k-m-1)}{k!} \right) = (1 + (-1)^k) \frac{k-1}{k!} \quad \text{for } k \geq 3$$

### General case

#### Coefficients of $\zeta(k_1, \dots, k_r)$

#### Proof Overview

For example, we consider the coefficient of  $\zeta(k_1, \dots, k_r)$  when

calculating  $\zeta(m_1, \dots, m_l, k_l) * \zeta(k_1 - m_1, \dots, k_l - m_l, k_{l+1}, \dots, k_{l-1})$ .

$$\begin{aligned} (-1)^{l+i} \sum_{m_1=2}^{k_1-2} \dots \sum_{m_l=2}^{k_l-2} \left\{ (-1)^{m_1+\dots+m_l+k_l} (-1)^{k_1+\dots+k_l-1-m_1-\dots-m_l} \right\} \frac{(m_1-1) \dots (m_l-1)(k_l-1)}{m_1! \dots m_l! k_l!} \\ \times \frac{(k_1 - m_1 - 1) \dots (k_l - m_l - 1)(k_{l+1} - 1) \dots (k_{l-1} - 1) k_1! \dots k_l!}{(k_1 - m_1)! \dots (k_l - m_l)! k_{l+1}! \dots k_{l-1}! k_1! \dots k_l!} \\ = (-1)^{l+i} \{ (-1)^{k_l} (-1)^{k_1+\dots+k_l-1} \} \times \prod_{j=1}^l \left[ 1 + (-1)^{k_j} \right] \times \prod_{j=1}^l \frac{k_j - 1}{k_j!} \end{aligned}$$

Doing this in all cases completes the proof.

## References

- [1] T. Arakawa and M. Kaneko, Introduction to Multiple Zeta Values (in Japanese). MI Lecture Note Series, vol. 23. Kyushu University, Kyushu (2010).
- [2] M. Hoffman, The algebra of multiple harmonic series, J. Algebra, 194 (1997), 477–495.
- [3] K. Ihara, M. Kaneko and D. Zagier, Derivation and double shuffle relations for multiple zeta values, Compositio Math., 142 (2006), 307–338.
- [4] G. Racinet, Doubles mélanges des polylogarithmes multiples aux racines de l'unité, Publ. Math. Inst. Hautes Etudes Sci., 95 (2002), 185–231.
- [5] K. Ikeda and M. Sakata, Multiple zeta values and Euler's reflection formula for the gamma function, in preparation.

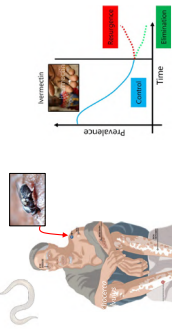
## Parameterising vector movement in an onchocerciasis transmission model with population genetic data.

PRESENTER:

Himal Shrestha  
@himal2007  
h.shrestha@latrobe.edu.au

### BACKGROUND

- Onchocerciasis is a neglected tropical disease common in sub-Saharan Africa where around **220 million people** are at risk of infection.
- Transmitted by the bites of blackflies and caused by a filarial parasite *Onchocerca volvulus*



- Persistence of onchocerciasis transmission** is attributed to movement of infected blackflies and humans.
- A transmission model with a spatial structure (patch model) was set up by McCulloch et. al. to address the problem.
- However, McCulloch et. al. focused on human movement alone. The effect of vector movement was not explored.

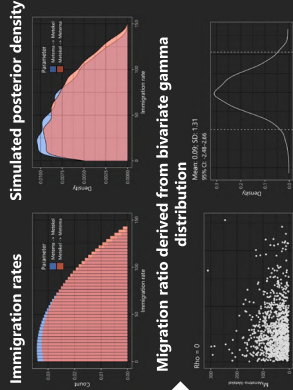
### OBJECTIVE

- Parameterise the vector movement parameters in the patch model with population genetic data
- Explore the effect of vector movement in a spatially explicit setting.

### METHODS

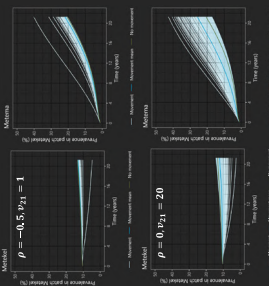
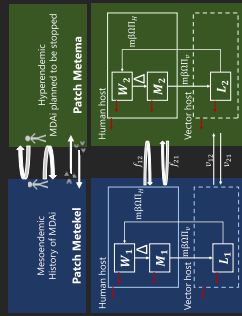
- We calculated the vector migration estimates between the two regions in Ethiopia, Metema and Metekel with genetic data from 134 blackflies using Migrate-n.
- We incorporated the directionality of migration rates into the patch model as a migration ratio.

# Incorporation of the population genetic data from blackflies shows the transmission dynamics of persisting onchocerciasis hotspot in Ethiopia.



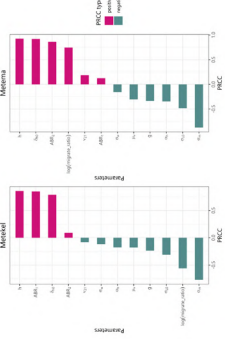
$$\frac{M_{12}}{M_{21}} = \frac{V_{12}}{V_{21}}$$

### Migration ratio



### RESULTS AND DISCUSSION

- There was asymmetric migration of blackflies between Metekel to Metema with blackfly migration greater to the Metema.
- With the simulation using estimates of the migration ratio from the population genetic data there is a prominent increase in onchocerciasis prevalence in the Metema focus.
- It can reach a microfilarial prevalence ~25% within a span of 20 years.
- Sensitivity analysis with Latin hypercube sampling (LHS) and PRCC revealed that parameters like Annual biting rate ( $ABR$ ),  $\delta_{hp}$ ,  $h$ ,  $\sigma_{hp}$ , and  $\sigma_{10}$  were the most influencing parameters in the model for prevalence in Metema and Metekel.



### CONCLUSION

- Estimates of migration derived from population genetic data can be used to inform vector movement parameters in the transmission model.

Himal Shrestha, Shannon M. Hedtke, Karen McCulloch, Warwick N. Grant, Rebecca Chisholm

**Acknowledgements:** Dr Rony Post, Dr Moses Katabarwa, Dr Peter Beerli, Mr Sindew M. Feleke, Dr Joel Miller, Dr Craig Wilding



## MI レクチャーノートシリーズ刊行にあたり

本レクチャーノートシリーズは、文部科学省 21 世紀 COE プログラム「機能数学の構築と展開」(H15-19 年度)において作成した COE Lecture Notes の続刊であり、文部科学省大学院教育改革支援プログラム「産業界が求める数学博士と新修士養成」(H19-21 年度)および、同グローバル COE プログラム「マス・フォア・インダストリ教育研究拠点」(H20-24 年度)において行われた講義の講義録として出版されてきた。平成 23 年 4 月のマス・フォア・インダストリ研究所 (IMI) 設立と平成 25 年 4 月の IMI の文部科学省共同利用・共同研究拠点として「産業数学の先進的・基礎的共同研究拠点」の認定を受け、今後、レクチャーノートは、マス・フォア・インダストリに関わる国内外の研究者による講義の講義録、会議録等として出版し、マス・フォア・インダストリの本格的な展開に資するものとする。

2022 年 10 月

マス・フォア・インダストリ研究所  
所長 梶原 健司

## Proceedings of Forum “Math-for-Industry” 2022 -Mathematics of Public Health and Sustainability-

発行 2023年 6 月 19 日  
編集 Philip Broadbridge, Luke Bennetts, Melanie Roberts and Kenji Kajiwara  
発行 九州大学マス・フォア・インダストリ研究所  
九州大学大学院数理学府  
〒819-0395 福岡市西区元岡744  
九州大学数理・IMI 事務室  
TEL 092-802-4402 FAX 092-802-4405  
URL <https://www.imi.kyushu-u.ac.jp/>

印刷 城島印刷株式会社  
〒810-0012 福岡市中央区白金 2 丁目 9 番 6 号  
TEL 092-531-7102 FAX 092-524-4411

## シリーズ既刊

Issue	Author/Editor	Title	Published
COE Lecture Note	Mitsuhiro T. NAKAO Kazuhiro YOKOYAMA	Computer Assisted Proofs - Numeric and Symbolic Approaches - 199pages	August 22, 2006
COE Lecture Note	M.J.Shai HARAN	Arithmetical Investigations - Representation theory, Orthogonal polynomials and Quantum interpolations- 174pages	August 22, 2006
COE Lecture Note Vol.3	Michal BENES Masato KIMURA Tatsuyuki NAKAKI	Proceedings of Czech-Japanese Seminar in Applied Mathematics 2005 155pages	October 13, 2006
COE Lecture Note Vol.4	宮田 健治	辺要素有限要素法による磁界解析 - 機能数理学特別講義 21pages	May 15, 2007
COE Lecture Note Vol.5	Francois APERY	Univariate Elimination Subresultants - Bezout formula, Laurent series and vanishing conditions - 89pages	September 25, 2007
COE Lecture Note Vol.6	Michal BENES Masato KIMURA Tatsuyuki NAKAKI	Proceedings of Czech-Japanese Seminar in Applied Mathematics 2006 209pages	October 12, 2007
COE Lecture Note Vol.7	若山 正人 中尾 充宏	九州大学産業技術数理研究センター キックオフミーティング 138pages	October 15, 2007
COE Lecture Note Vol.8	Alberto PARMEGGIANI	Introduction to the Spectral Theory of Non-Commutative Harmonic Oscillators 233pages	January 31, 2008
COE Lecture Note Vol.9	Michael I.TRIBELSKY	Introduction to Mathematical modeling 23pages	February 15, 2008
COE Lecture Note Vol.10	Jacques FARAUT	Infinite Dimensional Spherical Analysis 74pages	March 14, 2008
COE Lecture Note Vol.11	Gerrit van DIJK	Gelfand Pairs And Beyond 60pages	August 25, 2008
COE Lecture Note Vol.12	Faculty of Mathematics, Kyushu University	Consortium "MATH for INDUSTRY" First Forum 87pages	September 16, 2008
COE Lecture Note Vol.13	九州大学大学院 数理学研究院	プロシーディング「損保数理に現れる確率モデル」 — 日新火災・九州大学 共同研究2008年11月 研究会 — 82pages	February 6, 2009



## シリーズ既刊

Issue	Author/Editor	Title	Published
COE Lecture Note Vol.14	Michal Beneš, Tohru Tsujikawa Shigetoshi Yazaki	Proceedings of Czech-Japanese Seminar in Applied Mathematics 2008 77pages	February 12, 2009
COE Lecture Note Vol.15	Faculty of Mathematics, Kyushu University	International Workshop on Verified Computations and Related Topics 129pages	February 23, 2009
COE Lecture Note Vol.16	Alexander Samokhin	Volume Integral Equation Method in Problems of Mathematical Physics 50pages	February 24, 2009
COE Lecture Note Vol.17	矢嶋 徹 及川 正行 梶原 健司 辻 英一 福本 康秀	非線形波動の数理と物理 66pages	February 27, 2009
COE Lecture Note Vol.18	Tim Hoffmann	Discrete Differential Geometry of Curves and Surfaces 75pages	April 21, 2009
COE Lecture Note Vol.19	Ichiro Suzuki	The Pattern Formation Problem for Autonomous Mobile Robots —Special Lecture in Functional Mathematics— 23pages	April 30, 2009
COE Lecture Note Vol.20	Yasuhide Fukumoto Yasunori Maekawa	Math-for-Industry Tutorial: Spectral theories of non-Hermitian operators and their application 184pages	June 19, 2009
COE Lecture Note Vol.21	Faculty of Mathematics, Kyushu University	Forum "Math-for-Industry" Casimir Force, Casimir Operators and the Riemann Hypothesis 95pages	November 9, 2009
COE Lecture Note Vol.22	Masakazu Suzuki Hoon Hong Hirokazu Anai Chee Yap Yousuke Sato Hiroshi Yoshida	The Joint Conference of ASCM 2009 and MACIS 2009: Asian Symposium on Computer Mathematics Mathematical Aspects of Computer and Information Sciences 436pages	December 14, 2009
COE Lecture Note Vol.23	荒川 恒男 金子 昌信	多重ゼータ値入門 111pages	February 15, 2010
COE Lecture Note Vol.24	Fulton B.Gonzalez	Notes on Integral Geometry and Harmonic Analysis 125pages	March 12, 2010
COE Lecture Note Vol.25	Wayne Rossman	Discrete Constant Mean Curvature Surfaces via Conserved Quantities 130pages	May 31, 2010
COE Lecture Note Vol.26	Mihai Ciucu	Perfect Matchings and Applications 66pages	July 2, 2010

## シリーズ既刊

Issue	Author/Editor	Title	Published
COE Lecture Note Vol.27	九州大学大学院 数理学研究院	Forum “Math-for-Industry” and Study Group Workshop Information security, visualization, and inverse problems, on the basis of optimization techniques 100pages	October 21, 2010
COE Lecture Note Vol.28	ANDREAS LANGER	MODULAR FORMS, ELLIPTIC AND MODULAR CURVES LECTURES AT KYUSHU UNIVERSITY 2010 62pages	November 26, 2010
COE Lecture Note Vol.29	木田 雅成 原田 昌晃 横山 俊一	Magma で広がる数学の世界 157pages	December 27, 2010
COE Lecture Note Vol.30	原 隆 松井 卓 廣島 文生	Mathematical Quantum Field Theory and Renormalization Theory 201pages	January 31, 2011
COE Lecture Note Vol.31	若山 正人 福本 康秀 高木 剛 山本 昌宏	Study Group Workshop 2010 Lecture & Report 128pages	February 8, 2011
COE Lecture Note Vol.32	Institute of Mathematics for Industry, Kyushu University	Forum “Math-for-Industry” 2011 “TSUNAMI-Mathematical Modelling” Using Mathematics for Natural Disaster Prediction, Recovery and Provision for the Future 90pages	September 30, 2011
COE Lecture Note Vol.33	若山 正人 福本 康秀 高木 剛 山本 昌宏	Study Group Workshop 2011 Lecture & Report 140pages	October 27, 2011
COE Lecture Note Vol.34	Adrian Muntean Vladimír Chalupecký	Homogenization Method and Multiscale Modeling 72pages	October 28, 2011
COE Lecture Note Vol.35	横山 俊一 夫 紀恵 林 卓也	計算機代数システムの進展 210pages	November 30, 2011
COE Lecture Note Vol.36	Michal Beneš Masato Kimura Shigetoshi Yazaki	Proceedings of Czech-Japanese Seminar in Applied Mathematics 2010 107pages	January 27, 2012
COE Lecture Note Vol.37	若山 正人 高木 剛 Kirill Morozov 平岡 裕章 木村 正人 白井 朋之 西井 龍映 柴 伸一郎 穴井 宏和 福本 康秀	平成23年度 数学・数理科学と諸科学・産業との連携研究ワーク ショップ 拡がっていく数学 ～期待される“見えない力”～ 154pages	February 20, 2012

## シリーズ既刊

Issue	Author/Editor	Title	Published
COE Lecture Note Vol.38	Fumio Hiroshima Itaru Sasaki Herbert Spohn Akito Suzuki	Enhanced Binding in Quantum Field Theory 204pages	March 12, 2012
COE Lecture Note Vol.39	Institute of Mathematics for Industry, Kyushu University	Multiscale Mathematics: Hierarchy of collective phenomena and interrelations between hierarchical structures 180pages	March 13, 2012
COE Lecture Note Vol.40	井ノ口順一 太田 泰広 寛 三郎 梶原 健司 松浦 望	離散可積分系・離散微分幾何チュートリアル2012 152pages	March 15, 2012
COE Lecture Note Vol.41	Institute of Mathematics for Industry, Kyushu University	Forum “Math-for-Industry” 2012 “Information Recovery and Discovery” 91pages	October 22, 2012
COE Lecture Note Vol.42	佐伯 修 若山 正人 山本 昌宏	Study Group Workshop 2012 Abstract, Lecture & Report 178pages	November 19, 2012
COE Lecture Note Vol.43	Institute of Mathematics for Industry, Kyushu University	Combinatorics and Numerical Analysis Joint Workshop 103pages	December 27, 2012
COE Lecture Note Vol.44	萩原 学	モダン符号理論からポストモダン符号理論への展望 107pages	January 30, 2013
COE Lecture Note Vol.45	金山 寛	Joint Research Workshop of Institute of Mathematics for Industry (IMI), Kyushu University “Propagation of Ultra-large-scale Computation by the Domain-decomposition-method for Industrial Problems (PUCDIP 2012)” 121pages	February 19, 2013
COE Lecture Note Vol.46	西井 龍映 栄 伸一郎 岡田 勘三 落合 啓之 小磯 深幸 斎藤 新悟 白井 朋之	科学・技術の研究課題への数学アプローチ —数学モデリングの基礎と展開— 325pages	February 28, 2013
COE Lecture Note Vol.47	SOO TECK LEE	BRANCHING RULES AND BRANCHING ALGEBRAS FOR THE COMPLEX CLASSICAL GROUPS 40pages	March 8, 2013
COE Lecture Note Vol.48	溝口 佳寛 脇 隼人 平坂 貢 谷口 哲至 鳥袋 修	博多ワークショップ「組み合わせとその応用」 124pages	March 28, 2013

## シリーズ既刊

Issue	Author/Editor	Title	Published
COE Lecture Note Vol.49	照井 章 小原 功任 濱田 龍義 横山 俊一 穴井 宏和 横田 博史	マス・フォア・インダストリ研究所 共同利用研究集会 II 数式処理研究と産学連携の新たな発展 137pages	August 9, 2013
MI Lecture Note Vol.50	Ken Anjyo Hiroyuki Ochiai Yoshinori Dobashi Yoshihiro Mizoguchi Shizuo Kaji	Symposium MEIS2013: Mathematical Progress in Expressive Image Synthesis 154pages	October 21, 2013
MI Lecture Note Vol.51	Institute of Mathematics for Industry, Kyushu University	Forum “Math-for-Industry” 2013 “The Impact of Applications on Mathematics” 97pages	October 30, 2013
MI Lecture Note Vol.52	佐伯 修 岡田 勘三 高木 剛 若山 正人 山本 昌宏	Study Group Workshop 2013 Abstract, Lecture & Report 142pages	November 15, 2013
MI Lecture Note Vol.53	四方 義啓 櫻井 幸一 安田 貴徳 Xavier Dahan	平成25年度 九州大学マス・フォア・インダストリ研究所 共同利用研究集会 安全・安心社会基盤構築のための代数構造 ～サイバー社会の信頼性確保のための数理学～ 158pages	December 26, 2013
MI Lecture Note Vol.54	Takashi Takiguchi Hiroshi Fujiwara	Inverse problems for practice, the present and the future 93pages	January 30, 2014
MI Lecture Note Vol.55	栄 伸一郎 溝口 佳寛 脇 隼人 洪田 敬史	Study Group Workshop 2013 数学協働プログラム Lecture & Report 98pages	February 10, 2014
MI Lecture Note Vol.56	Yoshihiro Mizoguchi Hayato Waki Takafumi Shibuta Tetsuji Taniguchi Osamu Shimabukuro Makoto Tagami Hirotake Kurihara Shuya Chiba	Hakata Workshop 2014 ~ Discrete Mathematics and its Applications ~ 141pages	March 28, 2014
MI Lecture Note Vol.57	Institute of Mathematics for Industry, Kyushu University	Forum “Math-for-Industry” 2014: “Applications + Practical Conceptualization + Mathematics = fruitful Innovation” 93pages	October 23, 2014
MI Lecture Note Vol.58	安生健一 落合啓之	Symposium MEIS2014: Mathematical Progress in Expressive Image Synthesis 135pages	November 12, 2014

## シリーズ既刊

Issue	Author/Editor	Title	Published
MI Lecture Note Vol.59	西井 龍映 岡田 勘三 梶原 健司 高木 剛 若山 正人 脇 隼人 山本 昌宏	Study Group Workshop 2014 数学協働プログラム Abstract, Lecture & Report 196pages	November 14, 2014
MI Lecture Note Vol.60	西浦 博	平成26年度九州大学 IMI 共同利用研究・研究集会 (I) 感染症数理モデルの実用化と産業及び政策での活用のための新たな展開 120pages	November 28, 2014
MI Lecture Note Vol.61	溝口 佳寛 Jacques Garrigue 萩原 学 Reynald Affeldt	研究集会 高信頼な理論と実装のための定理証明および定理証明器 Theorem proving and provers for reliable theory and implementations (TPP2014) 138pages	February 26, 2015
MI Lecture Note Vol.62	白井 朋之	Workshop on “ $\beta$ -transformation and related topics” 59pages	March 10, 2015
MI Lecture Note Vol.63	白井 朋之	Workshop on “Probabilistic models with determinantal structure” 107pages	August 20, 2015
MI Lecture Note Vol.64	落合 啓之 土橋 宜典	Symposium MEIS2015: Mathematical Progress in Expressive Image Synthesis 124pages	September 18, 2015
MI Lecture Note Vol.65	Institute of Mathematics for Industry, Kyushu University	Forum “Math-for-Industry” 2015 “The Role and Importance of Mathematics in Innovation” 74pages	October 23, 2015
MI Lecture Note Vol.66	岡田 勘三 藤澤 克己 白井 朋之 若山 正人 脇 隼人 Philip Broadbridge 山本 昌宏	Study Group Workshop 2015 Abstract, Lecture & Report 156pages	November 5, 2015
MI Lecture Note Vol.67	Institute of Mathematics for Industry, Kyushu University	IMI-La Trobe Joint Conference “Mathematics for Materials Science and Processing” 66pages	February 5, 2016
MI Lecture Note Vol.68	古庄 英和 小谷 久寿 新甫 洋史	結び目と Grothendieck-Teichmüller 群 116pages	February 22, 2016
MI Lecture Note Vol.69	土橋 宜典 鍛冶 静雄	Symposium MEIS2016: Mathematical Progress in Expressive Image Synthesis 82pages	October 24, 2016
MI Lecture Note Vol.70	Institute of Mathematics for Industry, Kyushu University	Forum “Math-for-Industry” 2016 “Agriculture as a metaphor for creativity in all human endeavors” 98pages	November 2, 2016
MI Lecture Note Vol.71	小磯 深幸 二宮 嘉行 山本 昌宏	Study Group Workshop 2016 Abstract, Lecture & Report 143pages	November 21, 2016

## シリーズ既刊

Issue	Author/Editor	Title	Published
MI Lecture Note Vol.72	新井 朝雄 小嶋 泉 廣島 文生	Mathematical quantum field theory and related topics 133pages	January 27, 2017
MI Lecture Note Vol.73	穴田 啓晃 Kirill Morozov 須賀 祐治 奥村 伸也 櫻井 幸一	Secret Sharing for Dependability, Usability and Security of Network Storage and Its Mathematical Modeling 211pages	March 15, 2017
MI Lecture Note Vol.74	QUISPEL, G. Reinout W. BADER, Philipp MCLAREN, David I. TAGAMI, Daisuke	IMI-La Trobe Joint Conference Geometric Numerical Integration and its Applications 71pages	March 31, 2017
MI Lecture Note Vol.75	手塚 集 田上 大助 山本 昌宏	Study Group Workshop 2017 Abstract, Lecture & Report 118pages	October 20, 2017
MI Lecture Note Vol.76	宇田川誠一	Tzitzéica 方程式の有限間隙解に付随した極小曲面の構成理論 —Tzitzéica 方程式の楕円関数解を出発点として— 68pages	August 4, 2017
MI Lecture Note Vol.77	松谷 茂樹 佐伯 修 中川 淳一 田上 大助 上坂 正晃 Pierluigi Cesana 濱田 裕康	平成29年度 九州大学マス・フォア・インダストリ研究所 共同利用研究会 (I) 結晶の界面, 転位, 構造の数理 148pages	December 20, 2017
MI Lecture Note Vol.78	瀧澤 重志 小林 和博 佐藤憲一郎 斎藤 努 清水 正明 間瀬 正啓 藤澤 克樹 神山 直之	平成29年度 九州大学マス・フォア・インダストリ研究所 プロジェクト研究 研究会 (I) 防災・避難計画の数理モデルの高度化と社会実装へ向けて 136pages	February 26, 2018
MI Lecture Note Vol.79	神山 直之 畔上 秀幸	平成29年度 AIMaP チュートリアル 最適化理論の基礎と応用 96pages	February 28, 2018
MI Lecture Note Vol.80	Kirill Morozov Hiroaki Anada Yuji Suga	IMI Workshop of the Joint Research Projects Cryptographic Technologies for Securing Network Storage and Their Mathematical Modeling 116pages	March 30, 2018
MI Lecture Note Vol.81	Tsuyoshi Takagi Masato Wakayama Keisuke Tanaka Noboru Kunihiro Kazufumi Kimoto Yasuhiko Ikematsu	IMI Workshop of the Joint Research Projects International Symposium on Mathematics, Quantum Theory, and Cryptography 246pages	September 25, 2019
MI Lecture Note Vol.82	池森 俊文	令和2年度 AIMaP チュートリアル 新型コロナウイルス感染症にかかわる諸問題の数理 145pages	March 22, 2021

## シリーズ既刊

Issue	Author/Editor	Title	Published
MI Lecture Note Vol.83	早川健太郎 軸丸 芳揮 横須賀洋平 可香谷 隆 林 和希 堺 雄亮	シエル理論・膜理論への微分幾何学からのアプローチと その建築曲面設計への応用 49pages	July 28, 2021
MI Lecture Note Vol.84	Taketoshi Kawabe Yoshihiro Mizoguchi Junichi Kako Masakazu Mukai Yuji Yasui	SICE-JSAE-AIMaP Tutorial Advanced Automotive Control and Mathematics 110pages	December 27, 2021
MI Lecture Note Vol.85	Hiroaki Anada Yasuhiko Ikematsu Koji Nuida Satsuya Ohata Yuntao Wang	IMI Workshop of the Joint Usage Research Projects Exploring Mathematical and Practical Principles of Secure Computation and Secret Sharing 114pages	February 9, 2022
MI Lecture Note Vol.86	濱田 直希 穴井 宏和 梅田 裕平 千葉 一永 佐藤 寛之 能島 裕介 加藤田雄太朗 一木 俊助 早野 健太 佐伯 修	2020年度採択分 九州大学マス・フォア・インダストリ研究所 共同利用研究集会 進化計算の数理 135pages	February 22, 2022
MI Lecture Note Vol.87	Osamu Saeki, Ho Tu Bao, Shizuo Kaji, Kenji Kajiwara, Nguyen Ha Nam, Ta Hai Tung, Melanie Roberts, Masato Wakayama, Le Minh Ha, Philip Broadbridge	Proceedings of Forum “Math-for-Industry” 2021 -Mathematics for Digital Economy- 122pages	March 28, 2022
MI Lecture Note Vol.88	Daniel PACKWOOD Pierluigi CESANA, Shigenori FUJIKAWA, Yasuhide FUKUMOTO, Petros SOFRONIS, Alex STAYKOV	Perspectives on Artificial Intelligence and Machine Learning in Materials Science, February 4-6, 2022 74pages	November 8, 2022

MI Lecture Note Vol.89	松谷 茂樹 落合 啓之 井上 和俊 小磯 深幸 佐伯 修 白井 朋之 垂水 竜一 内藤 久資 中川 淳一 濱田 裕康 松江 要 加葉田雄太朗	2020年度採択分 九州大学マス・フォア・インダストリ研究所 共同利用研究集会 材料科学における幾何と代数 III 356pages	December 7, 2022
MI Lecture Note Vol.90	中山 尚子 谷川 拓司 品野 勇治 近藤 正章 石原 亨 鍛冶 静雄 藤澤 克樹	2022年度採択分 九州大学マス・フォア・インダストリ研究所 共同利用研究集会 データ格付けサービス実現のための数理基盤の構築 58pages	December 12, 2022
MI Lecture Note Vol.91	Katsuki Fujisawa Shizuo Kaji Toru Ishihara Masaaki Kondo Yuji Shinano Takuji Tanigawa Naoko Nakayama	IMI Workshop of the Joint Usage Research Projects Construction of Mathematical Basis for Realizing Data Rating Service 610pages	December 27, 2022
MI Lecture Note Vol.92	丹田 聡 三宮 俊 廣島 文生	2022年度採択分 九州大学マス・フォア・インダストリ研究所 共同利用研究集会 時間・量子測定・準古典近似の理論と実験 ～古典論と量子論の境界～ 150pages	January 6, 2023





Institute of Mathematics for Industry  
Kyushu University

九州大学マス・フォア・インダストリ研究所  
九州大学大学院 数理学府

〒819-0395 福岡市西区元岡744 TEL 092-802-4402 FAX 092-802-4405  
URL <http://www.imi.kyushu-u.ac.jp/>